Aus dem Institut/der Klinik für Pädiatrie mit Schwerpunkt Onkologie und Hämatologie
der Medizinischen Fakultät Charité – Universitätsmedizin Berlin

DISSERTATION

Targeting ATR in pediatric solid tumors
ATR als therapeutischer Angriffspunkt bei pädiatrischen soliden Tumoren

zur Erlangung des akademischen Grades
Doctor of Philosophy (PhD)

vorgelegt der Medizinischen Fakultät
Charité – Universitätsmedizin Berlin

von

Heathcliff Dorado García

Datum der Promotion: 30.06.2024

Table of contents

List of figures ii

List of abbreviations iii

Abstract 1

1. Introduction 3

2. Methods 9

3. Results 13

4. Discussion 23

5. Reference list 28

6. Statutory Declaration 37

7. Declaration of your own contribution to the publications 38

8. Excerpt from Journal Summary List 39

9. Printing copies of the publications 41

10. Curriculum Vitae 98

11. Publication list 102

12. Acknowledgments 105

List of figures

Figure 1. ATR inhibition has antitumor activity in ARMS cell lines. 14

Figure 2. ATR inhibition leads to homologous recombination deficiency in ARMS cells. 15

Figure 3. PAX3-FOXO1 is sufficient to increase sensitivity to ATR inhibition. 16

Figure 4. FOS family gene activation is important for ATR inhibitor resistance. 18

Figure 5. ATR inhibition is an effective antitumor therapy in ARMS PDX models. 20

Figure 6. Aurora A and ATR inhibitors have strong antitumor activity in *MYCN*-amplified NB PDX. 22

List of abbreviations

ADP	Adenosine-5’-diphosphate
AKT	Ak strain transforming
ALK	Anaplastic lymphoma kinase
ALT	Alternative lengthening of telomeres
AP-1	Activation protein 1
ARMS	Alveolar rhabdomyosarcoma
ATM	Ataxia-telangiectasia mutated
ATR	ATM- and Rad3-related
ATRX	Alpha-thalassemia/mental retardation, X-linked
BCA	Bicinchoninic acid
BER	Base excision repair
BRCA1/2	Breast Cancer 1/2
BRD4	Bromodomain 4
BSA	Bovine serum albumin
CAR-T cell	Chimeric antigen receptor-T cell
CDK4	Cyclin-dependent kinase 4
CHD4	Chromodomain-helicase-DNA-binding protein 4
CHK1/2	Checkpoint kinase 1/2
c-MYC	Myelocytomatosis oncogene (human)
CNS	Central nervous system
c-Raf	Rapidly accelerated fibrosarcoma (human)
CRISPR	Clustered regularly interspaced short palindromic repeats
DAPI	4’, 6-diamidino-2-phenylindole
DDR	DNA damage repair
DMEM	Dubelco’s Modified Eagle Medium

DMSO	Dimethyl sulfoxide
DNA	Deoxyribonucleic acid
DNA-PK	DNA protein kinase
Dox.	Doxycycline
DSB	Double strand break
ECL	Enhanced chemoluminescence
ERK1/2	Extracellular-signal regulated kinase 1/2
ERMS	Embryonal rhabdomyosarcoma
EWS	Ewing sarcoma
FACS	Flow-assisted cytometry system
FDR	False discovery rate
FLI1	Friend leukemia virus integration 1
FOS(B)	Finkel-Biskis-Jinkins murine osteogenic sarcoma (B)
FOSL1/2	FOS ligand 1/2
FOXO1	Forkhead Box O1
GD2	Disiaganglioside GD2
H3	Histone 3
HDAC	Histone deacetylase
HR	Homologous recombination
HU	Hydroxyurea
IC_{50}	Inhibitory concentration 50
IVA	Ifosfamide, vincristine, actinomycin D
MAGeCK	Model-based analysis of genome-wide CRISPR/Cas9 knock-out
MAPK	Mitogen-activated protein kinase
MMR	Mismatch-mediated repair

MOI	Multiplicity of infection
MSKCC	Memorial Sloan Kettering Cancer Center
MYCN	Myelocytomatosis oncogene N
NB	Neuroblastoma
NCOA1	Nuclear receptor coactivator 1
NER	Nucleotide excision repair
NHEJ	Non-homologous end joining
NRAS	N-Rat sarcoma virus
P3F/P7F	PAX3-FOXO1/PAX7-FOXO1
PARP1	Poly [ADP-ribose] polymerase 1
PAX3/7	Paired box 3/7
PBS	Phosphate buffer saline
PDX	Patient-derived xenograft
PGBD5	PiggyBac transposable element derived 5
PI3K	Phosphoinositide 3-kinase
PVDF	Polyvinylidene fluoride
RAS	Rat sarcoma virus
RMS	Rhabdomyosarcoma
RNA	Ribonucleic acid
RPA32	Replication protein A 32
RPMI	Roswell Park Memorial Institute
RRA	Robust rank aggregation
RTK	Receptor tyrosine kinase
SEER	Surveillance, epidemiology and end results
sgRNA	single guide RNA
SSB	Single strand break

TdT	Terminal deoxynucleotidyl transferase
TERT	Telomerase reverse transcriptase
TP53	Tumor protein 53
TP53BP1	TP53 binding protein 1
TUNEL	TdT-dependent UTP nick-end labelling
US	United States
UTP	Uridine-5’-triphosphate
UV	Ultraviolet
VAC	Vincistrine, actinomycin D, cyclophosphamide
γH2A.X	Serine 139-phosphorylated Histone 2A.X

Abstract

Pediatric solid tumors represent a unique challenge for cancer therapeutics, due to their unique genetic background. Despite advances in cancer treatment, some forms of pediatric cancer continue having a poor outcome. Here we look at the effectiveness of ATR inhibitors in two pediatric solid tumors, alveolar rhabdomyosarcoma and *MYCN*-amplified neuroblastoma. ATR inhibitors showed a strong antitumor activity in alveolar rhabdomyosarcomas, observed as an accumulation of DNA damage and genomic instability that resulted in cell death. Using phosphoproteomics, we identified BRCA1, and more broadly homologous recombination, as being compromised upon ATR inhibition, and hypothesize that defects in DNA repair are responsible for sensitivity to ATR inhibitors. We also identified PAX3-FOXO1, a fusion oncoprotein characteristic of alveolar rhabdomyosarcoma, as a factor that increases replication stress and sensitizes alveolar rhabdomyosarcomas to ATR inhibition. Because resistance to therapy is frequently the cause of treatment failure, we looked at potential mechanisms of resistance to ATR inhibitors and identified the FOS family genes as candidates for ATR inhibitor resistance in alveolar rhabdomyosarcoma. Finally, we looked at the efficacy of ATR inhibitors in patient-derived xenograft models of alveolar rhabdomyosarcoma as a monotherapy and in combination with the PARP1 inhibitor olaparib. ATR inhibitors as a monotherapy were sufficient to achieve stable disease in alveolar rhabdomyosarcoma with minimal side effects, while the combination with olaparib resulted in total remission of the tumors. In *MYCN*-amplified neuroblastoma, together with Prof. Dr. Martin Eilers, we looked at the combination of ATR inhibitors to Aurora A kinase inhibitors. Previously, they identified Aurora A kinas as an interaction partner of MYCN important for MYCN activity regulation. Inhibition of Aurora A kinase resulted in increased replication stress, which we hypothesized could be further exacerbated by adding ATR inhibitors. Our result show a strong antitumor effect of the combination thanks to the recruitment of immune cells to the tumor site. Together, both studies demonstrate the potential of ATR inhibitors as a novel therapy in pediatric solid tumors.

Zusammenfassung

Pädiatrische solide Tumore stellen aufgrund ihrer einzigartigen genetischen Komposition eine besondere Herausforderung für die Krebstherapie dar. Trotz der Fortschritte in den Therapieansätzen sind die Behandlungsergebnisse bei einigen Formen von Kinderkrebs nach wie vor unzureichend. Hier untersuchen wir die Wirksamkeit von ATR-Inhibitoren bei zwei pädiatrischen soliden Tumoren, dem alveolären Rhabdomyosarkom und dem MYCN-amplifizierten Neuroblastom. ATR-Inhibitoren zeigten bei alveolären Rhabdomyosarkomen eine starke Antitumoraktivität, die sich in einer Anhäufung von DNA-Schäden und genomischer Instabilität äußert, welche zum Zelltod führen. Mithilfe der Phosphoproteomik haben wir BRCA1 und damit die homologe Rekombination als durch ATR-Inhibition beeinträchtigt identifiziert. Dadurch stellen wir die Hypothese auf, dass Defekte in der DNA-Reparatur für die Empfindlichkeit gegenüber ATR-Inhibitoren verantwortlich sind. Wir haben außerdem PAX3-FOXO1, ein für alveoläre Rhabdomyosarkome charakteristisches Fusionsonkoprotein, als einen Faktor identifiziert, der den Replikationsstress erhöht und alveoläre Rhabdomyosarkome für eine ATR-Inhibition sensibilisiert. Da Therapieresistenz häufig die Ursache für ein Versagen der Behandlung ist, untersuchten wir mögliche Resistenzmechanismen gegen ATR-Inhibitoren und identifizierten die Gene der FOS-Familie als Kandidaten für die ATR-Inhibitorresistenz bei alveolären Rhabdomyosarkomen. Schließlich untersuchten wir die Wirksamkeit von ATR-Inhibitoren in von Patienten abgeleiteten Xenotransplantationsmodellen des alveolären Rhabdomyosarkoms als Monotherapie und in Kombination mit dem PARP1-Inhibitor Olaparib. ATR-Inhibitoren als Monotherapie reichen aus, um bei alveolärem Rhabdomyosarkom eine stabile Erkrankung zu erreichen und rufe dabei nur minimale Nebenwirkungen hervor. Die Kombination mit Olaparib führt zu einer vollständigen Remission der Tumore. Beim MYCN-amplifizierten Neuroblastom haben wir zusammen mit Prof. Dr. Martin Eilers die Kombination von ATR-Inhibitoren mit Aurora-A-Kinase-Inhibitoren untersucht. Zuvor hatte seine Arbeitsgruppe Aurora-A-Kinasen als Interaktionspartner und Regulatoren von MYCN identifiziert. Die Hemmung der Aurora-A-Kinase führte zu einem erhöhten Replikationsstress, der, so unsere Hypothese, durch die Zugabe von ATR-Inhibitoren noch verstärkt wird. Unsere Ergebnisse zeigen eine starke antitumorale Wirkung der Kombinationstherapie auf Grund der Infiltration von Immunzellen in den Tumor. Beide Studien zusammengenommen zeigen das Potenzial von ATR-Inhibitoren als neuartige Therapie bei pädiatrischen soliden Tumoren.

1. Introduction

1.1. Pediatric solid tumors

Cancer is a disease predominantly associated with age, but can also happen during the first two decades of life, coinciding with the active growth and development phase. Around 40% of early life cancers are leukemias and lymphomas, with the rest being pediatric solid tumors(1). Of those, the most common are tumors affecting the central nervous system (CNS), neuroblastoma (NB) and soft tissue sarcomas, including rhabdomyosarcoma (RMS), Ewing sarcoma (EWS) and osteosarcoma(2). In this work, I focus on two pediatric solid tumor types, RMS and NB, as both provide unique clinical and research challenges.

1.1.1. Rhabdomyosarcoma

Rhabdomyosarcoma (RMS) is a cancer of the muscle that is presumed to arise from muscle progenitor cells(3, 4). It has an incidence of 4.5 new cases per 1,000,000 children per year, being the most common soft tissue sarcoma in childhood and the third most common pediatric solid tumor(5). There are two major subtypes of the disease, embryonal and alveolar RMS. Embryonal rhabdomyosarcomas (ERMS) represent 75% of the RMS cases, with a better overall survival (70-90%)(6, 7). Alveolar rhabdomyosarcomas (ARMS) are less common, about 20% of all cases, but have much worse prognosis, with a five-year survival of 30%(6, 7).

Molecularly, ERMS and ARMS are driven by different oncogenes and biological pathways. Most ERMS present mutations in the RAS and PI3K pathways, with up to 30% of ERMS having an NRAS mutation(8). ARMS on the other hand present a balanced chromosome translocation between chromosomes 2 and 13, which creates a fusion oncoprotein involving the PAX3 and FOXO1 genes(9-11). Other translocations that appear in ARMS are PAX7-FOXO1 and PAX3-NCOA1, but the specific differences between them are uncharacterized(10). Besides the fusion translocation, ARMS present amplifications of *MYCN* and *CDK4*(8). About 20% of ARMS do not present the fusion oncoprotein. These tumors resemble ERMS at the molecular level, suggesting that classification of RMS based on their genotype is more precise than the traditional histological approach(12).

RMS are treated according to their risk assessment. Low-risk RMS are treated with a combination of vincristine, actinomycin D and cyclophosphamide (VAC, in the USA) or ifosfamide (IVA, in Europe), whereas high-risk RMS have additionally cixutumumab or temozolomide(13). Despite advances in cancer therapeutics, RMS treatment has remained unchanged over the last four decades. New approaches for treatment of RMS are being developed(14), with the most promising ones being BRD4 and CHD4 inhibitors(15, 16), which disrupt transcription of PAX3-FOXO1 targets. A phase I clinical trial for histone deacetylase (HDAC) inhibitors in pediatric solid tumors recently showed good tolerability, but the effectiveness in RMS treatment remains uncertain(17). Similarly, inhibitors against receptor tyrosine kinases (RTK), RAS and PI3K pathways, which are frequently mutated in RMS, are under study, but show limited efficacy, due to the high redundancy and cross-talk among these factors(18-20). Immunotherapy approaches have also shown limited efficacy in RMS, partly due to the lack of neoantigens and accessibility of immune cells(21, 22). Taken together, novel approaches are urgently needed, particularly for ARMS, which have dismal survival with current chemotherapy treatments.

1.1.2. Neuroblastoma

Neuroblastoma (NB) is an embryonal tumor that typically develops in the adrenal medulla or paraspinal ganglia. The cell of origin is a precursor cell derived from neural-crest tissue(23). It has an incidence of 10.2 cases per million children, being the most common solid tumor in childhood. According to the Surveillance, Epidemiology and End Results database (SEER), the survival rate for NB has increased to 80%, mainly due to the improved treatment of the more benign forms of NB. High-risk NB, however, have a survival rate of 50%(24, 25).

Molecularly, NB present few somatic mutations, but frequent copy number alterations(26). Among them, *MYCN* amplifications are the most important prognostic factor for poor outcome(27). MYCN is a neuronal paralog of the c-MYC transcription factor that can bind to multiple promoter and enhancers and promote gene expression(28). *MYCN* amplification can co-occur with *ALK* mutations and amplifications(29). ALK is a receptor tyrosine kinase that can activate the RAS-MAPK and PI3K-AKT pathways(30). Tumors harboring both *MYCN* amplifications and *ALK* alterations are a particularly high-risk subgroup(29, 31). Additionally, telomere maintenance mechanisms are activated in NB. In

high-risk, *MYCN*-non amplified NB, alternative lengthening of telomeres (ALT) is present, usually due to mutations in the epigenetic regulator ATRX(32-34). Alternatively, telomerase upregulation is achieved by chromosomal rearrangements that drive TERT overexpression(35, 36).

NB treatment varies according to the risk group. Some NB spontaneously regress(37), particularly in patients under one year of age, and therefore only monitoring is required. For intermediate and high-risk NB, a combination of surgery and chemotherapy is required, followed by myeloablative chemotherapy and autologous stem cell transplantation(38). Nonetheless, relapses remain frequent, urging for novel, targeted therapies. Antibodies against the glucoside GD2, frequently expressed in NB, have shown efficacy against high-risk NB(39). Similarly, a CAR-T cells against GD2 are currently under investigation(40). ALK inhibitors are currently being studied in NB with *ALK* aberrations(41, 42), and are expected to be included in the current therapy regimes. Targeting MYCN is an attractive albeit challenging approach. Aurora A is an interaction partner of MYCN that stabilizes it, while also controlling MYCN-dependent expression during S-phase(43). Aurora A kinase inhibitors have been shown to promote MYCN destabilization and degradation(44, 45) and are currently in a phase II clinical trial in combination with chemotherapy(46). Future research could help improve current and developing treatments to increase the survival rate of neuroblastoma.

1.2. DNA damage and cancer

Genome stability is critical to support survival and reproduction. However, DNA is subjected to mutations, either caused by external agents (UV light, radiation) or as a product of their own metabolism (reactive oxygen species, errors introduced during DNA replication). DNA damage can severely affect the normal activity of biological processes, either by creating structures that interrupt or block DNA replication and transcription, or by introducing mutations in the DNA sequence that affect the protein function. As such, cells are equipped with sophisticated regulatory pathways, the DNA damage response (DDR) to ensure that upon detection of the DNA damage, the cell cycle is stopped until the DNA is repaired, and if the damage is too severe to be fixed, the cell is removed from the tissue through cell death.

1.2.1. The DNA damage repair pathways

There are multiple DNA repair pathways that will respond to specific types of DNA damage and are active at different phases of cell cycle. When the damage affects the DNA base, but not the strand, three main DNA repair pathways can be activated, depending of the type of damage. Base excision repair (BER) responds to modifications of a single nucleotide base, such as oxidation or alkylation, by removing the base and introducing the new one using the complementary strand as a template. Nucleotide excision repair (NER) responds to more bulky lesions such as pyrimidine dimers formed by UV light. The affected nucleotides and their surrounding will be removed to allow the synthesis of a repaired strand using the complementary strand as a template. Mismatch repair (MMR) responds to post-replicative mismatch bases that can occur when the wrong nucleotide is introduced or after polymerase slippage. The damaged strand will be open, cut, and the new strand will be synthesized using the complementary strand as a template.

DNA damage affecting the complete strand are more severe, as the DNA sequence is interrupted. It can affect only one strand (single strand break, SSB) or both (double strand break, DSB) and can be repaired through two pathways: non-homologous end joining (NHEJ) and homologous recombination (HR). NHEJ is active thorough the cell cycle, but HR is preferred after DNA replication, when a sister chromatid is available as a template for repair(47, 48).

There are three kinases that orchestrate the response to SSB and DSB: DNA protein kinase (DNA-PK), Ataxia-telangiectasia mutated (ATM) and ATM- and Rad3-related (ATR). The three of them share a similar structure and preferentially phosphorylate serine and threonine amino acids followed by glutamine (S/T-Q)(49-51). This means that many of their substrates can be phosphorylated by all three kinases, and therefore there is an overlap between their function. Nonetheless, each kinase responds to a specific stimulus and have unique targets, thus increasing the specificity and complexity of the DDR. DNA-PK responds predominantly to DSBs and promotes NHEJ(52). ATM also responds predominantly to DSBs(53, 54), but it is capable of recruiting factors for NHEJ(55, 56) and HR(57-60). ATR on the other hand responds primarily to SSBs, which can occur after replication stress(61) and are also an intermediate step in DSB repair(62). Unlike DNA-PK and ATM, ATR is an essential protein(63-65). Mice without ATR fail to develop, indicating that ATR has a fundamental role in some of those processes. Furthermore, mice

with reduced levels of ATR are also more resistant to tumor development, indicating that ATR can protect cells from mutagenesis(66, 67).

Because of its critical role in genome stability maintenance, mutations in genes of the DDR are common in cancer, as it allows for the accumulation of mutations that promote cancer development. At the same time, cancer cells rely on the DDR to sustain the increased DNA damage induced by their metabolism, particularly replication stress, thus making the DDR promising targets for anticancer drug development.

1.2.2. DNA Damage response as a therapeutic option for cancer

Despite the differences among cancer types, there are some characteristics that are common to all cancers. These characteristics, termed hallmark of cancer by Douglas Hanahan, were first described in the year 2000 and revisited in 2011 and 2022 to incorporate the growing knowledge of cancer biology(68-70). One of those hallmarks is genomic instability, as a higher mutation rate favors the acquisition of pathogenic mutations that promote proliferation and survival of tumor cells. Genomic instability is frequently acquired by impairing the activity of the DDR and avoiding the safeguards in place when a lesion occurs. Loss of function of many genes important for DDR are associated with cancer and syndromes with increased cancer susceptibility, such as loss of TP53(71, 72) (associated with Li Fraumeni syndrome and mutated in almost 50% of tumors), BRCA1(73) (associated with hereditary breast and ovarian cancer), and ATM (associated with breast cancer and ataxia-telangiectasia syndrome)(74, 75). Additionally, some oncogenes can induce DNA damage as a consequence of their activity. Overexpression of cyclines, important for cell division and proliferation, induces dormant origin firing(76-78). Some transcription factors, such as MYCN or EWS-FLI1, also induce replication stress by disrupting the transcription and replication machinery(79, 80). Oncogene-induced replication stress has recently been proposed as a cancer-specific vulnerability with therapeutic potential. These types of stressors typically generate DNA damage repaired by ATR, making ATR-dependent DNA repair the most therapeutically interesting pathway for cancer treatment.

There are many ATR inhibitors currently in preclinical and clinical trials with a similar molecular structure. The most advanced in clinical trials are AZD6738 (ceralasertib), cur-

rently in clinical trials for both solid tumors and leukemia, in combination with chemotherapy, PARP1 inhibitors or immunotherapy (NCT05450692, NCT04417062, NCT03682289 and others), and BAY 1895344 (elimusertib), for which recently it was reported the first-in-human clinical trial(81) and is currently in phase I/II for other tumors, including pediatric solid tumors (NCT05071209, NCT03188965, NCT04616534 and others).

1.3. Hypothesis

Given the fundamental role of ATR and the effectiveness of ATR inhibition for treating several types of cancer, we wanted to investigate whether pediatric solid tumors could benefit from small molecule inhibitors. Of note, recent publications show that EWS responds well to ATR inhibitors. EWS is, similar to RMS, a soft tissue sarcoma driven by a fusion oncoprotein. These reports show that this fusion oncoprotein induce replication stress. It is tempting to speculate that the same would also be true for ARMS. Additionally, MYCN has been shown to increase replication stress due to its role as a transcription activator. Thus, *MYCN*-amplified NB could also be a candidate for ATR inhibition.

During my PhD, my group and I have been focusing on developing ATR inhibitors as a therapeutic option for pediatric solid tumors, providing a rationale for their use and looking for biomarkers that predict response to ATR inhibition. We focused mainly on two tumor entities, NB, through a collaboration with Prof. Dr. Martin Eilers in the university of Würzburg, which led to a publication in *Nature Cancer*(82), and ARMS, the main focus of my PhD that was published in *Nature Communications*(83). Furthermore, we provide an insight on potential resistance mechanisms to ATR inhibitors that could emerge in ARMS, and start a preclinical trial of elimusertib in mice, which serves as a proof of concept to launch a clinical trial (NCT05071209) in the US with our collaborators in Memorial Sloan Kettering Cancer Center (MSKCC) in New York.

2. Methods

All methods are described in detail in Dorado García *et al.* (83) and Roeschert *et al.* (82).

2.1. Cell culture

Cells were grown in RPMI-1640 or DMEM (Thermo Fisher) supplemented with 10% fetal calf serum (Thermo Fisher) and penicillin/streptomycin (Thermo Fisher). The absence of Mycoplasma sp. was assesed using MycoAlert system (Lonza).

Human primary myoblasts were derived from muscle biopsies from healthy donors. Myoblast isolation was done at the HELIOS Hospital Berlin Buch with approval by the regulatory agencies (Ethics committee of Charité Universitätsmedizin Berlin, in compliance with the Declaration of Helsinki, approval number EA2/175/17) and consent from the patients. Cells were grown in Skeletal Muscle Growth Medium (Provitro) without antibiotics.

2.2. Lentiviral transduction

To produce virus, HEK293T cells were transfected using TransIT-LT1 (Mirus), following the manufacturer's protocol, with pMD2.G, psPAX and the lentiviral plasmid of interestat a 1:1:2 ratio. Viral supernatant was collected, pooled and filtered 2 to 3 days after transfection. To transduce mammalian cells with the lentivirus, a mixture of lentivirus with 8 µg/mL polybrene (Sigma Aldrich) was added for 24 hours. Selection was carried out with the corresponding antibiotic.

2.3. CRISPRa screening and sequencing

Cells were sequencially transduced with the lentiMPH v2 plasmid (Addgene #89308) and an sgRNA library targeting the promoter of 20,000 genes at a multiplicity of infection (MOI) of <0.3. Cells were divided into a group incubated with AZD6738 at 750 nM and a mock-

treated control group. The sgRNA sequences were isolated and amplified from the genomic DNA and prepared for sequencing. Sequencing was performed on a NextSeq500 with Mid Output. Samples were demultiplexed and analyzed using MAGeCK.

2.4. Cell viability

Cell viability was assessed using CellTiter-Glo (Promega). 1000 cells were seeded in white 96-well plates one day before adding the drugs. After 72h of drug treatment, luminescence was measured after incubation with CellTiter-Glo, following the manufacturers' protocol. To evaluate synergistic relationships between drugs, cells were simultaneously treated with a range of drug concentrations, and the synergism score was calculated using the R package SynergyFinder.

2.5. Immunoblotting

Proteins were extracted from frozen cells using Radioimmunoprecipitation assay buffer (RIPA) supplemented with cOmplete Protease inhibitor (Roche) and PhosphStop (Roche). Concentration of protein was measured by bicinchoninic acid assay (BCA, Thermo Fisher). For electrophoresis, 10µg of denaturated protein (diluted in Laemmli buffer and boiled for 5 minutes) were loaded onto 16% or 10% Tris-Glycin gels (Thermo Fisher). Proteins were transferred onto Polyvinylidene fluoride (PVDF) membranes (Roche) for 90 minutes at 90V. The membranes were blocked with 5% dry milk for 1 h, and incubated with primary antibodies overnight at 4 °C, then secondary antibodies conjugated with peroxidase for 1 h at room temperature. Using Enhanced chemiluminescence (ECL) Western Blotting Substrate (Thermo Fisher), chemoluminescent signal was measured in a Fusion FX7 imaging system (Vilber Lourmat).

2.6. Immunofluorescence

Cells were grown on a glass coverlid for 24 h (micronuclei quantification) and treated with 1000 ng/mL doxycycline for another 48 h. Cells were washed with PBS and fixed for

10 min with 4% paraformaldehyde, washed again and permeabilized with PBS containing 0.1% Triton-X100. Cells were blocked with 5% BSA in PBS and incubated overnight at 4 °C with the primary antibody. The next day, cells were carefully washed three times with PBS-T (0.05% Tween-20 in PBS), incubated for 1 h with the secondary antibody in the dark and room temperature, washed three times with PBS-T and mounted with DAPI-containing mounting media. For micronuclei detection, cells were directly mounted on a slide with DAPI-containing mounting media after fixation.

2.7. Fluorescence-activated cell sorting (FACS)

The different flow cytometry-based assays were performed with the kits Click-IT EdU Alexa Fluor 488 Flow Cytometry Assay kit (Thermo Fisher), APO-BrdU TUNEL Assay Kit (Thermo Fisher) and CellEvent Caspase3/7 Green Flow Cytometry kit (Thermo Fisher), according to the manufacturer's descriptions. The measurements were done at BD LSR Fortessa flow cytometer (BD Biosciences, Franklin Lakes, NJ, USA).

2.8. Patient-derived xenograft (PDX) treatment

All experiments were in accordance to the institutional animal protocols and the national laws and regulations and approved by the Charité University Medicine. Fragments from RMS or NB patients were transplanted into NOD.Cg-Prkdcscid Il2rgtm1Sug/JicTac (Taconic, Rensselaer, NY, USA) or NSG-H (NOD.Cg-Prkdcscid Hprtem1Mvw Il2rgtm1Wjl/MvwJ; for the PAX7-FOXO1 ARMS PDXs) mice. Caliper measurements were conducted to follow tumor growth, and the volume was calculated with the formula length x width^2/2. Mice were randomly split into four groups with at least 3 mice to receive AZD6738 (50 mg/kg day, oral), olaparib (50 mg/kg day, oral), MLN8237 (7.5 mg/kg 5 days on/2 days off), a combination of AZD6738 and olaparib, a combination of AZD6738 and MLN8237 or vehicle. For the BAY 1895344 study, mice were administered 40 mg/kg body weight on a 3 days on/ 4 days off regime twice daily (orally). Ifosfamide was administered intravenously at a 50 mg/mL concentration up to 80 mg/kg body weight per day twice weekly. Vincristine was administered daily intravenously at 1 mg/mL up to 1 mg/kg body weight per day. Solutions in which the drugs were dissolved were used as vehicle controls

respectively. Mice were sacrificed by cervical dislocation once the tumor volume exceeded 2000 mm^3 or body weight loss was higher than 10%. For the toxicity study, blood was drawn, and blood count was analyzed by Synlab. Organ tissue was collected, fixed with formalin and embedded into paraffin, sliced, and stained with hematoxylin & eosin following the standard diagnostics protocol. For immunohistochemistry staining of cleaved caspase 3 and Ki67, snap frozen tumor fragments were cut and stained following the standard protocol.

2.9. RNA-seq of ATR inhibitor resistant cells

Cells were cultured with increasing concentrations of ATR inhibitors over the course of four months. Resistant cells were collected and prepared for RNA-seq using TruSeq Standard mRNA library prep, according to the manufacturer's instructions. Samples were sequenced (pair ended 2x75bp reads, using a NextSeq500 mid output). And processed using trimGalore!, STAR and HTSeq, and the hg19 genome as a reference.

3. Results

3.1. Dorado García *et al*. Therapeutic targeting of ATR in alveolar rhabdomyosarcoma

In Dorado Garcia *et al.*(83), we first assessed the effectiveness of the ATR inhibitors AZD6738 and BAY 1895344 in a set of pediatric solid tumor cell lines, including ARMS, ERMS and EWS (as a positive control), compared to five human untransformed myogenic cells (Figure 1a-d). In all cases, tumor cells were more sensitive to ATR inhibitors than untransformed myogenic cells, underscoring the potential of ATR inhibitors as a cancer treatment option. Of note, ARMS were more sensitive to ATR inhibitors than ERMS, and had a similar response as EWS's. Encouraged by this finding, we focused on ARMS, as it represents the most urgent clinical challenge. In response to ATR inhibitors, ARMS cell lines showed increased levels of DNA damage and genomic instability, as shown by TUNEL and micronuclei formation (Figure 1e, 1f). Because ATR is a key regulator of the intra-S and G2/M checkpoints, we looked at the cell cycle distribution of cells in response to ATR inhibitors, and found that most cells were stuck in mitosis, as shown by Histone 3 Serine 10 phosphorylation, a marker specific of mitosis, and consistent with the abrogation of the cell cycle checkpoints controlled by ATR (Figure 1g). Cells also showed higher levels of apoptosis after ATR inhibition (Figure 1h), which we hypothesize is caused by the accumulation of unrepaired DNA damage in mitosis, leading to improper missegregation of chromosomes and micronucleation.

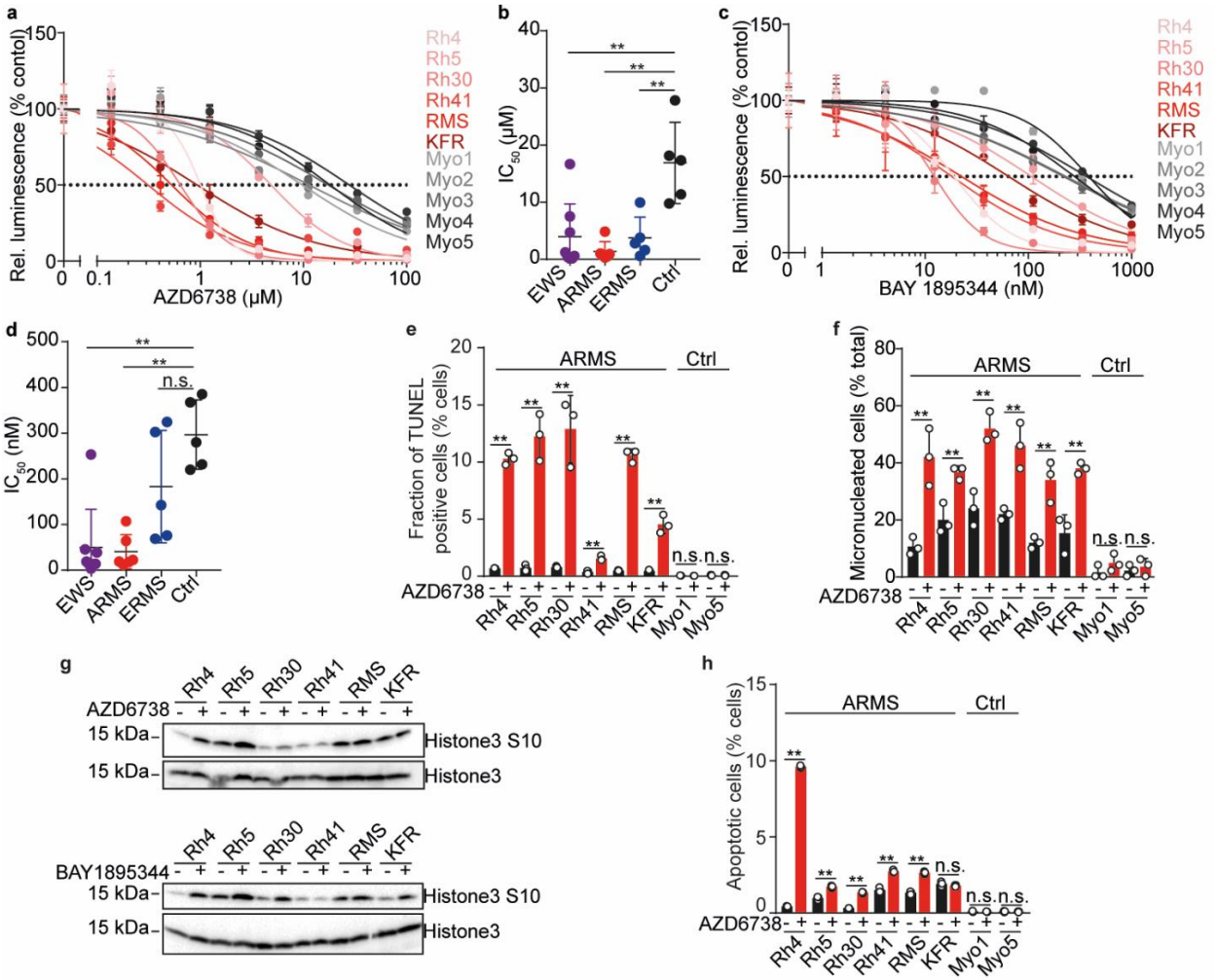

Figure 1. ATR inhibition has antitumor activity in ARMS cell lines. (a) Dose-response curves of cell viability for ARMS cell lines (red) and primary myoblasts (greyscale) in response to the ATR inhibitor AZD6738. (b) Comparison of the IC_{50} concentration for AZD6738 in different pediatric solid tumors, including EWS (purple), ARMS (red), ERMS (blue) and primary myoblasts (black). (c) Dose-response curves of cell viability for ARMS cell lines (red) and primary myoblasts (greyscale) in response to the ATR inhibitor BAY 1895344. (d) Comparison of the IC_{50} concentration for BAY 1895344 in different pediatric solid tumors, including EWS (purple), ARMS (red), ERMS (blue) and primary myoblasts (black). (e) TUNEL signal in cells treated with AZD6738 for 72 hours. (f) Micronucleation in cells treated with AZD6738 for 72 hours. (g) Western immunoblot of histone 3 phosphorylation at serine 10 (S10) in six ARMS cell lines treated with AZD6738 (top) or BAY 1895344 (bottom). (g) Apoptosis signal in cells treated with AZD6738 for 72 hours. Figure modified from Dorado García *et al*.(83).

To confirm the on-target activity of AZD6738 in ARMS, we performed phosphoproteomics in response to short-term treatment with AZD6738 (Figure 2a). We identified that the ATR pathway was the most hypophosphorylated pathway, consistent with on-target inhibition of ATR (Figure 2b). When looking at specific targets, we found BRCA1 and TP53 to be

hypophosphorylated at Serine 1524 and 15, respectively (Figure 2a). Because of its critical role controlling HR, we looked at what effects ATR inhibitors have in HR activity. After treatment, there was a strong reduction in HR activity, which could in part explain the accumulation of DNA damage (Figure 2c). Because of this, we sought to investigate the combination of ATR inhibitors and the PARP1 inhibitor olaparib. To varying degrees, the combination was synergistic (Figure 2d), suggesting the potential of a combination with ATR and PARP1 inhibitors in treating ARMS.

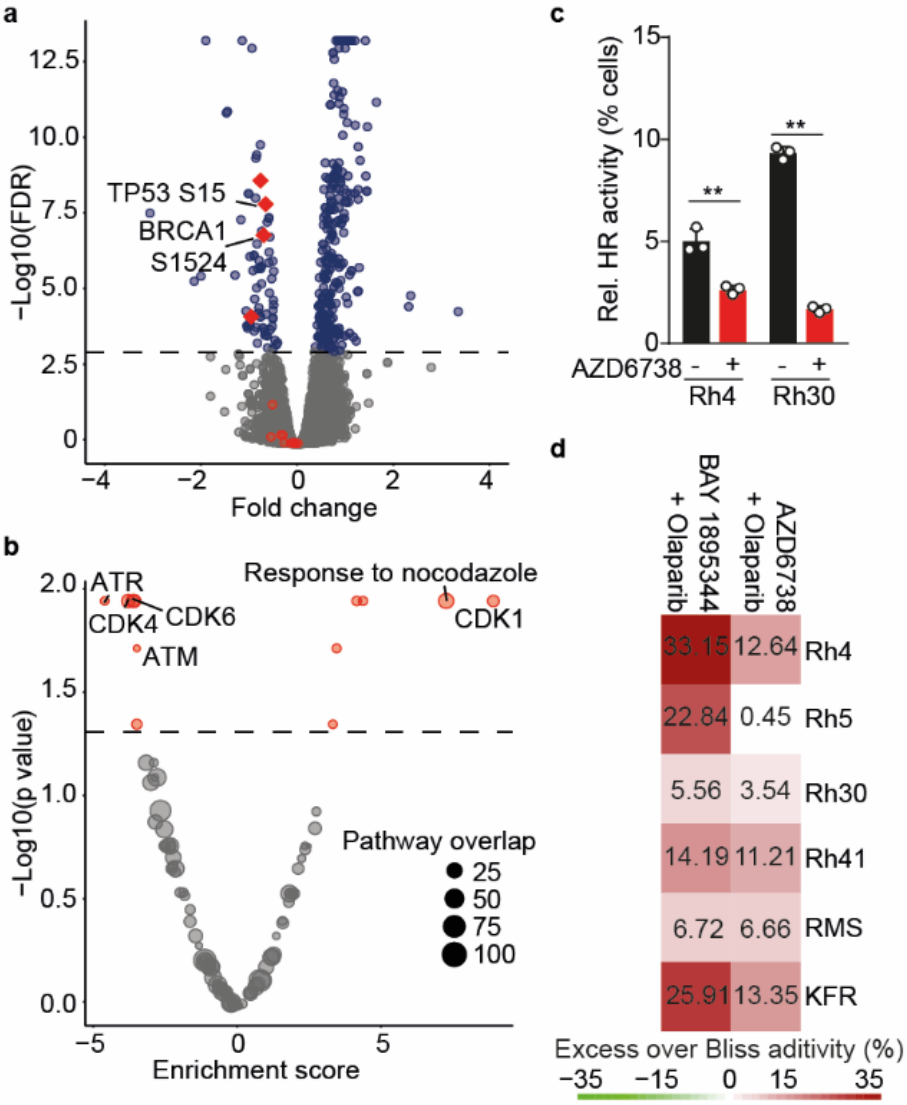

Figure 2. ATR inhibition leads to homologous recombination deficiency in ARMS cells. (a) Volcano plot showing changes in peptide phosphorylation after 2 hours incubation with AZD6738. Known ATR targets marked in red. (b) Pathway enrichment analysis based on phospho-peptide abundance after two hours of treatment with AZD6738. (c) Relative HR activity in two ARMS cell lines with and without AZD6738. (d) Synergistic score of a combination of the ATR inhibitors BAY 1895344 and AZD6738 with the PARP1 inhibitor olaparib. Figure modified from Dorado García *et al.*(83).

We then looked at which factors could render ARMS more sensitive to ATR inhibitors. Only MYCN correlated with ATR inhibitor sensitivity. Because MYCN is a target of PAX3-FOXO1, and previous reports showed that a similar fusion oncoprotein, EWS-FLI1, increased sensitivity to ATR inhibitors in EWS, we looked at whether PAX3-FOXO1 could increase sensitivity to ATR inhibitors. Indeed, PAX3-FOXO1 overexpression in a mouse myoblast cell line, C2C12 (Figure 3a), increased sensitivity to both ATR inhibitors (Figure 3b, 3c), and similarly, PAX3-FOXO1 knockdown in ARMS cell lines reduced it (Figure 3d). We observed that after PAX3-FOXO1 overexpression, cells had high levels of γH2AX, an early marker of DNA damage, indicating that these cells could be more dependent on DNA damage repair. Consistently, RPA32 T21 levels were much higher in PAX3-FOXO1 overexpressing cells after ATR inhibition (Figure 3a). Together, our data suggests that PAX3-FOXO1 increases DNA damage and dependency on DNA repair pathways, therefore making cells more vulnerable to ATR inhibition.

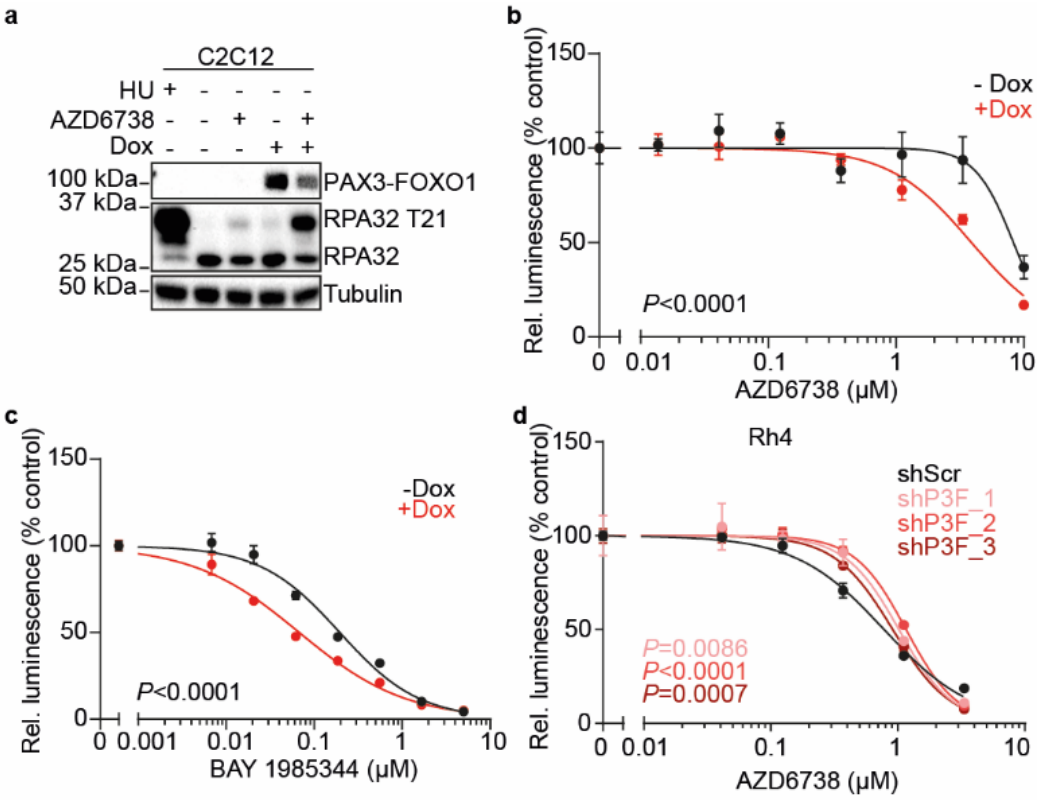

Figure 3. PAX3-FOXO1 is sufficient to increase sensitivity to ATR inhibition. (a) Western immunoblot in C2C12 cells modified to induce PAX3-FOXO1 upon doxycycline treatment, showing levels of PAX3-FOXO1 and RPA32 phosphorylation at T21 after treatment with AZD6738. Hydroxyurea (HU) served as a control of replication stress. (b-c) Cell viability of C2C12 cells expressing PAX3-FOXO1 in response to AZD6738 (b) or BAY 1895344 (c). (d) Dose-response curves in Rh4 cells modified to express shRNA targeting PAX3-FOXO1 (or a mock control) in response to doxycycline, and treated with AZD6738. Figure modified from Dorado García *et al*.(83).

To identify mechanisms of resistance that can emerge after using ATR inhibitors, we used two independent approaches. We used a genome-wide CRISPR-based activation screen, that allows us to identify genes that confer an advantage while cells are exposed to ATR inhibition (Figure 4a). We identified FOSB, FOSL1 and FOSL2 as genes that increase resistance to ATR inhibitors (Figure 4b). These genes belong to the FOS family and are part of the AP-1 transcription factor. We validated that overexpression of FOSB, FOSL1 and FOSL2 led to higher resistance to ATR inhibitors, and that cells with high levels of those genes presented less DNA damage, as shown by RPA32 T21 phosphorylation (Figure 4c). The second approach is long-term exposure of cells to increasing concentrations of ATR inhibitors, in order to isolate colonies that are naturally resistant to the drugs (Figure 4d). Using both AZD6738 and BAY 1895344, we cultured ARMS cells over four months and collected the surviving population for gene expression analysis. We identified the RAS/MAPK pathway to be more active in cells exposed to the drugs after four months (Figure 4e) and validated the results by measuring phosphorylation of key MAPK pathway factors, such as ERK1/2 T202/T204 phosphorylation and c-Raf S338 (Figure 4f). Interestingly, the FOS family genes are also regulated by the RAS/MAPK pathway (Figure 4f). We confirmed that FOSB protein levels were higher in cells exposed to the drug, providing a second line of evidence that AP-1 is important for ATR inhibitor resistance in ARMS.

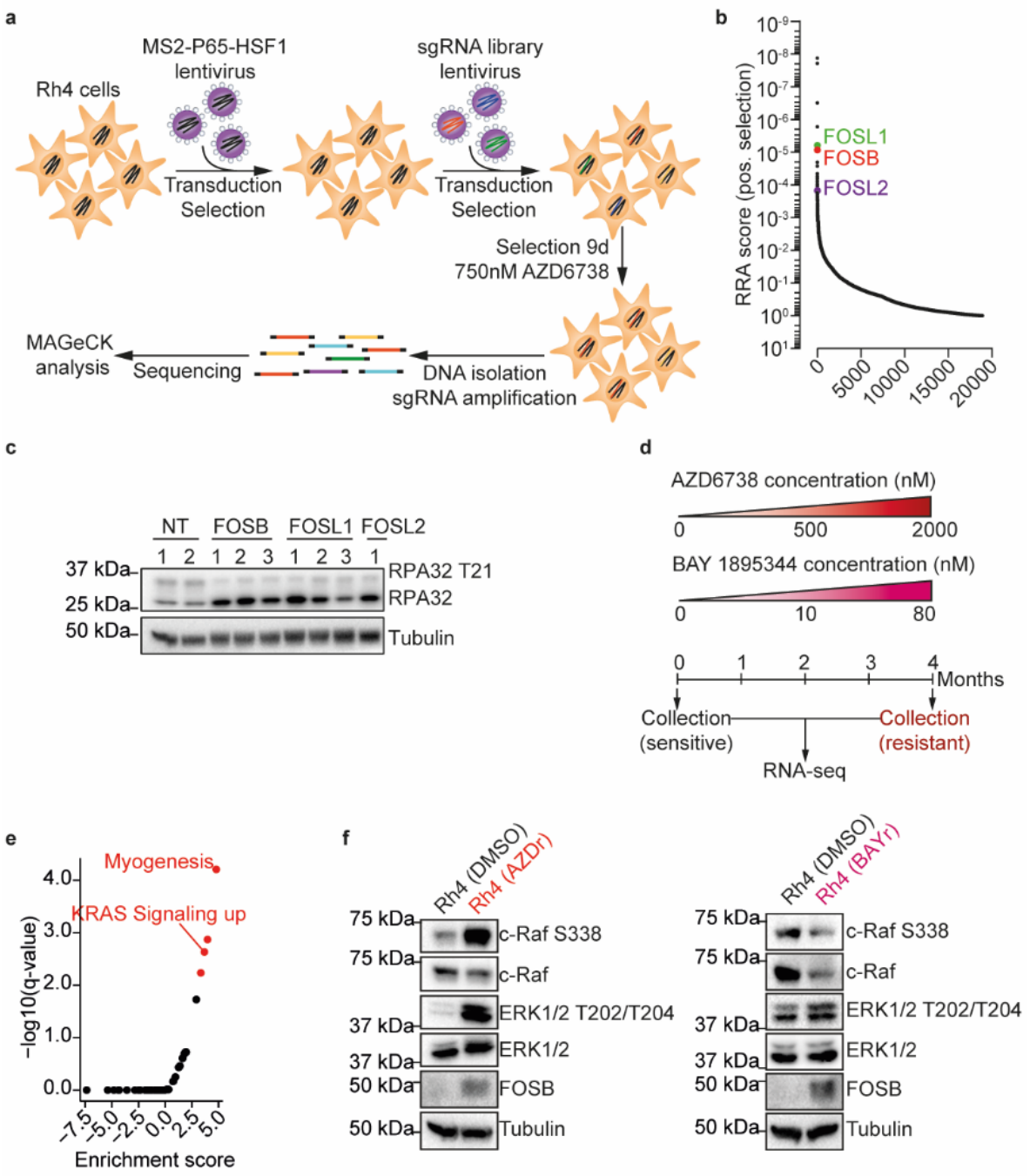

Figure 4. FOS family gene activation is important for ATR inhibitor resistance. (a) Schematic representation of the genome wide CRISPRa screen experimental design. (b) Waterfall plot showing the positive robust rank aggregation (RRA) score of sgRNAs in Rh4 cells incubated in the presence of AZD6738 for 9 days compared to DMSO treated cells as analyzed using MAGeCK. (c) Western immunoblot of RPA32 phosphorylation at T21 in Rh4 cells expressing sgRNAs targeting FOS family members *FOSB*, *FOSL1* or *FOSL2*. (d) Schematic representation of the generation of ATR inhibitor-resistant cells by long-term exposure to increasing doses of the ATR inhibitors AZD6738 and BAY 1895344. (e) (Positive) enrichment score of hallmark pathways in cells resistant to ATR inhibitors. (f) Western immunoblotting of RAS-MAPK pathway members c-Raf and ERK1/2 (and their phosphorylated forms), as well as FOSB, in cells resistant to AZD6738 (left) or BAY 1895344 (right) compared to treatment-naïve cells. Figure modified from Dorado García *et al*.(83).

Encouraged by our findings *in vitro*, we tested the potential of ATR inhibition in a patient-derived xenograft model for ARMS (Figure 5a, 5b). This model was derived from a patient suffering from a third ARMS relapse at the Charité University Medicine. Both AZD6738 and elimusertib greatly inhibited tumor growth, but the combination of AZD6738 with olaparib achieved total regression of the tumor (Figure 5a). We also treated with elimusertib mice harboring a two PDX model from a PAX7-FOXO1 ARMS patient. These PDXs were derived from a primary tumor, and a relapse from the same patient that presented an additional *MYCN* amplification. In both cases, elimusertib reduced tumor growth, but the response was slightly worse in the relapsed tumor (Figure 5c). This data suggests that ATR inhibition, alone and in combination, has strong antitumor activity in ARMS *in vivo*, and could potentially represent a therapeutic option in the treatment of ARMS patients.

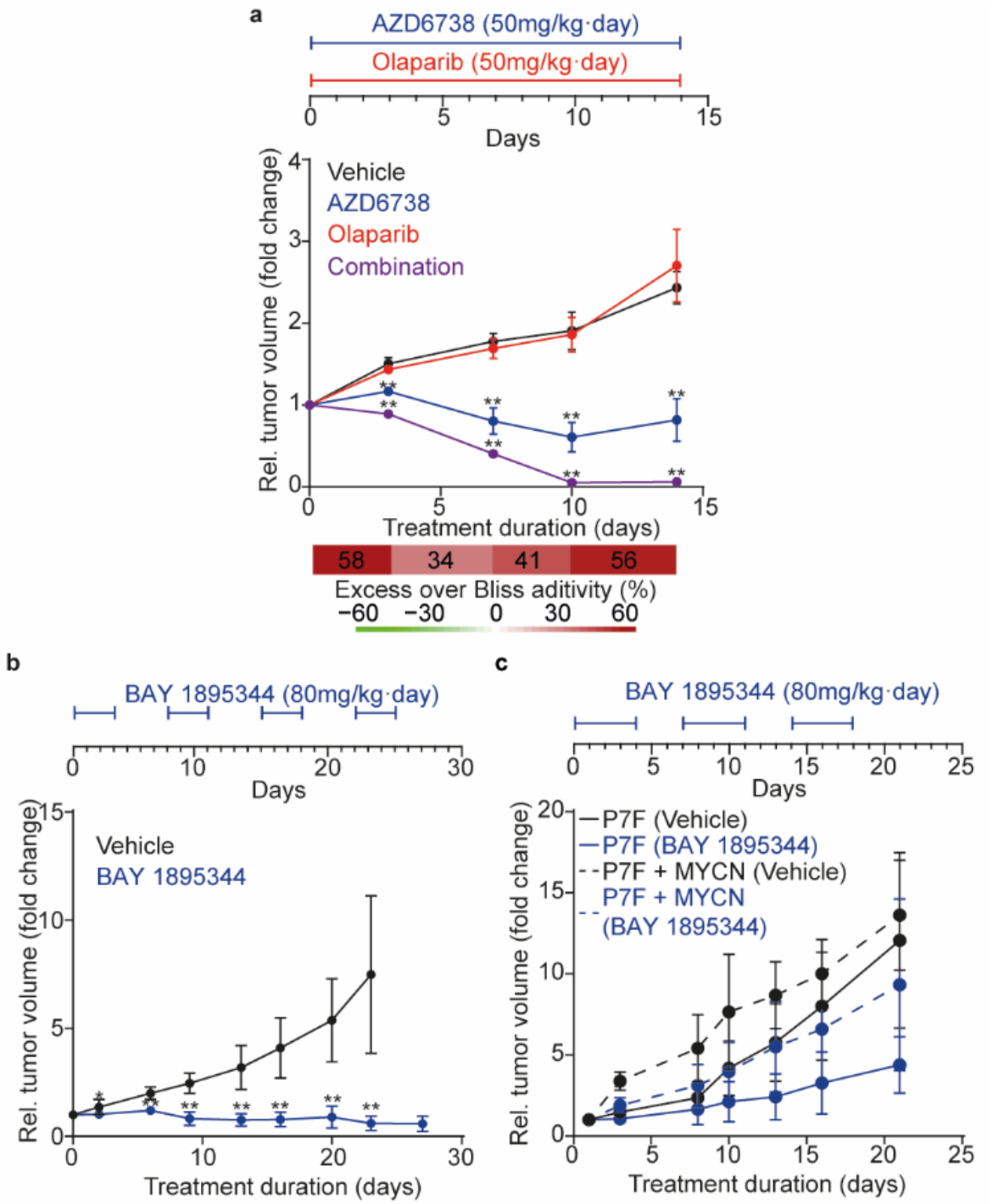

Figure 5. ATR inhibition is an effective antitumor therapy in ARMS PDX models. (a) Tumor volume change of a FP-RMS PDX model subcutaneously xenografted and treated with AZD6738 (oral gavage, 50mg/kg per day), olaparib (oral gavage, 50mg/kg per day) or both compared to vehicle treated mice. (b) Tumor volume change of a FP-RMS PDX model subcutaneously xenografted and treated with BAY 1895344 (twice daily by oral gavage, 40mg/kg per application, 3 days on/4 days off schedule) as compared to vehicle treated mice. (c) Tumor volume change of an ARMS PDX harboring a PAX7-FOXO1 and a relapse from the same patient with an additional *MYCN* amplification, treated with BAY 1895344 (twice daily by oral gavage, 40mg/kg per application, 3 days on/4 days off schedule) as compared to vehicle treated mice. Figure modified from Dorado García *et al*.(83).

3.2. Roeschert *et al*. Combined inhibition of Aurora-A and ATR kinase results in regression of *MYCN*-amplified neuroblastoma.

Together with Prof. Martin Eilers, we evaluated the potential of ATR inhibitors in NB. Prof. Eilers research focus is the understanding of *MYCN* biology in high-risk, *MYCN*-amplified NB. In a previous study, they identified Aurora A kinase as a protein interactor of MYCN that stabilizes it and limit MYCN-dependent transcription during S phase to coordinate it with DNA replication(43). They observed that when treating NB cell lines with the Aurora A kinase inhibitor alisertib (MLN8237), replication stress increases, leading to activation of ATR-mediated DNA repair (Figure 6a). Using our experience with ATR inhibitors, we tested AZD6738 in combination with alisertib in a cohort of NB PDXs, including four *MYCN*-amplified NB (Figure 6b). The combination of alisertib with AZD6738 reduced tumor growth better than the single agents in three out of the four tumor models, with two models achieving partial regression (Figure 6a). However, the response was weakened by the fact that the mice lacked an active immune system, pointing at the importance of the immune response engagement to further increase the antitumor potential of the drugs (Figure 6c). Taken together, this data suggests that combining ATR and Aurora A Kinase inhibitors have strong antitumor effect in *MYCN*-amplified NB, but require the host immune system for tumor elimination.

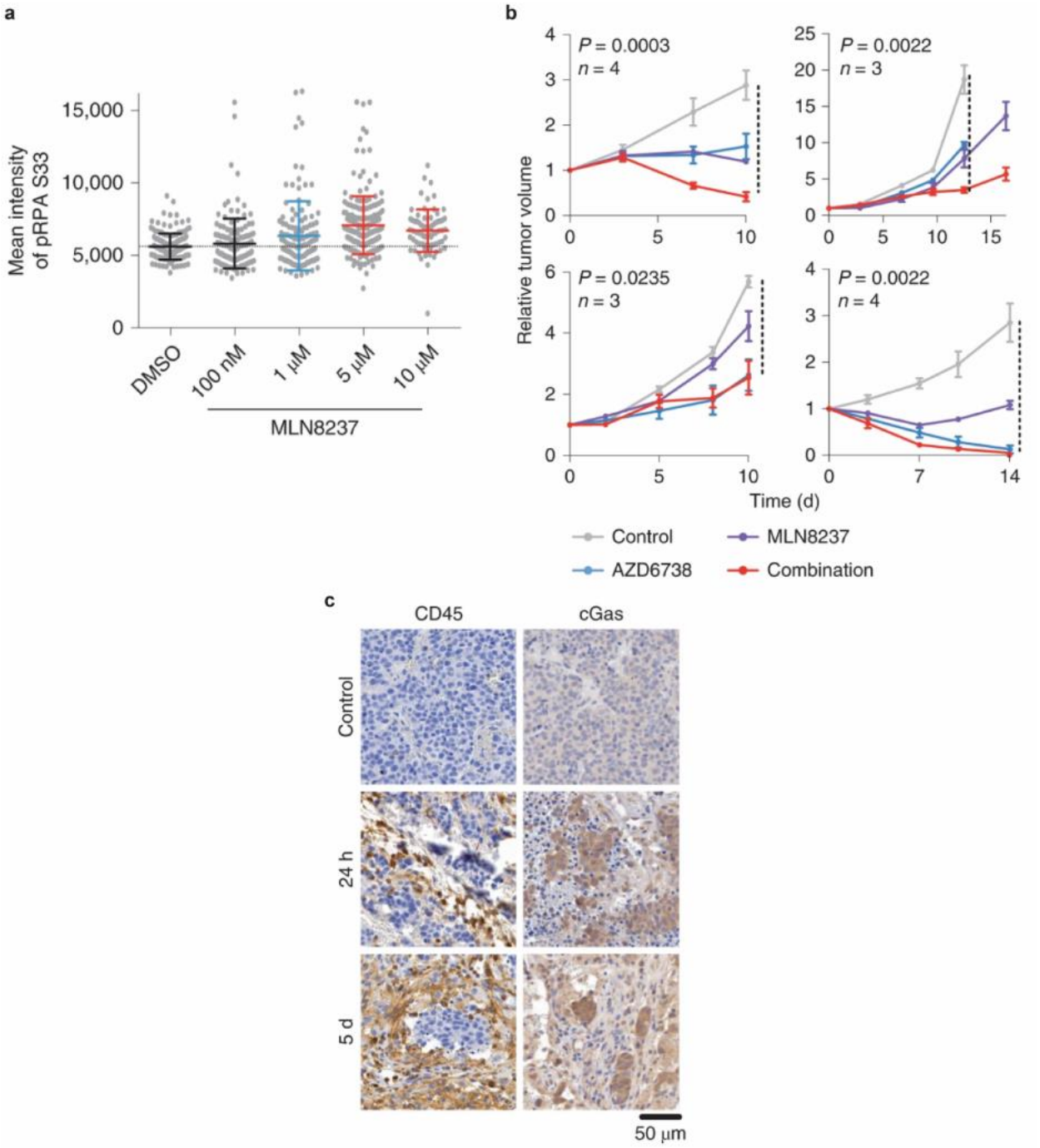

Figure 6. Aurora A and ATR inhibitors have strong antitumor activity in *MYCN*-amplified NB PDX. (a) RPA32 S33 phosphorylation staining in IMR-5 cells treated for 8 h with the indicated concentrations of Aurora-A inhibitor MLN8237. (b) Relative changes in tumor volume of four *MYCN*-amplified PDX models during treatment with MLN8237, AZD6738 or a combination of both. (c) Histology of representative tumor sections showing CD45- and cGAS-positive cells in tumors of TH-MYCN mice treated with combined Aurora-A/ATR kinase inhibition. Figure modified from Roeschert *et al*.(82)

4. Discussion

4.1. Short summary of results

Here we show that ATR inhibitors have therapeutic potential for treating ARMS. Our cohort of eleven RMS cell lines, six of them ARMS, responded better to ATR inhibitors than five human myogenic cells used as control. In response to two ATR inhibitors, we observe that ARMS cell lines accumulate DNA damage and enter apoptosis. Furthermore, we observe a reduced G2/M checkpoint activity, as observed by an increase in mitotic cells despite persistent DNA damage. These findings are consistent with ATR being the key regulator of the G2/M checkpoint, as well as on-target activity of both small molecule inhibitors. To our knowledge, this is the first study that compares the response of ARMS to ATR inhibitors. Our data suggests that ATR inhibitors have a strong antitumor activity against ARMS. Upon inhibition of ATR, cells accumulate DNA damage, but the lack of activation of the ATR-controlled cell cycle checkpoints allows the entry in mitosis, triggering apoptosis due to the high levels of genomic instability. These findings are in line with previous reports of ATR inhibitors in multiple tumors, including leukemia, ATM- and TP53-deficient tumors (67, 84-92).

Mechanistically, ATR inhibition leads to hypophosphorylation of multiple proteins important for DNA repair and checkpoint activation. We here focus on BRCA1 because of its key role in HR. *BRCA1* is frequently mutated in breast and ovarian cancer(73), and its role as a tumor suppressor is widely characterized. Phosphorylation of BRCA1, specifically at its C-terminal region, is important for HR regulation(93). Interestingly, we identified S1524 to be hypophosphorylated after ATR inhibition. While there is no direct evidence of the role of S1524, it is located in the same region as other sites described to be required for HR(93) and it is a known target of another DNA damage repair protein, ATM(94). We believe that other sites not identified in our phosphoproteomics experiment might be affected by the inhibition of ATR. Consistently, we observed a reduction in HR activity, in line with other reports(93). Because BRCA1- and HR-deficient tumors are sensitive to PARP1 inhibitors, we hypothesized that adding olaparib to ATR inhibitors could result in stronger antitumor activity. Our results suggest that the combination is synergistic in ARMS, although at different levels. The synergistic potential of the combination can be affected by multiple factors, including how well the inhibitors work as a monotherapy.

Nonetheless, our data suggests that the combination is an interesting therapeutic option of ARMS treatment.

We are able to show that PAX3-FOXO1 is sufficient to increase sensitivity to ATR inhibition by increasing the basal levels of replication stress. Likewise, PAX3-FOXO1 knockdown reduced sensitivity of ARMS cells to ATR inhibition. The results are in line with our hypothesis based on the previous knowledge that the transcription factor activity of another fusion oncoprotein, EWS-FLI1, confers sensitivity to ATR inhibitors in EWS. After PAX3-FOXO1 overexpression, we observed an increase in γH2AX phosphorylation, a marker of DNA damage, as well as a mild increase in RPA32 T21 phosphorylation. More significantly, HR activity was higher, suggesting higher levels of DNA damage and higher dependency on HR repair. After ATR inhibition, we observe a strong reduction and high levels of RPA32 T21 in PAX3-FOXO1 overexpressing cells, consistent with increased DNA damage. These results are in line with previous reports identifying factors that lead to vulnerability to ATR inhibitors, such as PGBD5, ATM and TP53(84, 86, 95).

We also investigated potential resistance mechanisms that could emerge during treatment with ATR inhibitors. We identify AP-1, and specifically FOSB, as a mediator of ATR inhibitor resistance, but the specific mechanism of action remains unclear. Studies in melanoma have shown that overactivation of AP-1 mediates multidrug resistance(96-99), including resistance to BRAF inhibitors(100, 101), part of the RAS/MAPK pathway. Future research in the topic could help understand how AP-1, and FOSB in particular, are connected with drug resistance and to identify new treatments that overcome it. A study in osteosarcoma demonstrated that *FOS* activates CHK1 and protect cells from replication stress(97). It is tempting to speculate that by activating AP-1 cells are able to partially overcome ATR activation by directly activating CHK1. Simultaneously, a combination treatment of ATR and CHK1 inhibitors could potentially overcome this resistance mechanism.

Finally, we explored the potential of ATR inhibitors *in vivo* as a monotherapy or in combination with olaparib and alisertib. ATR inhibitors are synergistic with olaparib in all cell lines tested, consistent with the observed reduction of HR activity and BRCA1 phosphorylation and previous literature(86, 102-104). As a monotherapy, both celarasertib and elimusertib show strong antitumor activity in a PAX3-FOXO1 and a PAX7-FOXO1 ARMS PDX models, but the response was even stronger when combined with Olaparib. In combination with Prof. Dr. Martin Eilers, we also analyzed the combination of AZD6738 and

alisertib in NB, based on their observations that Aurora A kinase inhibition leads to increased genomic instability in *MYCN*-amplified NB. We observed a synergistic activity of AZD6738 and alisertib in *MYCN*-amplified NB cell lines and PDX models, suggesting a potential therapeutic option for *MYCN*-amplified NB. Our data opens the possibility to introduce ATR inhibitors in the clinic for treating ARMS, with strong response and limited toxicity, as well as *MYCN*-amplified NB in combination with Aurora A kinase inhibitors.

4.2. Strengths and weaknesses of the studies

This study is a step forward toward new, targeted therapies against pediatric solid tumors. One of the advantages of using ATR inhibitors to treat cancer is that it relies on an intrinsic characteristic of cancer, genomic instability, instead of a specific mutation or factor that is present in a subset of tumors. This broad vulnerability allows us to expand our research to molecularly and histologically different tumors, such as *MYCN*-amplified NB and ARMS. This is particularly important for pediatric oncology, as they are rare and thus samples available for research are few and scarce, making it difficult to identify specific vulnerabilities for each tumor type.

Simultaneously, one of the limitations of the study is the scarcity of models available for research, particularly for PDXs. As such, one of the next steps the lab is currently working on is a preclinical study of elimusertib in multiple pediatric solid tumor PDXs, including ARMS and *MYCN*-amplified NB. This future study will enable us to better characterize the response to ATR inhibitors, identify biomarkers and explore novel vulnerabilities in pediatric solid tumors, as well as getting us closer to a clinical trial that tests the efficacy and safety of ATR inhibitors in patients.

Finally, a novelty of this study is that we not only look at the efficacy of ATR inhibitors in pediatric solid tumors, but also, we attempt to identify resistance mechanisms that might emerge during treatment. Targeted therapy, including ATR inhibitors, often stop being effective after a subpopulation of the tumor acquires new characteristics to survive in the presence of the drug. These could be by physically excluding the drug from the cells, such as overexpression of efflux pumps(105, 106), blocking the induction of apoptosis(107) or more specific resistance mechanisms may emerge specific for the drug or pathway affected, such as mutations in *BRCA2* or deletion of *TP53BP1* in BRCA1-deficient tumors treated with olaparib(108, 109). We here identify overexpression of the AP-

1 transcription factor, and more specifically FOSB, to confer resistance to ATR inhibitors by two independent experiments. How FOSB activity interferes with ATR inhibitors, as well as alternative treatments to offer for patients that develop resistance remains unclear and will be part of a future project specifically addressing these issues.

4.3. Implications for practice and/or future research

Here we are able to provide a rationale for the inclusion of ATR inhibitors in the therapeutic options for ARMS, *MYCN*-amplified NB and potentially other pediatric solid tumors with common characteristics, such as medulloblastoma and EWS. There has not been any new drug approved for the treatment of ARMS and *MYCN*-amplified NB in the last four decades. Furthermore, due to the rarity of pediatric solid tumors, there is no economic incentive to develop novel treatments. Repurposing drugs that are currently available or under investigation in adult cancers for use in pediatric solid tumors is a less expensive approach that would accelerate the introduction of novel, more effective and safer treatments.

One of the current limitations of cancer therapies is the emergence of resistances. Resistance to treatment can either be intrinsic (e.g. cancer stem cells that do not respond to chemotherapy(110-112) or acquired (e.g. Loss of 53BP1 and mutations in *BRCA2* in BRCA1-deficient tumors receiving PARP1 inhibitors(108, 109). Early detection of resistance allows us to change the treatment to a more effective one and avoid unnecessary toxicities and side effects. Here, we attempted to predict resistance mechanisms to ATR inhibitors, in hopes to identify markers to monitor and predict response to ATR inhibitors. While we could not suggest an alternative treatment to overcome, or at least delay, resistance to ATR inhibitor, further research could identify new agents that extend the efficacy of ATR inhibitors.

Our data provides a starting point to introduce ATR inhibitors in the clinic, but more extensive research is needed, particularly in more complex models that better simulate human biology. Our lab is currently working on a preclinical trial for elimusertib using over 30 PDX models from several pediatric solid tumors. This knowledge would further improve our understanding of ATR inhibitors and allow us to better select patients that would benefit from them. Importantly, American and European RMS leading researchers are pushing WEE1 inhibitors, a downstream target of ATR, in combination with vincristine

and irinotecan for RMS clinical trial design(113, 114). My PhD project provides a rationale for inhibiting the ATR/CHK1/WEE1 axis and suggests PAX3-FOXO1 as a biomarker for sensitivity to ATR inhibitors. A clinical trial in the United States is currently recruiting patients for receiving elimusertib in several pediatric solid tumors, including refractory ARMS. This clinical trial is directed by one of our collaborators and was partially inspired by the results of my PhD project. We are currently working towards starting a clinical trial in Europe to treat patients with ATR inhibitors in combination with other small molecule inhibitors, including olaparib. If successful, it could help establish Berlin and Charité as a reference center in Europe for pediatric sarcoma research.

5. Reference list

1. Steliarova-Foucher E, Colombet M, Ries LAG, Moreno F, Dolya A, Bray F, Hesseling P, Shin HY, Stiller CA, contributors I-. International incidence of childhood cancer, 2001-10: a population-based registry study. Lancet Oncol. 2017;18(6):719-31.
2. Siegel RL, Miller KD, Fuchs HE, Jemal A. Cancer Statistics, 2021. CA Cancer J Clin. 2021;71(1):7-33.
3. Rudzinski ER, Anderson JR, Hawkins DS, Skapek SX, Parham DM, Teot LA. The World Health Organization Classification of Skeletal Muscle Tumors in Pediatric Rhabdomyosarcoma: A Report From the Children's Oncology Group. Arch Pathol Lab Med. 2015;139(10):1281-7.
4. Qualman SJ, Coffin CM, Newton WA, Hojo H, Triche TJ, Parham DM, Crist WM. Intergroup Rhabdomyosarcoma Study: update for pathologists. Pediatr Dev Pathol. 1998;1(6):550-61.
5. Ognjanovic S, Linabery AM, Charbonneau B, Ross JA. Trends in childhood rhabdomyosarcoma incidence and survival in the United States, 1975-2005. Cancer. 2009;115(18):4218-26.
6. Perkins SM, Shinohara ET, DeWees T, Frangoul H. Outcome for children with metastatic solid tumors over the last four decades. PLoS One. 2014;9(7):e100396.
7. Crist W, Gehan EA, Ragab AH, Dickman PS, Donaldson SS, Fryer C, Hammond D, Hays DM, Herrmann J, Heyn R, et al. The Third Intergroup Rhabdomyosarcoma Study. J Clin Oncol. 1995;13(3):610-30.
8. Shern JF, Chen L, Chmielecki J, Wei JS, Patidar R, Rosenberg M, Ambrogio L, Auclair D, Wang J, Song YK, Tolman C, Hurd L, Liao H, Zhang S, Bogen D, Brohl AS, Sindiri S, Catchpoole D, Badgett T, Getz G, Mora J, Anderson JR, Skapek SX, Barr FG, Meyerson M, Hawkins DS, Khan J. Comprehensive genomic analysis of rhabdomyosarcoma reveals a landscape of alterations affecting a common genetic axis in fusion-positive and fusion-negative tumors. Cancer Discov. 2014;4(2):216-31.
9. Douglass EC, Valentine M, Etcubanas E, Parham D, Webber BL, Houghton PJ, Houghton JA, Green AA. A specific chromosomal abnormality in rhabdomyosarcoma. Cytogenet Cell Genet. 1987;45(3-4):148-55.
10. Douglass EC, Rowe ST, Valentine M, Parham DM, Berkow R, Bowman WP, Maurer HM. Variant translocations of chromosome 13 in alveolar rhabdomyosarcoma. Genes Chromosomes Cancer. 1991;3(6):480-2.
11. Keller C, Arenkiel BR, Coffin CM, El-Bardeesy N, DePinho RA, Capecchi MR. Alveolar rhabdomyosarcomas in conditional Pax3:Fkhr mice: cooperativity of Ink4a/ARF and Trp53 loss of function. Genes Dev. 2004;18(21):2614-26.
12. Williamson D, Missiaglia E, de Reyniès A, Pierron G, Thuille B, Palenzuela G, Thway K, Orbach D, Laé M, Fréneaux P, Pritchard-Jones K, Oberlin O, Shipley J, Delattre O. Fusion gene-negative alveolar rhabdomyosarcoma is clinically and molecularly indistinguishable from embryonal rhabdomyosarcoma. J Clin Oncol. 2010;28(13):2151-8.
13. Crist WM, Anderson JR, Meza JL, Fryer C, Raney RB, Ruymann FB, Breneman J, Qualman SJ, Wiener E, Wharam M, Lobe T, Webber B, Maurer HM, Donaldson SS. Intergroup rhabdomyosarcoma study-IV: results for patients with nonmetastatic disease. J Clin Oncol. 2001;19(12):3091-102.
14. Chen C, Dorado Garcia H, Scheer M, Henssen AG. Current and Future Treatment Strategies for Rhabdomyosarcoma. Front Oncol. 2019;9:1458.

15. Gryder BE, Yohe ME, Chou HC, Zhang X, Marques J, Wachtel M, Schaefer B, Sen N, Song Y, Gualtieri A, Pomella S, Rota R, Cleveland A, Wen X, Sindiri S, Wei JS, Barr FG, Das S, Andresson T, Guha R, Lal-Nag M, Ferrer M, Shern JF, Zhao K, Thomas CJ, Khan J. PAX3-FOXO1 Establishes Myogenic Super Enhancers and Confers BET Bromodomain Vulnerability. Cancer Discov. 2017;7(8):884-99.
16. Böhm M, Wachtel M, Marques JG, Streiff N, Laubscher D, Nanni P, Mamchaoui K, Santoro R, Schäfer BW. Helicase CHD4 is an epigenetic coregulator of PAX3-FOXO1 in alveolar rhabdomyosarcoma. J Clin Invest. 2016;126(11):4237-49.
17. Bukowinski A, Chang B, Reid JM, Liu X, Minard CG, Trepel JB, Lee MJ, Fox E, Weigel BJ. A phase 1 study of entinostat in children and adolescents with recurrent or refractory solid tumors, including CNS tumors: Trial ADVL1513, Pediatric Early Phase-Clinical Trial Network (PEP-CTN). Pediatr Blood Cancer. 2021;68(4):e28892.
18. Li SQ, Cheuk AT, Shern JF, Song YK, Hurd L, Liao H, Wei JS, Khan J. Targeting wild-type and mutationally activated FGFR4 in rhabdomyosarcoma with the inhibitor ponatinib (AP24534). PLoS One. 2013;8(10):e76551.
19. Pappo AS, Vassal G, Crowley JJ, Bolejack V, Hogendoorn PC, Chugh R, Ladanyi M, Grippo JF, Dall G, Staddon AP, Chawla SP, Maki RG, Araujo DM, Geoerger B, Ganjoo K, Marina N, Blay JY, Schuetze SM, Chow WA, Helman LJ. A phase 2 trial of R1507, a monoclonal antibody to the insulin-like growth factor-1 receptor (IGF-1R), in patients with recurrent or refractory rhabdomyosarcoma, osteosarcoma, synovial sarcoma, and other soft tissue sarcomas: results of a Sarcoma Alliance for Research Through Collaboration study. Cancer. 2014;120(16):2448-56.
20. Yohe ME, Gryder BE, Shern JF, Song YK, Chou HC, Sindiri S, Mendoza A, Patidar R, Zhang X, Guha R, Butcher D, Isanogle KA, Robinson CM, Luo X, Chen JQ, Walton A, Awasthi P, Edmondson EF, Difilippantonio S, Wei JS, Zhao K, Ferrer M, Thomas CJ, Khan J. MEK inhibition induces MYOG and remodels super-enhancers in RAS-driven rhabdomyosarcoma. Sci Transl Med. 2018;10(448).
21. Rodeberg DA, Nuss RA, Heppelmann CJ, Celis E. Lack of effective T-lymphocyte response to the PAX3/FKHR translocation area in alveolar rhabdomyosarcoma. Cancer Immunol Immunother. 2005;54(6):526-34.
22. DeRenzo C, Krenciute G, Gottschalk S. The Landscape of CAR T Cells Beyond Acute Lymphoblastic Leukemia for Pediatric Solid Tumors. Am Soc Clin Oncol Educ Book. 2018;38:830-7.
23. Hoehner JC, Gestblom C, Hedborg F, Sandstedt B, Olsen L, Påhlman S. A developmental model of neuroblastoma: differentiating stroma-poor tumors' progress along an extra-adrenal chromaffin lineage. Lab Invest. 1996;75(5):659-75.
24. Yan P, Qi F, Bian L, Xu Y, Zhou J, Hu J, Ren L, Li M, Tang W. Comparison of Incidence and Outcomes of Neuroblastoma in Children, Adolescents, and Adults in the United States: A Surveillance, Epidemiology, and End Results (SEER) Program Population Study. Med Sci Monit. 2020;26:e927218.
25. Maris JM, Hogarty MD, Bagatell R, Cohn SL. Neuroblastoma. Lancet. 2007;369(9579):2106-20.
26. Pugh TJ, Morozova O, Attiyeh EF, Asgharzadeh S, Wei JS, Auclair D, Carter SL, Cibulskis K, Hanna M, Kiezun A, Kim J, Lawrence MS, Lichenstein L, McKenna A, Pedamallu CS, Ramos AH, Shefler E, Sivachenko A, Sougnez C, Stewart C, Ally A, Birol I, Chiu R, Corbett RD, Hirst M, Jackman SD, Kamoh B, Khodabakshi AH, Krzywinski M, Lo A, Moore RA, Mungall KL, Qian J, Tam A, Thiessen N, Zhao Y, Cole KA, Diamond M, Diskin SJ, Mosse YP, Wood AC, Ji L, Sposto R, Badgett T, London WB, Moyer Y, Gastier-Foster JM, Smith MA, Guidry Auvil JM, Gerhard DS, Hogarty MD, Jones SJ, Lander ES,

Gabriel SB, Getz G, Seeger RC, Khan J, Marra MA, Meyerson M, Maris JM. The genetic landscape of high-risk neuroblastoma. Nat Genet. 2013;45(3):279-84.
27. Brodeur GM, Seeger RC, Schwab M, Varmus HE, Bishop JM. Amplification of N-myc in untreated human neuroblastomas correlates with advanced disease stage. Science. 1984;224(4653):1121-4.
28. Zimmerman MW, Liu Y, He S, Durbin AD, Abraham BJ, Easton J, Shao Y, Xu B, Zhu S, Zhang X, Li Z, Weichert-Leahey N, Young RA, Zhang J, Look AT. Drives a Subset of High-Risk Pediatric Neuroblastomas and Is Activated through Mechanisms Including Enhancer Hijacking and Focal Enhancer Amplification. Cancer Discov. 2018;8(3):320-35.
29. Bellini A, Pötschger U, Bernard V, Lapouble E, Baulande S, Ambros PF, Auger N, Beiske K, Bernkopf M, Betts DR, Bhalshankar J, Bown N, de Preter K, Clément N, Combaret V, Font de Mora J, George SL, Jiménez I, Jeison M, Marques B, Martinsson T, Mazzocco K, Morini M, Mühlethaler-Mottet A, Noguera R, Pierron G, Rossing M, Taschner-Mandl S, Van Roy N, Vicha A, Chesler L, Balwierz W, Castel V, Elliott M, Kogner P, Laureys G, Luksch R, Malis J, Popovic-Beck M, Ash S, Delattre O, Valteau-Couanet D, Tweddle DA, Ladenstein R, Schleiermacher G. Frequency and Prognostic Impact of. J Clin Oncol. 2021;39(30):3377-90.
30. Mossé YP, Laudenslager M, Longo L, Cole KA, Wood A, Attiyeh EF, Laquaglia MJ, Sennett R, Lynch JE, Perri P, Laureys G, Speleman F, Kim C, Hou C, Hakonarson H, Torkamani A, Schork NJ, Brodeur GM, Tonini GP, Rappaport E, Devoto M, Maris JM. Identification of ALK as a major familial neuroblastoma predisposition gene. Nature. 2008;455(7215):930-5.
31. Zhu S, Lee JS, Guo F, Shin J, Perez-Atayde AR, Kutok JL, Rodig SJ, Neuberg DS, Helman D, Feng H, Stewart RA, Wang W, George RE, Kanki JP, Look AT. Activated ALK collaborates with MYCN in neuroblastoma pathogenesis. Cancer Cell. 2012;21(3):362-73.
32. Ackermann S, Cartolano M, Hero B, Welte A, Kahlert Y, Roderwieser A, Bartenhagen C, Walter E, Gecht J, Kerschke L, Volland R, Menon R, Heuckmann JM, Gartlgruber M, Hartlieb S, Henrich KO, Okonechnikov K, Altmüller J, Nürnberg P, Lefever S, de Wilde B, Sand F, Ikram F, Rosswog C, Fischer J, Theissen J, Hertwig F, Singhi AD, Simon T, Vogel W, Perner S, Krug B, Schmidt M, Rahmann S, Achter V, Lang U, Vokuhl C, Ortmann M, Büttner R, Eggert A, Speleman F, O'Sullivan RJ, Thomas RK, Berthold F, Vandesompele J, Schramm A, Westermann F, Schulte JH, Peifer M, Fischer M. A mechanistic classification of clinical phenotypes in neuroblastoma. Science. 2018;362(6419):1165-70.
33. Koneru B, Lopez G, Farooqi A, Conkrite KL, Nguyen TH, Macha SJ, Modi A, Rokita JL, Urias E, Hindle A, Davidson H, Mccoy K, Nance J, Yazdani V, Irwin MS, Yang S, Wheeler DA, Maris JM, Diskin SJ, Reynolds CP. Telomere Maintenance Mechanisms Define Clinical Outcome in High-Risk Neuroblastoma. Cancer Res. 2020;80(12):2663-75.
34. Brady SW, Liu Y, Ma X, Gout AM, Hagiwara K, Zhou X, Wang J, Macias M, Chen X, Easton J, Mulder HL, Rusch M, Wang L, Nakitandwe J, Lei S, Davis EM, Naranjo A, Cheng C, Maris JM, Downing JR, Cheung NV, Hogarty MD, Dyer MA, Zhang J. Pan-neuroblastoma analysis reveals age- and signature-associated driver alterations. Nat Commun. 2020;11(1):5183.
35. Peifer M, Hertwig F, Roels F, Dreidax D, Gartlgruber M, Menon R, Krämer A, Roncaioli JL, Sand F, Heuckmann JM, Ikram F, Schmidt R, Ackermann S, Engesser A, Kahlert Y, Vogel W, Altmüller J, Nürnberg P, Thierry-Mieg J, Thierry-Mieg D, Mariappan A, Heynck S, Mariotti E, Henrich KO, Gloeckner C, Bosco G, Leuschner I, Schweiger MR, Savelyeva L, Watkins SC, Shao C, Bell E, Höfer T, Achter V, Lang U, Theissen J, Volland

R, Saadati M, Eggert A, de Wilde B, Berthold F, Peng Z, Zhao C, Shi L, Ortmann M, Büttner R, Perner S, Hero B, Schramm A, Schulte JH, Herrmann C, O'Sullivan RJ, Westermann F, Thomas RK, Fischer M. Telomerase activation by genomic rearrangements in high-risk neuroblastoma. Nature. 2015;526(7575):700-4.
36. Valentijn LJ, Koster J, Zwijnenburg DA, Hasselt NE, van Sluis P, Volckmann R, van Noesel MM, George RE, Tytgat GA, Molenaar JJ, Versteeg R. TERT rearrangements are frequent in neuroblastoma and identify aggressive tumors. Nat Genet. 2015;47(12):1411-4.
37. Yamamoto K, Hanada R, Kikuchi A, Ichikawa M, Aihara T, Oguma E, Moritani T, Shimanuki Y, Tanimura M, Hayashi Y. Spontaneous regression of localized neuroblastoma detected by mass screening. J Clin Oncol. 1998;16(4):1265-9.
38. Simon T, Hero B, Schulte JH, Deubzer H, Hundsdoerfer P, von Schweinitz D, Fuchs J, Schmidt M, Prasad V, Krug B, Timmermann B, Leuschner I, Fischer M, Langer T, Astrahantseff K, Berthold F, Lode H, Eggert A. 2017 GPOH Guidelines for Diagnosis and Treatment of Patients with Neuroblastic Tumors. Klin Padiatr. 2017;229(3):147-67.
39. Mody R, Naranjo A, Van Ryn C, Yu AL, London WB, Shulkin BL, Parisi MT, Servaes SE, Diccianni MB, Sondel PM, Bender JG, Maris JM, Park JR, Bagatell R. Irinotecan-temozolomide with temsirolimus or dinutuximab in children with refractory or relapsed neuroblastoma (COG ANBL1221): an open-label, randomised, phase 2 trial. Lancet Oncol. 2017;18(7):946-57.
40. Straathof K, Flutter B, Wallace R, Jain N, Loka T, Depani S, Wright G, Thomas S, Cheung GW, Gileadi T, Stafford S, Kokalaki E, Barton J, Marriott C, Rampling D, Ogunbiyi O, Akarca AU, Marafioti T, Inglott S, Gilmour K, Al-Hajj M, Day W, McHugh K, Biassoni L, Sizer N, Barton C, Edwards D, Dragoni I, Silvester J, Dyer K, Traub S, Elson L, Brook S, Westwood N, Robson L, Bedi A, Howe K, Barry A, Duncan C, Barone G, Pule M, Anderson J. Antitumor activity without on-target off-tumor toxicity of GD2-chimeric antigen receptor T cells in patients with neuroblastoma. Sci Transl Med. 2020;12(571).
41. Foster JH, Voss SD, Hall DC, Minard CG, Balis FM, Wilner K, Berg SL, Fox E, Adamson PC, Blaney SM, Weigel BJ, Mossé YP. Activity of Crizotinib in Patients with ALK-Aberrant Relapsed/Refractory Neuroblastoma: A Children's Oncology Group Study (ADVL0912). Clin Cancer Res. 2021;27(13):3543-8.
42. Fischer M, Moreno L, Ziegler DS, Marshall LV, Zwaan CM, Irwin MS, Casanova M, Sabado C, Wulff B, Stegert M, Wang L, Hurtado FK, Branle F, Geoerger B, Schulte JH. Ceritinib in paediatric patients with anaplastic lymphoma kinase-positive malignancies: an open-label, multicentre, phase 1, dose-escalation and dose-expansion study. Lancet Oncol. 2021;22(12):1764-76.
43. Büchel G, Carstensen A, Mak KY, Roeschert I, Leen E, Sumara O, Hofstetter J, Herold S, Kalb J, Baluapuri A, Poon E, Kwok C, Chesler L, Maric HM, Rickman DS, Wolf E, Bayliss R, Walz S, Eilers M. Association with Aurora-A Controls N-MYC-Dependent Promoter Escape and Pause Release of RNA Polymerase II during the Cell Cycle. Cell Rep. 2017;21(12):3483-97.
44. Brockmann M, Poon E, Berry T, Carstensen A, Deubzer HE, Rycak L, Jamin Y, Thway K, Robinson SP, Roels F, Witt O, Fischer M, Chesler L, Eilers M. Small molecule inhibitors of aurora-a induce proteasomal degradation of N-myc in childhood neuroblastoma. Cancer Cell. 2013;24(1):75-89.
45. Gustafson WC, Meyerowitz JG, Nekritz EA, Chen J, Benes C, Charron E, Simonds EF, Seeger R, Matthay KK, Hertz NT, Eilers M, Shokat KM, Weiss WA. Drugging MYCN through an allosteric transition in Aurora kinase A. Cancer Cell. 2014;26(3):414-27.
46. DuBois SG, Mosse YP, Fox E, Kudgus RA, Reid JM, McGovern R, Groshen S, Bagatell R, Maris JM, Twist CJ, Goldsmith K, Granger MM, Weiss B, Park JR, Macy ME,

Cohn SL, Yanik G, Wagner LM, Hawkins R, Courtier J, Lai H, Goodarzian F, Shimada H, Boucher N, Czarnecki S, Luo C, Tsao-Wei D, Matthay KK, Marachelian A. Phase II Trial of Alisertib in Combination with Irinotecan and Temozolomide for Patients with Relapsed or Refractory Neuroblastoma. Clin Cancer Res. 2018;24(24):6142-9.
47. Beucher A, Birraux J, Tchouandong L, Barton O, Shibata A, Conrad S, Goodarzi AA, Krempler A, Jeggo PA, Löbrich M. ATM and Artemis promote homologous recombination of radiation-induced DNA double-strand breaks in G2. EMBO J. 2009;28(21):3413-27.
48. Karanam K, Kafri R, Loewer A, Lahav G. Quantitative live cell imaging reveals a gradual shift between DNA repair mechanisms and a maximal use of HR in mid S phase. Mol Cell. 2012;47(2):320-9.
49. Bannister AJ, Gottlieb TM, Kouzarides T, Jackson SP. c-Jun is phosphorylated by the DNA-dependent protein kinase in vitro; definition of the minimal kinase recognition motif. Nucleic Acids Res. 1993;21(5):1289-95.
50. Chen YR, Lees-Miller SP, Tegtmeyer P, Anderson CW. The human DNA-activated protein kinase phosphorylates simian virus 40 T antigen at amino- and carboxy-terminal sites. J Virol. 1991;65(10):5131-40.
51. Lees-Miller SP, Anderson CW. The human double-stranded DNA-activated protein kinase phosphorylates the 90-kDa heat-shock protein, hsp90 alpha at two NH2-terminal threonine residues. J Biol Chem. 1989;264(29):17275-80.
52. Jette N, Lees-Miller SP. The DNA-dependent protein kinase: A multifunctional protein kinase with roles in DNA double strand break repair and mitosis. Prog Biophys Mol Biol. 2015;117(2-3):194-205.
53. Andegeko Y, Moyal L, Mittelman L, Tsarfaty I, Shiloh Y, Rotman G. Nuclear retention of ATM at sites of DNA double strand breaks. J Biol Chem. 2001;276(41):38224-30.
54. Bekker-Jensen S, Lukas C, Kitagawa R, Melander F, Kastan MB, Bartek J, Lukas J. Spatial organization of the mammalian genome surveillance machinery in response to DNA strand breaks. J Cell Biol. 2006;173(2):195-206.
55. Goodarzi AA, Yu Y, Riballo E, Douglas P, Walker SA, Ye R, Härer C, Marchetti C, Morrice N, Jeggo PA, Lees-Miller SP. DNA-PK autophosphorylation facilitates Artemis endonuclease activity. EMBO J. 2006;25(16):3880-9.
56. Jiang W, Crowe JL, Liu X, Nakajima S, Wang Y, Li C, Lee BJ, Dubois RL, Liu C, Yu X, Lan L, Zha S. Differential phosphorylation of DNA-PKcs regulates the interplay between end-processing and end-ligation during nonhomologous end-joining. Mol Cell. 2015;58(1):172-85.
57. Adams KE, Medhurst AL, Dart DA, Lakin ND. Recruitment of ATR to sites of ionising radiation-induced DNA damage requires ATM and components of the MRN protein complex. Oncogene. 2006;25(28):3894-904.
58. Cuadrado M, Martinez-Pastor B, Murga M, Toledo LI, Gutierrez-Martinez P, Lopez E, Fernandez-Capetillo O. ATM regulates ATR chromatin loading in response to DNA double-strand breaks. J Exp Med. 2006;203(2):297-303.
59. Jazayeri A, Falck J, Lukas C, Bartek J, Smith GC, Lukas J, Jackson SP. ATM- and cell cycle-dependent regulation of ATR in response to DNA double-strand breaks. Nat Cell Biol. 2006;8(1):37-45.
60. Myers JS, Cortez D. Rapid activation of ATR by ionizing radiation requires ATM and Mre11. J Biol Chem. 2006;281(14):9346-50.
61. Byun TS, Pacek M, Yee MC, Walter JC, Cimprich KA. Functional uncoupling of MCM helicase and DNA polymerase activities activates the ATR-dependent checkpoint. Genes Dev. 2005;19(9):1040-52.

62. Raderschall E, Golub EI, Haaf T. Nuclear foci of mammalian recombination proteins are located at single-stranded DNA regions formed after DNA damage. Proc Natl Acad Sci U S A. 1999;96(5):1921-6.
63. Saldivar JC, Cortez D, Cimprich KA. The essential kinase ATR: ensuring faithful duplication of a challenging genome. Nat Rev Mol Cell Biol. 2017;18(10):622-36.
64. Buisson R, Boisvert JL, Benes CH, Zou L. Distinct but Concerted Roles of ATR, DNA-PK, and Chk1 in Countering Replication Stress during S Phase. Mol Cell. 2015;59(6):1011-24.
65. Cimprich KA, Cortez D. ATR: an essential regulator of genome integrity. Nat Rev Mol Cell Biol. 2008;9(8):616-27.
66. Murga M, Bunting S, Montaña MF, Soria R, Mulero F, Cañamero M, Lee Y, McKinnon PJ, Nussenzweig A, Fernandez-Capetillo O. A mouse model of ATR-Seckel shows embryonic replicative stress and accelerated aging. Nat Genet. 2009;41(8):891-8.
67. Murga M, Campaner S, Lopez-Contreras AJ, Toledo LI, Soria R, Montaña MF, Artista L, Schleker T, Guerra C, Garcia E, Barbacid M, Hidalgo M, Amati B, Fernandez-Capetillo O. Exploiting oncogene-induced replicative stress for the selective killing of Myc-driven tumors. Nat Struct Mol Biol. 2011;18(12):1331-5.
68. Hanahan D, Weinberg RA. The hallmarks of cancer. Cell. 2000;100(1):57-70.
69. Hanahan D. Hallmarks of Cancer: New Dimensions. Cancer Discov. 2022;12(1):31-46.
70. Hanahan D, Weinberg RA. Hallmarks of cancer: the next generation. Cell. 2011;144(5):646-74.
71. Varley J. TP53, hChk2, and the Li-Fraumeni syndrome. Methods Mol Biol. 2003;222:117-29.
72. Bielas JH, Loeb LA. Mutator phenotype in cancer: timing and perspectives. Environ Mol Mutagen. 2005;45(2-3):206-13.
73. Bertwistle D, Ashworth A. Functions of the BRCA1 and BRCA2 genes. Curr Opin Genet Dev. 1998;8(1):14-20.
74. Renwick A, Thompson D, Seal S, Kelly P, Chagtai T, Ahmed M, North B, Jayatilake H, Barfoot R, Spanova K, McGuffog L, Evans DG, Eccles D, Easton DF, Stratton MR, Rahman N, (UK) BCSC. ATM mutations that cause ataxia-telangiectasia are breast cancer susceptibility alleles. Nat Genet. 2006;38(8):873-5.
75. Lavin MF, Shiloh Y. Ataxia-telangiectasia: a multifaceted genetic disorder associated with defective signal transduction. Curr Opin Immunol. 1996;8(4):459-64.
76. Jones RM, Mortusewicz O, Afzal I, Lorvellec M, García P, Helleday T, Petermann E. Increased replication initiation and conflicts with transcription underlie Cyclin E-induced replication stress. Oncogene. 2013;32(32):3744-53.
77. Bartkova J, Rezaei N, Liontos M, Karakaidos P, Kletsas D, Issaeva N, Vassiliou LV, Kolettas E, Niforou K, Zoumpourlis VC, Takaoka M, Nakagawa H, Tort F, Fugger K, Johansson F, Sehested M, Andersen CL, Dyrskjot L, Ørntoft T, Lukas J, Kittas C, Helleday T, Halazonetis TD, Bartek J, Gorgoulis VG. Oncogene-induced senescence is part of the tumorigenesis barrier imposed by DNA damage checkpoints. Nature. 2006;444(7119):633-7.
78. Bartkova J, Horejsí Z, Koed K, Krämer A, Tort F, Zieger K, Guldberg P, Sehested M, Nesland JM, Lukas C, Ørntoft T, Lukas J, Bartek J. DNA damage response as a candidate anti-cancer barrier in early human tumorigenesis. Nature. 2005;434(7035):864-70.
79. Herold S, Kalb J, Büchel G, Ade CP, Baluapuri A, Xu J, Koster J, Solvie D, Carstensen A, Klotz C, Rodewald S, Schülein-Völk C, Dobbelstein M, Wolf E, Molenaar

J, Versteeg R, Walz S, Eilers M. Recruitment of BRCA1 limits MYCN-driven accumulation of stalled RNA polymerase. Nature. 2019;567(7749):545-9.
80. Gorthi A, Romero JC, Loranc E, Cao L, Lawrence LA, Goodale E, Iniguez AB, Bernard X, Masamsetti VP, Roston S, Lawlor ER, Toretsky JA, Stegmaier K, Lessnick SL, Chen Y, Bishop AJR. EWS-FLI1 increases transcription to cause R-loops and block BRCA1 repair in Ewing sarcoma. Nature. 2018;555(7696):387-91.
81. Yap TA, Tan DSP, Terbuch A, Caldwell R, Guo C, Goh BC, Heong V, Haris NRM, Bashir S, Drew Y, Hong DS, Meric-Bernstam F, Wilkinson G, Hreiki J, Wengner AM, Bladt F, Schlicker A, Ludwig M, Zhou Y, Liu L, Bordia S, Plummer R, Lagkadinou E, de Bono JS. First-in-Human Trial of the Oral Ataxia Telangiectasia and RAD3-Related (ATR) Inhibitor BAY 1895344 in Patients with Advanced Solid Tumors. Cancer Discov. 2021;11(1):80-91.
82. Roeschert I, Poon E, Henssen AG, Garcia HD, Gatti M, Giansanti C, Jamin Y, Ade CP, Gallant P, Schülein-Völk C, Beli P, Richards M, Rosenfeldt M, Altmeyer M, Anderson J, Eggert A, Dobbelstein M, Bayliss R, Chesler L, Büchel G, Eilers M. Combined inhibition of Aurora-A and ATR kinase results in regression of MYCN-amplified neuroblastoma. Nat Cancer. 2021;2(3):312-26.
83. Dorado García H, Pusch F, Bei Y, von Stebut J, Ibáñez G, Guillan K, Imami K, Gürgen D, Rolff J, Helmsauer K, Meyer-Liesener S, Timme N, Bardinet V, Chamorro González R, MacArthur IC, Chen CY, Schulz J, Wengner AM, Furth C, Lala B, Eggert A, Seifert G, Hundsoerfer P, Kirchner M, Mertins P, Selbach M, Lissat A, Dubois F, Horst D, Schulte JH, Spuler S, You D, Dela Cruz F, Kung AL, Haase K, DiVirgilio M, Scheer M, Ortiz MV, Henssen AG. Therapeutic targeting of ATR in alveolar rhabdomyosarcoma. Nat Commun. 2022;13(1):4297.
84. Kwok M, Davies N, Agathanggelou A, Smith E, Oldreive C, Petermann E, Stewart G, Brown J, Lau A, Pratt G, Parry H, Taylor M, Moss P, Hillmen P, Stankovic T. ATR inhibition induces synthetic lethality and overcomes chemoresistance in TP53- or ATM-defective chronic lymphocytic leukemia cells. Blood. 2016;127(5):582-95.
85. Wallez Y, Dunlop CR, Johnson TI, Koh SB, Fornari C, Yates JWT, Bernaldo de Quirós Fernández S, Lau A, Richards FM, Jodrell DI. The ATR Inhibitor AZD6738 Synergizes with Gemcitabine. Mol Cancer Ther. 2018;17(8):1670-82.
86. Lloyd RL, Wijnhoven PWG, Ramos-Montoya A, Wilson Z, Illuzzi G, Falenta K, Jones GN, James N, Chabbert CD, Stott J, Dean E, Lau A, Young LA. Combined PARP and ATR inhibition potentiates genome instability and cell death in ATM-deficient cancer cells. Oncogene. 2020;39(25):4869-83.
87. Gilad O, Nabet BY, Ragland RL, Schoppy DW, Smith KD, Durham AC, Brown EJ. Combining ATR suppression with oncogenic Ras synergistically increases genomic instability, causing synthetic lethality or tumorigenesis in a dosage-dependent manner. Cancer Res. 2010;70(23):9693-702.
88. Foote KM, Lau A, Nissink JW. Drugging ATR: progress in the development of specific inhibitors for the treatment of cancer. Future Med Chem. 2015;7(7):873-91.
89. Karnitz LM, Zou L. Molecular Pathways: Targeting ATR in Cancer Therapy. Clin Cancer Res. 2015;21(21):4780-5.
90. Reaper PM, Griffiths MR, Long JM, Charrier JD, Maccormick S, Charlton PA, Golec JM, Pollard JR. Selective killing of ATM- or p53-deficient cancer cells through inhibition of ATR. Nat Chem Biol. 2011;7(7):428-30.
91. Fokas E, Prevo R, Hammond EM, Brunner TB, McKenna WG, Muschel RJ. Targeting ATR in DNA damage response and cancer therapeutics. Cancer Treat Rev. 2014;40(1):109-17.

92. Morgado-Palacin I, Day A, Murga M, Lafarga V, Anton ME, Tubbs A, Chen HT, Ergan A, Anderson R, Bhandoola A, Pike KG, Barlaam B, Cadogan E, Wang X, Pierce AJ, Hubbard C, Armstrong SA, Nussenzweig A, Fernandez-Capetillo O. Targeting the kinase activities of ATR and ATM exhibits antitumoral activity in mouse models of MLL-rearranged AML. Sci Signal. 2016;9(445):ra91.
93. Beckta JM, Dever SM, Gnawali N, Khalil A, Sule A, Golding SE, Rosenberg E, Narayanan A, Kehn-Hall K, Xu B, Povirk LF, Valerie K. Mutation of the BRCA1 SQ-cluster results in aberrant mitosis, reduced homologous recombination, and a compensatory increase in non-homologous end joining. Oncotarget. 2015;6(29):27674-87.
94. Cortez D, Wang Y, Qin J, Elledge SJ. Requirement of ATM-dependent phosphorylation of brca1 in the DNA damage response to double-strand breaks. Science. 1999;286(5442):1162-6.
95. Henssen AG, Reed C, Jiang E, Garcia HD, von Stebut J, MacArthur IC, Hundsdoerfer P, Kim JH, de Stanchina E, Kuwahara Y, Hosoi H, Ganem NJ, Dela Cruz F, Kung AL, Schulte JH, Petrini JH, Kentsis A. Therapeutic targeting of PGBD5-induced DNA repair dependency in pediatric solid tumors. Sci Transl Med. 2017;9(414).
96. Smith LM, Wise SC, Hendricks DT, Sabichi AL, Bos T, Reddy P, Brown PH, Birrer MJ. cJun overexpression in MCF-7 breast cancer cells produces a tumorigenic, invasive and hormone resistant phenotype. Oncogene. 1999;18(44):6063-70.
97. Schulze J, Lopez-Contreras AJ, Uluçkan Ö, Graña-Castro O, Fernandez-Capetillo O, Wagner EF. Fos-dependent induction of Chk1 protects osteoblasts from replication stress. Cell Cycle. 2014;13(12):1980-6.
98. Daschner PJ, Ciolino HP, Plouzek CA, Yeh GC. Increased AP-1 activity in drug resistant human breast cancer MCF-7 cells. Breast Cancer Res Treat. 1999;53(3):229-40.
99. Pennanen PT, Sarvilinna NS, Toimela T, Ylikomi TJ. Inhibition of FOSL1 overexpression in antiestrogen-resistant MCF-7 cells decreases cell growth and increases vacuolization and cell death. Steroids. 2011;76(10-11):1063-8.
100. Vitorino FNL, Montoni F, Moreno JN, de Souza BF, Lopes MC, Cordeiro B, Fonseca CS, Gilmore JM, Sardiu MI, Reis MS, Florens LA, Washburn MP, Armelin HA, da Cunha JPC. FGF2 Antiproliferative Stimulation Induces Proteomic Dynamic Changes and High Expression of FOSB and JUNB in K-Ras-Driven Mouse Tumor Cells. Proteomics. 2018;18(17):e1800203.
101. Vallejo A, Perurena N, Guruceaga E, Mazur PK, Martinez-Canarias S, Zandueta C, Valencia K, Arricibita A, Gwinn D, Sayles LC, Chuang CH, Guembe L, Bailey P, Chang DK, Biankin A, Ponz-Sarvise M, Andersen JB, Khatri P, Bozec A, Sweet-Cordero EA, Sage J, Lecanda F, Vicent S. An integrative approach unveils FOSL1 as an oncogene vulnerability in KRAS-driven lung and pancreatic cancer. Nat Commun. 2017;8:14294.
102. Wilson Z, Odedra R, Wallez Y, Wijnhoven PWG, Hughes AM, Gerrard J, Jones GN, Bargh-Dawson H, Brown E, Young LA, O'Connor MJ, Lau A. ATR Inhibitor AZD6738 (Ceralasertib) Exerts Antitumor Activity as a Monotherapy and in Combination with Chemotherapy and the PARP Inhibitor Olaparib. Cancer Res. 2022;82(6):1140-52.
103. Jette NR, Radhamani S, Arthur G, Ye R, Goutam S, Bolyos A, Petersen LF, Bose P, Bebb DG, Lees-Miller SP. Combined poly-ADP ribose polymerase and ataxia-telangiectasia mutated/Rad3-related inhibition targets ataxia-telangiectasia mutated-deficient lung cancer cells. Br J Cancer. 2019;121(7):600-10.
104. Kim H, George E, Ragland R, Rafail S, Zhang R, Krepler C, Morgan M, Herlyn M, Brown E, Simpkins F. Targeting the ATR/CHK1 Axis with PARP Inhibition Results in Tumor Regression in. Clin Cancer Res. 2017;23(12):3097-108.

105. Townsend DM, Tew KD. The role of glutathione-S-transferase in anti-cancer drug resistance. Oncogene. 2003;22(47):7369-75.
106. Choi CH. ABC transporters as multidrug resistance mechanisms and the development of chemosensitizers for their reversal. Cancer Cell Int. 2005;5:30.
107. Fan S, el-Deiry WS, Bae I, Freeman J, Jondle D, Bhatia K, Fornace AJ, Magrath I, Kohn KW, O'Connor PM. p53 gene mutations are associated with decreased sensitivity of human lymphoma cells to DNA damaging agents. Cancer Res. 1994;54(22):5824-30.
108. Edwards SL, Brough R, Lord CJ, Natrajan R, Vatcheva R, Levine DA, Boyd J, Reis-Filho JS, Ashworth A. Resistance to therapy caused by intragenic deletion in BRCA2. Nature. 2008;451(7182):1111-5.
109. Jaspers JE, Kersbergen A, Boon U, Sol W, van Deemter L, Zander SA, Drost R, Wientjens E, Ji J, Aly A, Doroshow JH, Cranston A, Martin NM, Lau A, O'Connor MJ, Ganesan S, Borst P, Jonkers J, Rottenberg S. Loss of 53BP1 causes PARP inhibitor resistance in Brca1-mutated mouse mammary tumors. Cancer Discov. 2013;3(1):68-81.
110. Dallas NA, Xia L, Fan F, Gray MJ, Gaur P, van Buren G, Samuel S, Kim MP, Lim SJ, Ellis LM. Chemoresistant colorectal cancer cells, the cancer stem cell phenotype, and increased sensitivity to insulin-like growth factor-I receptor inhibition. Cancer Res. 2009;69(5):1951-7.
111. Bertolini G, Roz L, Perego P, Tortoreto M, Fontanella E, Gatti L, Pratesi G, Fabbri A, Andriani F, Tinelli S, Roz E, Caserini R, Lo Vullo S, Camerini T, Mariani L, Delia D, Calabrò E, Pastorino U, Sozzi G. Highly tumorigenic lung cancer CD133+ cells display stem-like features and are spared by cisplatin treatment. Proc Natl Acad Sci U S A. 2009;106(38):16281-6.
112. Carnero A, Garcia-Mayea Y, Mir C, Lorente J, Rubio IT, LLeonart ME. The cancer stem-cell signaling network and resistance to therapy. Cancer Treat Rev. 2016;49:25-36.
113. Yohe ME, Heske CM, Stewart E, Adamson PC, Ahmed N, Antonescu CR, Chen E, Collins N, Ehrlich A, Galindo RL, Gryder BE, Hahn H, Hammond S, Hatley ME, Hawkins DS, Hayes MN, Hayes-Jordan A, Helman LJ, Hettmer S, Ignatius MS, Keller C, Khan J, Kirsch DG, Linardic CM, Lupo PJ, Rota R, Shern JF, Shipley J, Sindiri S, Tapscott SJ, Vakoc CR, Wexler LH, Langenau DM. Insights into pediatric rhabdomyosarcoma research: Challenges and goals. Pediatr Blood Cancer. 2019;66(10):e27869.
114. Kahen E, Yu D, Harrison DJ, Clark J, Hingorani P, Cubitt CL, Reed DR. Identification of clinically achievable combination therapies in childhood rhabdomyosarcoma. Cancer Chemother Pharmacol. 2016;78(2):313-23.

6. Statutory Declaration

“I, Heathcliff Dorado García, by personally signing this document in lieu of an oath, hereby affirm that I prepared the submitted dissertation on the topic “Targeting ATR in pediatric solid tumors/ATR als therapeutischer Angriffspunkt bei pädiatrischen soliden Tumoren”, independently and without the support of third parties, and that I used no other sources and aids than those stated.
All parts which are based on the publications or presentations of other authors, either in letter or in spirit, are specified as such in accordance with the citing guidelines. The sections on methodology (in particular regarding practical work, laboratory regulations, statistical processing) and results (in particular regarding figures, charts and tables) are exclusively my responsibility.

Furthermore, I declare that I have correctly marked all of the data, the analyses, and the conclusions generated from data obtained in collaboration with other persons, and that I have correctly marked my own contribution and the contributions of other persons (cf. declaration of contribution). I have correctly marked all texts or parts of texts that were generated in collaboration with other persons.

My contributions to any publications to this dissertation correspond to those stated in the below joint declaration made together with the supervisor. All publications created within the scope of the dissertation comply with the guidelines of the ICMJE (International Committee of Medical Journal Editors; http://www.icmje.org) on authorship. In addition, I declare that I shall comply with the regulations of Charité – Universitätsmedizin Berlin on ensuring good scientific practice.

I declare that I have not yet submitted this dissertation in identical or similar form to another Faculty.

The significance of this statutory declaration and the consequences of a false statutory declaration under criminal law (Sections 156, 161 of the German Criminal Code) are known to me.”

Date Signature

7. Declaration of your own contribution to the publications

Heathcliff Dorado García contributed the following to the below listed publications:

Publication 1: **Heathcliff Dorado García**, Fabian Pusch, Yi Bei, Jennifer von Stebut, Glorymar Ibáñez, Kristina Guillan, Koshi Imami, Dennis Gürgen, Jana Rolff, Konstantin Helmsauer, Stephanie Meyer-Liesener, Natalie Timme, Victor Bardinet, Rocío Chamorro González, Ian C MacArthur, Celine Y Chen, Joachim Schulz, Antje M Wengner, Christian Furth, Birgit Lala, Angelika Eggert, Georg Seifert, Patrick Hundsoerfer, Marieluise Kirchner, Philipp Mertins, Matthias Selbach, Andrej Lissat, Frank Dubois, David Horst, Johannes H Schulte, Simone Spuler, Daoqi You, Filemon Dela Cruz, Andrew L Kung, Kerstin Haase, Michela DiVirgilio, Monika Scheer, Michael V Ortiz, Anton G Henssen. Therapeutic targeting of ATR in alveolar rhabdomyosarcoma. Nat Commun. (2022).
Contribution: Performed the experiments detailed in Figures 1, 2, 3, 4, 5 and 6, as well as Supplementary Figures 1, 2, 3, 4, 5, 6, 7, 8 and 9. For Figure 3a-b the candidate prepared the samples and got assistance from the lab of Prof. Selbach (phosphoproteomic run and data processing). For Figures 5a and 6d the candidate prepared the samples and they were sequenced by the MDC sequencing service (for sequencing run and data processing). The data from Figure 7a-d and Supplementary Figure 10 b-o was acquired by EPO GmbH. The data from Figure 7e-g was acquired by Prof. Ortiz's lab. The data from Figure 7h-j and Supplementary Figure 10p was acquired by iPATH. The doctoral candidate performed all data analysis (including the data from Figure 7 and Supplementary Figure 10) and prepared all the figures and text in collaboration with Prof. Henssen.

Publication 2: Isabelle Roeschert, Evon Poon, Anton G. Henssen **Heathcliff Dorado Garcia**, Marco Gatti, Celeste Giansanti, Yann Jamin, Carsten P. Ade, Peter Gallant, Christina Schülein-Völk, Petra Beli , Mark Richards, Mathias Rosenfeldt, Matthias Altmeyer, John Anderson, Angelika Eggert, Matthias Dobbelstein, Richard Bayliss , Louis Chesler, Gabriele Büchel and Martin Eilers. Combined inhibition of Aurora-A and ATR kinases results in regression of MYCN-amplified neuroblastoma. Nat Cancer, 2021.
Contribution: Figure 7a and Extended Data Fig. 6 were created based on the analysis performed by the doctoral candidate.

_____

Signature, date and stamp of first supervising university professor / lecturer

_____

Signature of doctoral candidate

8. Excerpt from Journal Summary List

8.1. Dorado García *et al*. Therapeutic targeting of ATR in alveolar rhabdomyosarcoma

Journal Data Filtered By: **Selected JCR Year: 2021** Selected Editions: SCIE,SSCI
Selected Categories: **"MULTIDISCIPLINARY SCIENCES"** Selected Category Scheme: WoS
Gesamtanzahl: 73 Journale

Rank	Full Journal Title	Total Cites	Journal Impact Factor	Eigenfaktor
1	NATURE	1,008,544	69.504	1.11428
2	SCIENCE	883,834	63.714	0.89813
3	Nature Human Behaviour	11,204	24.252	0.04187
4	National Science Review	10,508	23.178	0.01957
5	Science Bulletin	13,517	20.577	0.02141
6	Nature Communications	604,735	17.694	1.29690
7	Science Advances	104,068	14.957	0.28119
8	Journal of Advanced Research	8,207	12.822	0.00826
9	PROCEEDINGS OF THE NATIONAL ACADEMY OF SCIENCES OF THE UNITED STATES OF AMERICA	860,450	12.779	0.74016
10	Research	3,467	11.036	0.00574
11	Research Synthesis Methods	5,479	9.308	0.01057
12	Scientific Data	17,754	8.501	0.04575
13	GigaScience	8,120	7.658	0.01707
14	ANNALS OF THE NEW YORK ACADEMY OF SCIENCES	53,642	6.499	0.01954
15	iScience	13,293	6.107	0.02797
16	Frontiers in Bioengineering and Biotechnology	16,204	6.064	0.02051
17	Machine Learning-Science and Technology	791	6.013	0.00139
18	GLOBAL CHALLENGES	1,876	5.135	0.00443
19	Scientific Reports	696,320	4.996	1.17671
20	NPJ Microgravity	867	4.970	0.00142

8.2. Roeschert *et al*. Combined inhibition of Aurora-A and ATR kinase results in regression of *MYCN*-amplified neuroblastoma.

Journal Data Filtered By: **Selected JCR Year: 2021** Selected Editions: SCIE,SSCI
Selected Categories: **"ONCOLOGY"** Selected Category Scheme: WoS
Gesamtanzahl: 246 Journale

Rank	Full Journal Title	Total Cites	Journal Impact Factor	Eigenfaktor
1	CA-A CANCER JOURNAL FOR CLINICIANS	61,124	286.130	0.09703
2	NATURE REVIEWS CANCER	66,699	69.800	0.05330
3	Nature Reviews Clinical Oncology	22,751	65.011	0.04148
4	LANCET ONCOLOGY	79,244	54.433	0.13790
5	ANNALS OF ONCOLOGY	68,844	51.769	0.11379
6	JOURNAL OF CLINICAL ONCOLOGY	195,709	50.717	0.24244
7	Molecular Cancer	32,250	41.444	0.03386
8	CANCER CELL	57,294	38.585	0.07359
9	Cancer Discovery	31,182	38.272	0.06475
10	JAMA Oncology	27,216	33.006	0.08103
11	Nature Cancer	2,315	23.177	0.00816
12	Journal of Hematology & Oncology	15,318	23.168	0.02209
13	Journal of Thoracic Oncology	27,842	20.121	0.03995
14	Trends in Cancer	6,389	19.161	0.01397
15	SEMINARS IN CANCER BIOLOGY	14,777	17.012	0.01217
16	Cancer Communications	2,334	15.283	0.00391
17	CLINICAL CANCER RESEARCH	115,272	13.801	0.11972
18	CANCER TREATMENT REVIEWS	12,869	13.608	0.01455
19	Annual Review of Cancer Biology-Series	1,098	13.340	0.00327
20	CANCER RESEARCH	161,957	13.312	0.09051
21	NEURO-ONCOLOGY	20,825	13.029	0.02439

9. Printing copies of the publications

9.1. Dorado García *et al*. Therapeutic targeting of ATR in alveolar rhabdomyosarcoma

https://doi.org/10.1038/s41467-022-32023-7

nature communications

Article

https://doi.org/10.1038/s41467-022-32023-7

Therapeutic targeting of ATR in alveolar rhabdomyosarcoma

Received: 20 December 2020

Accepted: 11 July 2022

Published online: 25 July 2022

Check for updates

Heathcliff Dorado García[1,2,3], Fabian Pusch[1], Yi Bei[1,2,3], Jennifer von Stebut[1,2], Glorymar Ibáñez[4], Kristina Guillan[4], Koshi Imami[3], Dennis Gürgen[5], Jana Rolff[5], Konstantin Helmsauer[1,2], Stephanie Meyer-Liesener[1,3,6], Natalie Timme[2], Victor Bardinet[1,2], Rocío Chamorro González[1,2,3], Ian C. MacArthur[2], Celine Y. Chen[1,2], Joachim Schulz[2], Antje M. Wengner[7], Christian Furth[2], Birgit Lala[2], Angelika Eggert[2], Georg Seifert[2], Patrick Hundsoerfer[2], Marieluise Kirchner[3,8], Philipp Mertins[3,8], Matthias Selbach[3], Andrej Lissat[2], Frank Dubois[9,10], David Horst[9], Johannes H. Schulte[2], Simone Spuler[1,3,6,8,11], Daoqi You[4], Filemon Dela Cruz[4], Andrew L. Kung[4], Kerstin Haase[1], Michela DiVirgilio[3], Monika Scheer[2], Michael V. Ortiz[4] & Anton G. Henssen[1,2,3,8,12]

Despite advances in multi-modal treatment approaches, clinical outcomes of patients suffering from PAX3-FOXO1 fusion oncogene-expressing alveolar rhabdomyosarcoma (ARMS) remain dismal. Here we show that PAX3-FOXO1-expressing ARMS cells are sensitive to pharmacological ataxia telangiectasia and Rad3 related protein (ATR) inhibition. Expression of PAX3-FOXO1 in muscle progenitor cells is not only sufficient to increase sensitivity to ATR inhibition, but PAX3-FOXO1-expressing rhabdomyosarcoma cells also exhibit increased sensitivity to structurally diverse inhibitors of ATR. Mechanistically, ATR inhibition leads to replication stress exacerbation, decreased BRCA1 phosphorylation and reduced homologous recombination-mediated DNA repair pathway activity. Consequently, ATR inhibitor treatment increases sensitivity of ARMS cells to PARP1 inhibition in vitro, and combined treatment with ATR and PARP1 inhibitors induces complete regression of primary patient-derived ARMS xenografts in vivo. Lastly, a genome-wide CRISPR activation screen (CRISPRa) in combination with transcriptional analyses of ATR inhibitor resistant ARMS cells identifies the RAS-MAPK pathway and its targets, the *FOS* gene family, as inducers of resistance to ATR inhibition. Our findings provide a rationale for upcoming biomarker-driven clinical trials of ATR inhibitors in patients suffering from ARMS.

Rhabdomyosarcomas are the most common soft tissue tumors in childhood[1]. About 25% of cases present histologically as alveolar rhabdomyosarcoma (ARMS) and harbor pathognomonic chromosomal translocations involving genes encoding for the *PAX3* (and less frequently, *PAX7*) and *FOXO1* transcription factors[2,3]. PAX3/7-FOXO1 expression is not only sufficient to drive tumorigenesis[4], but it

A full list of affiliations appears at the end of the paper. e-mail: henssenlab@gmail.com

is significantly associated with adverse clinical outcome. Rhabdomyosarcomas expressing PAX3/7-FOXO1 have a high metastatic potential and are often refractory to chemotherapy[5]. Despite recent advances in cancer drug development, no new targeted treatment options were clinically approved for metastatic or recurrent rhabdomyosarcomas in the last ~30 years[6]. It is widely accepted that current treatment strategies have reached their limits. PAX3/7-FOXO1-driven rhabdomyosarcomas are rarely associated with therapeutically actionable genetic aberrations[7]. Thus, the identification of new therapeutic strategies for high-risk PAX3/7-FOXO1-expressing rhabdomyosarcoma remains urgent but challenging.

Most cancers depend on active DNA damage repair, explaining why genotoxic agents are among the most effective chemotherapeutic agents in cancer therapy[8]. The therapeutic window of genotoxic agents, however, is often narrow and considerable long-term sequelae occur in patients treated with such agents. Synthetic lethal cellular dependencies have emerged as tumor-specific vulnerabilities, which provide therapeutic targets offering much broader therapeutic windows[9]. In particular, DNA damage response (DDR) pathway dependencies are being successfully exploited for the development of novel therapies. As a prototypical example, *BRCA1* deficient tumors rely on PARP-mediated base-excision DNA repair (BER), a synthetic lethal relationship that was clinically translated in breast and ovarian cancers among other tumor entities[10,11]. Thus, exploiting DDR pathway dependencies may enable the development of novel therapeutic strategies for rhabdomyosarcomas.

Oncogenes, particularly those encoding for transcription factors and fusion transcription factors, can interfere with the normal function of the DNA replication machinery through deregulation of transcriptional activity[12]. Resulting transcription-induced replication fork stalling leads to activation of DDR pathways, during that unprotected single stranded DNA is bound by Replication Protein A (RPA32), subsequently recruiting the ataxia telangiectasia and Rad3 related (ATR) kinase[13–16]. This process has been termed oncogene-induced replication stress. Upon recognition of the DNA break, ATR activates checkpoint kinase 1 (CHK1) among other factors to stop cells from cycling and to coordinate DNA repair[17] (Fig. 1a). Unsurprisingly, many tumors depend on ATR activity to proliferate in the presence of oncogene-induced replication stress. Based on this observation, ATR has become a candidate target for pharmacological inhibition in cancer therapy and ATR inhibitors are being tested clinically (eg. NCT03682289, NCT05071209). Considering that molecular features creating synthetic lethal ATR dependencies, including *ATM* and *TP53* loss, MYC proto-oncogene expression, fusion oncogene expression, and PGBD5 expression[18–27], are present in a subset of rhabdomyosarcoma[7], we evaluated pharmacological ATR pathway inhibition as a therapeutic option for ARMS. Here, we show that ATR inhibitors exhibit antitumor activity against preclinical models of ARMS and that PAX3-FOXO1 is sufficient to increase sensitivity to ATR inhibition.

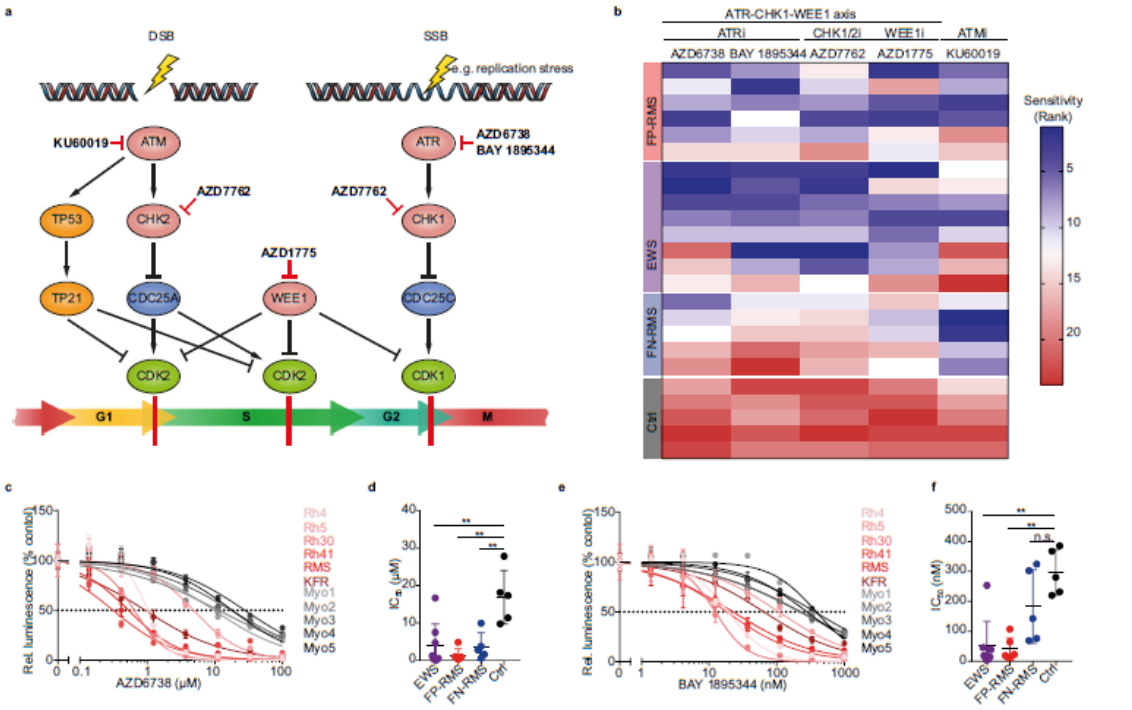

Fig. 1 | Fusion-positive ARMS cells are sensitive to pharmacological ATR inhibition. **a** Schematic of the DNA damage response pathway and small molecule inhibitor targeting proteins involved. DSB = Double Strand Break, SSB = Single Strand Break. **b** Heatmap showing sensitivity of ARMS (FP-RMS), Ewing sarcoma (EWS), ERMS (FN-RMS), and primary myoblast control cells (Ctrl) to the different DNA damage response inhibitors (blue indicates high sensitivity and red low sensitivity as defined by the rank of IC_{50} values). **c** Dose-response curves of cell viability for FP-RMS cell lines treated with the ATR inhibitor AZD6738 compared to primary myoblasts ($n = 3$). **d** IC_{50} values for FP-RMS, EWS, FN-RMS and Ctrl cells treated with AZD6738 ($P = 4.10 \times 10^{-3}$; 6.00×10^{-4}; 6.30×10^{-3} for EWS, FP-RMS and FN-RMS vs Ctrl, respectively; from left to right, $n = 8$, 6, 5, and 5 biologically independent cells). **e** Dose-response curves of cell viability for FP-RMS cell lines treated with the ATR inhibitor BAY 1895344 compared to primary myoblasts ($n = 3$). **f** IC_{50} values for FP-RMS, EWS, FN-RMS and Ctrl cells treated with BAY 1895344 ($P = 2.31 \times 10^{-4}$; 4.59×10^{-5}; 0.116 for EWS, FP-RMS and FN-RMS vs Ctrl, respectively; from left to right, $n = 8$, 6, 5, and 5 biologically independent cells). All statistical analyses correspond to two-sided student's t-test; data presented as mean value ± error bars representing standard deviation.

Results

ARMS cell lines are sensitive to pharmacological ATR pathway inhibition

To identify therapeutically actionable DDR pathway vulnerabilities, we screened six ARMS cell lines, eight Ewing sarcoma cell lines and five embryonal rhabdomyosarcoma (ERMS) cell lines compared to five primary untransformed myoblasts derived from healthy human donors for their sensitivity to small molecule inhibitors of DDR kinases ATR (AZD6738, BAY 1895344[28,29]), ATM (KU60019), CHK1/2 (AZD7762) and WEE1 (AZD1775) (Fig. 1a–f and Supplementary Fig. 1a–p). ARMS cell lines showed varying degrees of sensitivity to small molecule-mediated ATR, ATM, WEE1, and CHK1/2 inhibition, with inhibitory concentrations of 50% reduction in cell viability (IC_{50}) ranging between 10 nM and 15 μM (Supplementary Fig. 1a–p). ARMS cells were significantly more sensitive to all inhibitors compared to primary human myoblasts (Fig. 1b–f and Supplementary Fig. 1a–p), suggesting that a therapeutic index exists for these drugs. Sensitivity of ARMS cells to ATR pathway inhibition was similar to that of Ewing sarcoma cell lines (Fig. 1c–f), which were reported to be hypersensitive to ATR inhibition due to fusion oncogene-induced replication stress[30,31]. Thus, ARMS cells are sensitive to pharmacological ATR pathway inhibition.

ATR inhibition leads to replication stress, genomic instability, apoptosis, and cell cycle disruption in ARMS cells

Activated ATR is a key mediator of a multifaceted response to DNA replication stress, arrests the cell cycle, blocks replication, and increases repair of stalled replication forks[32,33]. Indeed, short hairpin RNA (shRNA)-mediated knock down of ATR in ARMS cells led to replication stress as evidenced by increased RPA32 T21 phosphorylation (Supplementary Fig. 2a). In line with on-target activity, pharmacological ATR inhibition with both AZD6738 and BAY 1895344, was also accompanied with increased RPA32 T21 phosphorylation (Fig. 2a, b). Consistent with increased replication stress, ARMS cells showed significant accumulation of unrepaired DNA double stranded breaks after incubation with ATR inhibitors or shRNA-mediated ATR knockdown, as measured by terminal deoxynucleotidyl transferase dUTP nick end labeling (TUNEL; Fig. 2c and Supplementary Figs. 2b and 3a). This was accompanied by an increase in micronucleated cells (Fig. 2d, e and Supplementary Fig. 2c), which are typically observed in the context of replication stress[34,35]. Furthermore, cell death, as measured by caspase 3 cleavage, increased in ARMS cells incubated in the presence of an ATR inhibitor or after shRNA-mediated ATR knockdown (Fig. 2f and Supplementary Figs. 2d and 3b). Because of the pivotal role of ATR in controlling the S phase and G2 to M transition checkpoints (Fig. 1a), we measured the cell cycle profiles of cells in response to ATR inhibition, by co-staining cells with 5-Ethynyl-2′-deoxyuridine (EdU) and propidium iodide (PI). After incubation with ATR inhibitors, ARMS cells accumulated in G2/M-phases with a corresponding reduction of cells in S-phase, indicating a bypass of intra-S phase cell cycle checkpoint (Fig. 2g and Supplementary Fig. 3c). This was associated with an increase in histone 3 S10 phosphorylation (Fig. 2h–j and Supplementary Fig. 2e), a marker of mitotic cells[36], suggesting accumulation in mitosis. The fraction of aneuploid cells was significantly larger after ATR inhibition (Fig. 2k and Supplementary Fig. 3c), pointing at chromosome missegregation due to erroneous repair of unresolved replication intermediates or mitotic catastrophe. Our data suggests that pharmacologic ATR inhibition exacerbates replication stress in ARMS cells, which enter mitosis with unrepaired DNA damage incompatible with cell survival.

Small molecule ATR inhibition has on-target effects on ATR kinase activity in ARMS cells in vitro at clinically achievable doses

We next sought to verify on-target activity of ATR inhibitors on ATR kinase activity as a mechanism of the observed cell cycle disruption, replication stress exacerbation and genomic instability in ARMS cells. To do so, we measured proteome-wide changes in phosphorylation using stable isotope labeling with amino acids in cell culture (SILAC)

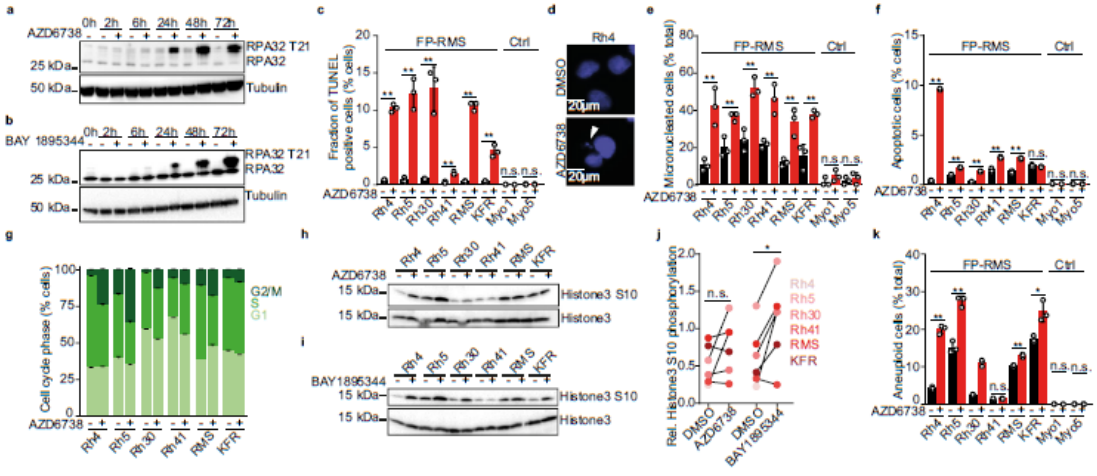

Fig. 2 | ATR inhibition induces replication stress-associated DNA damage, genomic instability, apoptosis and cell cycle disruption. Western immunoblot of RPA32 phosphorylation at T21 in Rh4 cells treated with ATR inhibitor AZD6738 (750 nM) (**a**) and BAY 1895344 (20 nM) (**b**). **c** Quantification of TUNEL signal in cells treated with AZD6738 for 72 h. ($n = 3$; from left to right, $P = 5.97 \times 10^{-6}$; 6.51×10^{-4}; 0.002; 0.001; 6.88×10^{-6}; 9.04×10^{-4}; 0.734; 0.980). **d** Representative photomicrographs of micronucleation in cells. White arrow represents micronuclei. **e** Fraction of micronucleated cells after treatment with AZD6738 for 72 h. ($n = 3$, with 50 nuclei counted per replicate; $P = 0.007$; 0.007; 0.004; 0.007; 0.007; 0.004; 0.206; 0.768). **f** Fraction of apoptotic cells after treatment with AZD6738 for 72 h. ($n = 3$; from left to right, $P = 4.54 \times 10^{-9}$; 7.12×10^{-4}; 6.12×10^{-6}; 2.46×10^{-4}; 6.52×10^{-5}; 0.313; 0.424; 0.713). **g** Cell cycle phase distribution of cells after treatment with AZD6738 for 72 h. ($n = 3$). Western immunoblot of histone 3 phosphorylation at S10 in six FP-RMS cells treated with AZD6738 (**h**) and BAY 1895344 (**i**) for 2 h. **j** Quantification of changes in histone 3 S10 phosphorylation ($P = 0.344$; 0.016; statistical analysis is sign test). **k** Fraction of aneuploid cells after treatment with AZD6738 for 72 h. ($n = 3$; from left to right, $P = 2.55 \times 10^{-5}$; 5.45×10^{-4}; 6.56×10^{-5}; 0.402; 5.13×10^{-4}; 0.012; 0.882; 0.565). All statistical analyses correspond to two-sided student's t-test except for (j) data presented as mean value ± error bars representing standard deviation.

https://doi.org/10.1038/s41467-022-32023-7

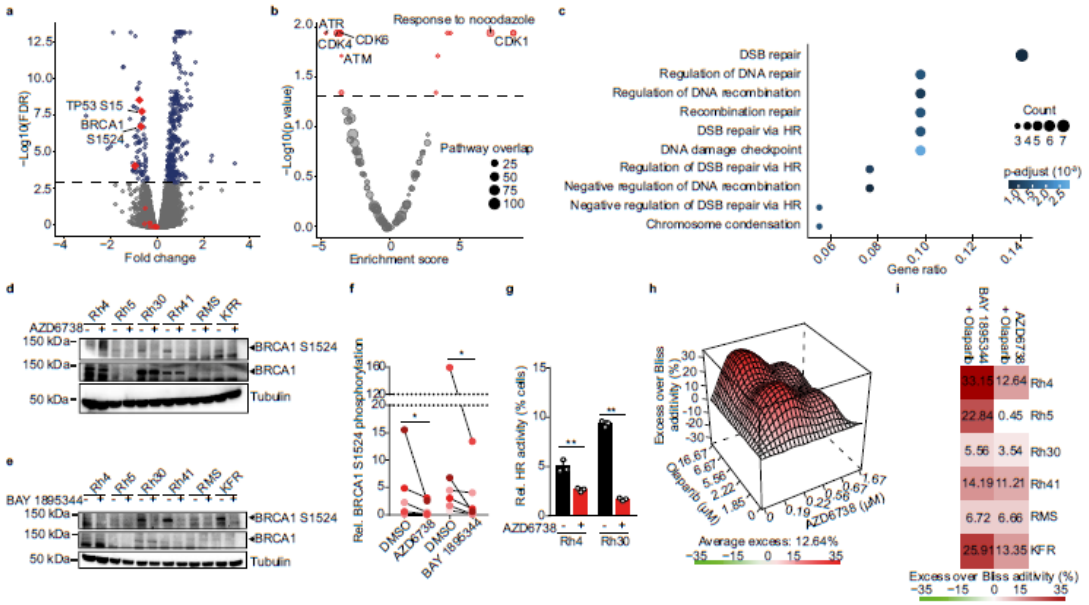

Fig. 3 | Pharmacological ATR inhibition has on-target activity and leads to reduced BRCA1 activation and repressed homologous recombination. a Volcano plot showing relative changes in phospho-peptide abundance in PAX3-FOXO1-expressing Rh30 cells after 2 h of incubation with AZD6738 (750 nM) measured using LC-MS/MS proteomics (red, known ATR targets; dotted line indicating a false discovery rate (FDR) of 0.001). b Volcano plot showing relative enrichment of molecular pathways in which differential phospho-peptide abundance was observed in cells treated with AZD6738 (750 nM) compared to DMSO-treated cells (dotted line indicating a false discovery rate of 0.05). c Cellular processes significantly enriched in differentially abundant phospho-peptides. Western immunoblotting of BRCA1 S1524 and total BRCA1 in six FP-RMS cells after 2 hours of treatment with AZD6738 (750 nM) (d) or BAY 1895344 (20 nM) (e). f Quantification of changes in BRCA1 S1524 phosphorylation ($P = 0.016$; 0.016 for d and e, respectively; statistical analysis is sign test). g Relative HR activity in Rh4 and Rh30 cells after incubation with AZD6738 (750 nM), measured as GFP reconstitution based on repair of an SceI-mediated DNA lesion via homologous recombination. ($n = 3$ biologically independent experiments; $P = 0.003$; 2.61×10^{-6} for Rh4 and Rh30, respectively). h Excess over Bliss analysis of combined treatment with olaparib and AZD6738 in Rh4 cells ($n = 3$). i Bliss synergy scores for six FP-RMS cell lines treated with AZD6738 and olaparib. All statistical analyses correspond to two-sided student's t-test except for 3f; data presented as mean value ± error bars representing standard deviation.

followed by liquid chromatography with tandem mass spectrometry (LC-MS/MS) phospho-proteomic analysis of cells incubated in the presence of AZD6738. Short-term incubation of ARMS cells with the ATR inhibitor at the same concentrations used in cell assays (Fig. 2a–k) significantly reduced phosphorylation of known ATR kinase target peptides (Fig. 3a), such as the direct ATR target TP53 S15[37], indicating on-target activity. Using a phosphosite-centered computational analysis tool[38], we inferred pathway activities after pharmacological ATR inhibition (Fig. 3b). The ATR pathway was the most significantly repressed pathway, again supporting on-target activity of AZD6738 at low doses in ARMS cells. In line with the observed mitotic arrest of cells after ATR inhibition (Fig. 2g–k), peptides from members of the CDK1 pathway and pathways activated in response to nocodazole, an inhibitor of microtubule formation leading to lack of mitotic spindle and M-phase arrest[39], were phosphorylated at higher degrees after ATR inhibitor treatment (Fig. 3b). Homologous recombination (HR), DNA damage checkpoint and DNA replication pathway proteins, on the other hand, were the most significantly de-phosphorylated after ATR inhibition (Fig. 3c), supporting our conclusion that the observed increase in genomic instability in cells was due to erroneous repair of unresolved replication intermediates and in line with ATR's role in these pathways[32,33].

A particularly high degree of differential phosphorylation was measured in BRCA1 peptides (Fig. 3a). BRCA1 is a known substrate of ATR[40], and is involved in HR at sites of replication stress[41–43]. A cluster of BRCA1 serine residues, including S1524, can be phosphorylated by ATR and serve as key regulatory sites for BRCA1 activity in DNA damage repair[40,44,45]. Using western immunoblotting, we tracked phosphorylation of one of these residues, BRCA1 S1524, in six different ARMS cell lines after 2 h incubation with AZD6738 and BAY 1895344 (Fig. 3d–f). BRCA1 S1524 phosphorylation was significantly reduced following AZD6738 treatment, confirming LC-MS/MS-based measurements (Fig. 3a). Next, we tested whether ATR inhibition affected HR activity by measuring HR on synthetic plasmids transfected into ARMS cells after incubation with AZD6738. Indeed, HR activity on such plasmids was significantly reduced in cells incubated with AZD6738 (Fig. 3g and Supplementary Fig. 3d). Thus, small molecule ATR inhibition has on target activity and represses BRCA1 activity and HR in ARMS cells.

Combined inhibition of ATR and PARP1 has synergistic anti-tumor effects in ARMS cells

Based on the known[40,44,46,47] and observed (Fig. 3a–h) effects of ATR inhibition on BRCA1 phosphorylation and HR pathway activity, we hypothesized that the reduced DNA damage repair via HR may increase cells' sensitivity to pharmacological poly (ADP-ribose) polymerase 1 (PARP1)-trapping on DNA, similarly as observed in *BRCA1*-deficient cancers[10]. Indeed, shRNA-mediated BRCA1 knock down in ARMS cells with three independent shRNAs led to increased sensitivity to PARP1 inhibition, with IC_{50} for olaparib changing from 90.1 μM for shGFP-expressing cells to 5.01, 7.19 and 6.42 μM for three independent shRNAs targeting BRCA1, respectively (Supplementary Fig. 4a, b). This confirmed that in the absence of BRCA1, rhabdomyosarcoma cells are sensitive to PARP-trapping. Consistently, BRCA1 knock down also sensitized rhabdomyosarcoma cells to ATR

https://doi.org/10.1038/s41467-022-32023-7

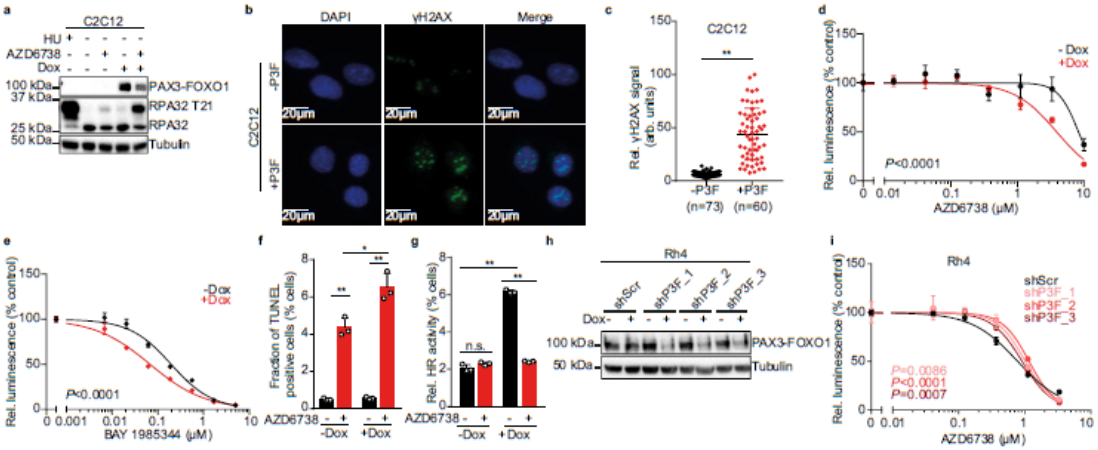

Fig. 4 | PAX3-FOXO1 is sufficient to increase sensitivity to ATR inhibition in myoblast cells. **a** Western immunoblot of PAX3-FOXO1 and RPA32 phosphorylation at T21 in C2C12 after doxycycline-induced expression of PAX3-FOXO1 (1000 ng/ml for 48 h) and treatment with AZD6738 (750 nM). Hydroxyurea (HU, 1 mM) was used as a control for replication stress. **b** Representative images of H2AX phosphorylation in C2C12 cells after ectopic expression of PAX3-FOXO1. **c** Quantification of H2AX phosphorylation in C2C12 cells after ectopic expression of PAX3-FOXO1 ($P = 9.57 \times 10^{-26}$). Dose-response curves of cell viability for C2C12 cells after ectopic expression of PAX3-FOXO1 and incubation with AZD6738 (**d**) or BAY 1895344 (**e**) ($n = 3$). **f** Quantification of TUNEL signal in C2C12 cells after induction of PAX3-FOXO1 with doxycycline and treatment with AZD6738 ($n = 3$; from top to bottom, $P = 0.016$; 1.84×10^{-4}; 1.99×10^{-4}). **g** Relative HR activity in C2C12 cells after induction of PAX3-FOXO1 with doxycycline (1000 ng/ml) and incubation with AZD6738 as measured using a GFP reconstitution assay based on repair of an SceI-mediated DNA lesion via homologous recombination ($n = 3$ biologically independent experiments; from top to bottom, $P = 5.19 \times 10^{-6}$; 3.67×10^{-7}; 0.114). **h** Western immunoblot of PAX3-FOXO1 in Rh4 cells after doxycycline-induced (1000 ng/mL) expression of shRNAs targeting PAX3-FOXO1 compared to scrambled shRNA control for 48 h. **i** Dose-response curves for Rh4 after doxycycline-induced (1000 ng/mL) expression of shRNAs targeting PAX3-FOXO1 compared to scrambled shRNA control and treated with AZD6738 ($n = 3$). All statistical analyses correspond to two-sided student's t-test; data presented as mean value ± error bars representing standard deviation.

inhibition (Supplementary Fig. 4c). We hypothesized that due to its effect on BRCA1 phosphorylation and HR activity, pharmacological ATR inhibition could sensitize rhabdomyosarcoma cells to PARP1 inhibition. Indeed, significant synergy of combined AZD6738 or BAY 1895344 and olaparib treatment was detected by Excess over Bliss analysis in six different ARMS cell lines (Fig. 3h–i and Supplementary Fig. 4d–n). Thus, ATR inhibition sensitizes ARMS cells to PARP inhibitor treatment in vitro.

PAX3-FOXO1 is sufficient to increase replication stress and sensitivity to pharmacological ATR inhibition

Several factors exist in synthetic lethal relationship with ATR[18–26]. To identify which of the known factors may influence rhabdomyosarcoma cells' sensitivity to ATR inhibition, we assessed their presence in eleven rhabdomyosarcoma cell lines and their association with ATR inhibitor sensitivity (Supplementary Fig. 5a–j). Even though some cell lines that were highly sensitive to ATR inhibition also presented reduced expression of TP53 and ATM, or high *PGBD5* and *CDC25A* mRNA expression, these associations were not statistically significant (Supplementary Fig. 5a–h). HR repair activity did not correlate with sensitivity to AZD6738 (Supplementary Fig. 5i, j), suggesting that differences in endogenous DNA damage levels rather than reduced repair activity was responsible for the observed differences in response to ATR inhibitors. In line with MYCN's ability to drive replication stress, high MYCN expression was associated with high ATR inhibitor sensitivity (Supplementary Fig. 5a, b). Ectopic expression of MYCN in untransformed mouse myoblast cells, however, did not increase cells' sensitivity to ATR inhibitors, suggesting that other factors in MYCN-expressing cells drive ATR inhibitor sensitivity (Supplementary Fig. 6a, b).

Based on previous reports showing that chimeric transcription factors, such as EWS-FLI1 in Ewing sarcoma, can themselves render cells sensitive to ATR inhibition through induction of replication stress[30,31], we hypothesized that PAX3-FOXO1 may contribute to replication stress and sensitivity to ATR inhibition in ARMS. To test this, we ectopically expressed PAX3-FOXO1 in untransformed mouse myoblast cells (C2C12, Fig. 4a). In line with oncogene-induced replication stress, ectopic PAX3-FOXO1 expression was associated with increased phosphorylation of RPA32 at T21, particularly in response to ATR inhibition with AZD6738 (Fig. 4a). This change in RPA32 phosphorylation was also observed in cells treated with hydroxyurea (HU), a potent inducer of replication stress (Fig. 4a). Consistent with increased oncogene-induced replication stress, H2AX phosphorylation, an early marker of DNA damage, increased in cells expressing PAX3-FOXO1 (Fig. 4b, c). This was accompanied by significantly increased sensitivity to the two structurally diverse ATR inhibitors, AZD6738 and BAY 1895344 (Fig. 4d, e). Furthermore, cells expressing PAX3-FOXO1 showed higher levels of TUNEL positive cells in response to AZD6738 than their counterpart control (Fig. 4f). Interestingly, overexpression of PAX3-FOXO1 led to an increase in HR activity, which was repressed by ATR inhibitor treatment (Fig. 4g). This indicates that myoblast cells depend on ATR activity in the presence of PAX3-FOXO1-induced replication stress to maintain increased HR activity.

To test whether PAX3-FOXO1 was required for ATR inhibitor sensitivity, we induced the expression of shRNAs directed against *PAX3-FOXO1* mRNA in PAX3-FOXO1-expressing ARMS cells (Fig. 4h). shRNA-mediated depletion of PAX3-FOXO1 led to reduced cell survival in ARMS cells (Supplementary Fig. 7a), consistent with the essential role of PAX3-FOXO1 in ARMS[48]. Even though the toxicity of PAX3-FOXO1 knockdown may affect the interpretation of our results, a significantly reduced sensitivity to ATR inhibitor treatment was observable after shRNA-mediated PAX3-FOXO1 knockdown (Fig. 4i, Supplementary Fig. 7b). Thus, the pathognomonic fusion oncoprotein PAX3-FOXO1 is not only sufficient to increase replication stress and ATR inhibitor sensitivity in myoblast cells, but is also required for ATR inhibitor sensitivity in ARMS cells.

https://doi.org/10.1038/s41467-022-32023-7

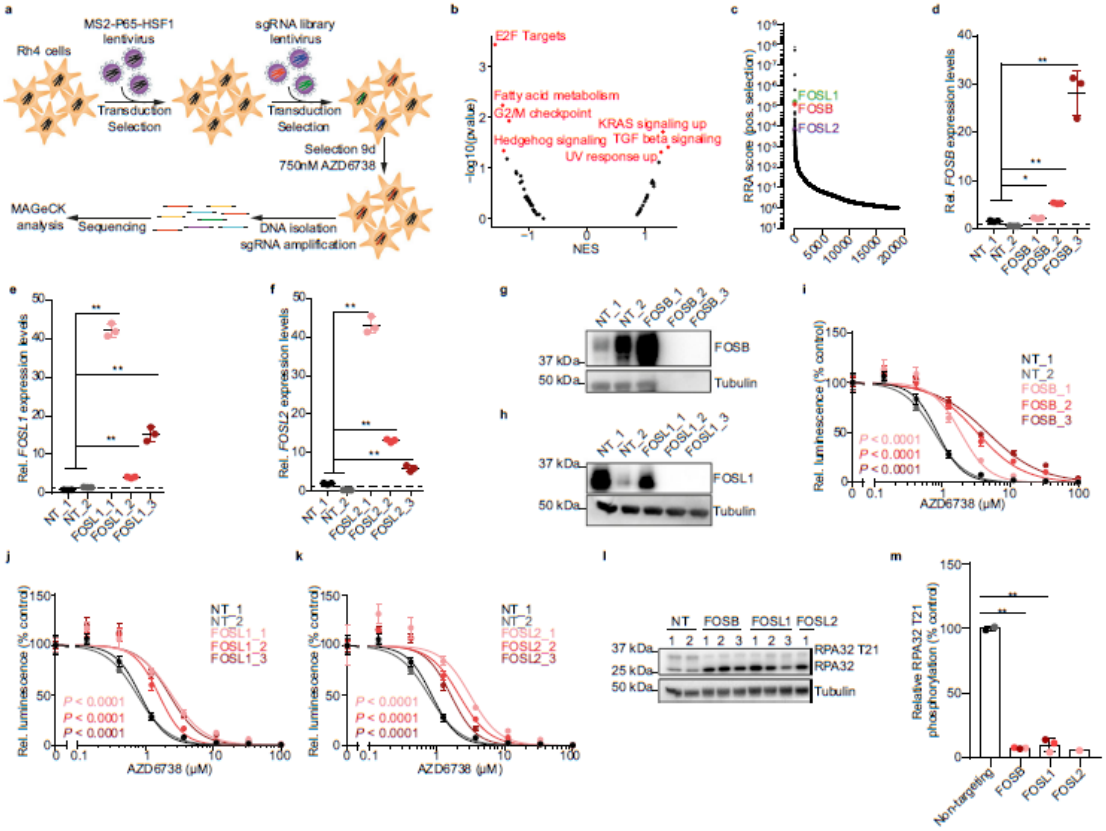

Fig. 5 | A genome wide CRISPR-based activation screen identifies molecular modifiers of sensitivity to ATR inhibition in PAX3-FOXO1-expressing ARMS cells. a Schematic representation of the genome wide CRISPRa screen experimental design. b Enrichment score for the GSEA hallmark pathways based on sgRNA enrichment. c Waterfall plot showing the positive robust rank aggregation (RRA) score of sgRNAs in Rh4 cells incubated in the presence of AZD6738 for 9 days compared to DMSO treated cells as analyzed using MAGeCK. *FOSB* (d, $P = 0.014$; 5.45×10^{-6}; 1.17×10^{-6}), *FOSL1* (e, $P = 9.09 \times 10^{-11}$; 5.16×10^{-6}; 2.19×10^{-7}) and *FOSL2* (f $P = 9.87 \times 10^{-10}$; 1.49×10^{-7}; 1.15×10^{-4}) mRNA expression measured using RT-qPCR in Rh30 cells expressing dCas9, lentiMPH and sgRNAs targeting *FOSB*, *FOSL1* or *FOSL2* ($n = 3$). Western immunoblot of FOSB (g) and FOSL1 (h) in Rh30 cells stably expressing dCas9, lentiMPH and sgRNAs targeting *FOSB* and *FOSL1*, respectively. Relative cell viability of Rh30 cells stably expressing dCas9, lentiMPH and sgRNAs targeting *FOSB* (i), *FOSL1* (j) and *FOSL2* (k) in the presence of varying concentrations of AZD6738. l Western immunoblot of RPA32 phosphorylation at T21 in Rh4 cells expressing sgRNAs targeting FOS family members *FOSB*, *FOSL1* or *FOSL2*. m Quantification of RPA32 phosphorylation at T21compared to the corresponding non-targeting control, ($P = 2.66 \times 10^{-6}$; 1.78×10^{-4}, respectively). All statistical analyses correspond to two-sided student's t-test; data presented as mean value ± error bars representing standard deviation.

A genome wide CRISPR activation screen identifies molecular factors reducing ATR inhibitor sensitivity in ARMS cells

Successful clinical translation of targeted therapies can be hampered by rapid occurrence of resistance[49]. Therefore, we aimed to identify factors altering sensitivity of ARMS cells to ATR inhibition, even in the presence of PAX3-FOXO1. To identify such factors, we used a genome-wide CRISPR-Cas9-based gene activation screen (CRISPRa) targeting over 70,000 genomic loci covering 20,000 gene promoters[50]. PAX3-FOXO1-expressing cells were genetically engineered to express endonuclease-deficient Cas9 (dCas9), transcriptional activation complex members and transduced with a single guide RNA (sgRNA) library. Next, cells were incubated for 9 days in the presence of the ATR inhibitor AZD6738 (Fig. 5a). sgRNAs significantly depleted in cells exposed to AZD6738 contained known sensitizers to ATR inhibition such as *MYC* and *CDC25A* (Supplementary Fig. 8a)[22]. Consistently, an unsupervised pathway analysis identified E2F targets and G2/M checkpoint genes enriched in sgRNAs depleted after AZD6738 exposure, i.e., associated with increased ATR inhibitor sensitivity (Fig. 5b). sgRNAs with increased abundance after AZD6738 exposure, on the other hand, were significantly enriched for KRAS-activated gene pathway members (Fig. 5b). This suggests that the RAS-MAPK pathway may promote ATR inhibitor resistance.

Interestingly, *FOSB*, *FOSL1*, and *FOSL2*, members of the AP-1 transcription factors and downstream targets of the RAS-MAPK pathway[51–54], were amongst the top genes targeted by sgRNAs with increased abundance in the presence of AZD6738 (Fig. 5c and Supplementary Fig. 8b). Efficient induction of *FOSB*, *FOSL1* and *FOSL2* mRNA and protein expression by CRISPRa was confirmed in two cell lines using RT-qPCR and western immunoblotting, respectively (Fig. 5d–h and Supplementary Fig. 8c–g). In line with increased resistance to ATR inhibition, cells expressing diverse *FOSB*, *FOSL1* and *FOSL2*-targeting sgRNAs and dCas9 were significantly less sensitive to ATR inhibition compared to cells expressing non-targeting sgRNAs, as evidenced by changes in dose-response relationship of two independent ARMS cell lines (Fig. 5i–k and Supplementary Fig. 8h–j). The AP-1 complex, including the *FOS* gene family members, are known modulators of DDR[55,56], leading us to hypothesize that *FOSB*, *FOSL1*, and *FOSL2* expression may reduce baseline replication stress in ARMS cells

https://doi.org/10.1038/s41467-022-32023-7

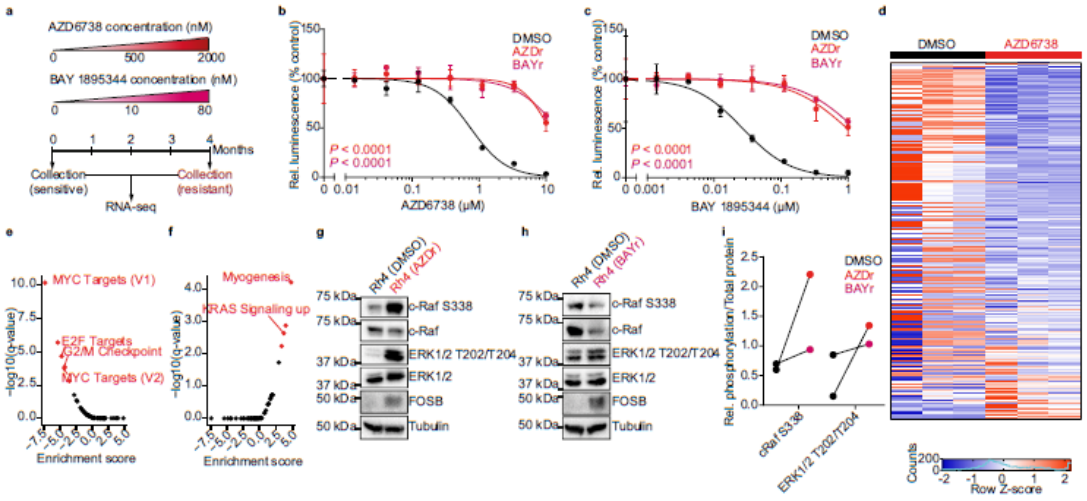

Fig. 6 | ATR inhibitor-resistant cells express FOSB and activated MAPK pathway. a Schematic representation of the generation of ATR inhibitor-resistant cells by long-term exposure to increasing doses of the ATR inhibitors AZD6738 and BAY 1895344. Dose-response curves of cell viability for resistant cells after incubation with AZD6738 (**b**) or BAY 1895344 (**c**) compared to treatment-naïve cells ($n = 3$ biologically independent experiments). **d** Heatmap of the 500 most variable genes based on RNA sequencing. Enrichment score for the GSEA hallmark pathways in ATR inhibitor-resistant cells based on RNA sequencing data, showing negatively (**e**) and positively enriched pathways (**f**). Western immunoblotting of RAS-MAPK pathway members in cells resistant to AZD6738 (**g**) or BAY 1895344 (**h**) compared to treatment-naïve cells. **i** Quantification of changes in c-Raf and ERK1/2 phosphorylation as measured in (g-h). All statistical analyses correspond to two-sided student's t-test; data presented as mean value ± error bars representing standard deviation.

even in the presence of PAX3-FOXO1. Indeed, CRISPRa-driven *FOS* gene family member expression was sufficient to reduce steady-state RPA32 T21 phosphorylation in ARMS cells, indicating reduced replication stress (Fig. 5l, m). Thus, *FOS* gene family member expression represents a mechanism through which ARMS cells can reduce replication stress, which is accompanied by reduced ATR inhibitor sensitivity.

ATR inhibitor resistance is associated with increased RAS-MAPK signaling and FOSB expression

To further investigate molecular mechanisms impeding ATR inhibitor sensitivity, we generated ATR inhibitor-resistant ARMS cells by incubating cells in the presence of AZD6738 and BAY 1895344 at increasing concentrations over a period of 4 months (Fig. 6a). We confirmed resistance of these cells to both inhibitors through dose-response measurements (Fig. 6b, c). Next, we performed RNA sequencing of ATR inhibitor-resistant cells and control cells and compared their gene expression. ATR inhibitor-resistant cells differed significantly with regards to their gene expression (Fig. 6d and Supplementary Fig. 9a). In line with the results from our CRISPRa screen (Fig. 5), gene expression pathway analysis identified MYC, E2F target, and G2/M checkpoint genes as being repressed in resistant cells (Fig. 6e and Supplementary Fig. 9b–e). The KRAS pathway, on the other hand, was one of the top pathways enriched in genes highly expressed in ATR inhibitor-resistant cells (Fig. 6f and Supplementary Fig. 9f, g). We confirmed higher RAS-MAPK pathway activity in ATR inhibitor-resistant cells compared to non-resistant cells by measuring c-Raf S338 and ERK1/2 T202/T204 phosphorylation (Fig. 6g–i). High RAS-MAPK activity was associated with high FOSB expression (Fig. 6g, h), further strengthening a functional link between RAS-MAPK activity, FOS family member expression, and ATR inhibitor resistance.

ATR inhibition suppresses tumor growth in ARMS patient-derived xenografts

Based on our results in human cell line models, we next sought to explore the effect of single agent ATR inhibition and its combination with olaparib in mice harboring patient-derived rhabdomyosarcoma xenografts (PDX). We measured the antitumoral effect of ATR inhibitors in an ARMS PDX derived from a 16-year-old female patient presenting with a relapsed ARMS in her forefoot. Histological analysis of the PDX and matching patient tumor confirmed that the PDX model adequately reflected ARMS histologically and expressed PAX3-FOXO1 (Supplementary Fig. 10a). Remarkably, this PDX was resistant to vincristine and ifosfamide, the two standard-of-care agents in ARMS therapy regimens[6] (Supplementary Fig. 10b–d). Both ATR inhibitors AZD6738 and BAY 1895344 had no significant effects on body weight stability (Supplementary Fig. 10e, f). Only mild reductions in erythrocyte counts were observed over the course of BAY 1895344 treatment (Supplementary Fig. 10g–o), consistent with the known on-target off-tumor toxicity of ATR inhibitors[29,57]. No histopathological differences were observed in six organs in mice treated with BAY 1895344 (Supplementary Fig. 10p), including muscle. In line with our observations in vitro, single-agent AZD6738 or BAY 1895344 treatment led to significant reductions in tumor burden over time in mice harboring the ARMS PDX (Fig. 7a–d). Next, we treated another ARMS PDX derived from a 4-year-old female with a PAX7-FOXO1-expressing relapsed ARMS in her left paraspinal mass. Treatment with BAY 1895344 significantly delayed tumor progression (Fig. 7e–g), suggesting that PAX7-FOXO1-harboring ARMS also respond to pharmacological ATR inhibition. In parallel, we treated a PDX derived from a different relapse of the same patient, in which a de novo *MYCN* amplification was detected. Even though BAY 1895344 treatment was accompanied by reduced PDX growth, the effects were less pronounced compared to the PDX lacking the *MYCN* amplification. Even though we cannot exclude the existence of additional genetic changes between the two PDX models derived from the same patient, the fact that a *MYCN* amplification was not associated with increased sensitivity of the PDX to ATR inhibition indicates that MYCN expression was not sufficient to alter ATR inhibitor sensitivity, in line with our observations in vitro (Supplementary Fig. 6). Tumors from mice treated with AZD6738 showed increased Caspase 3 cleavage and decreased

https://doi.org/10.1038/s41467-022-32023-7

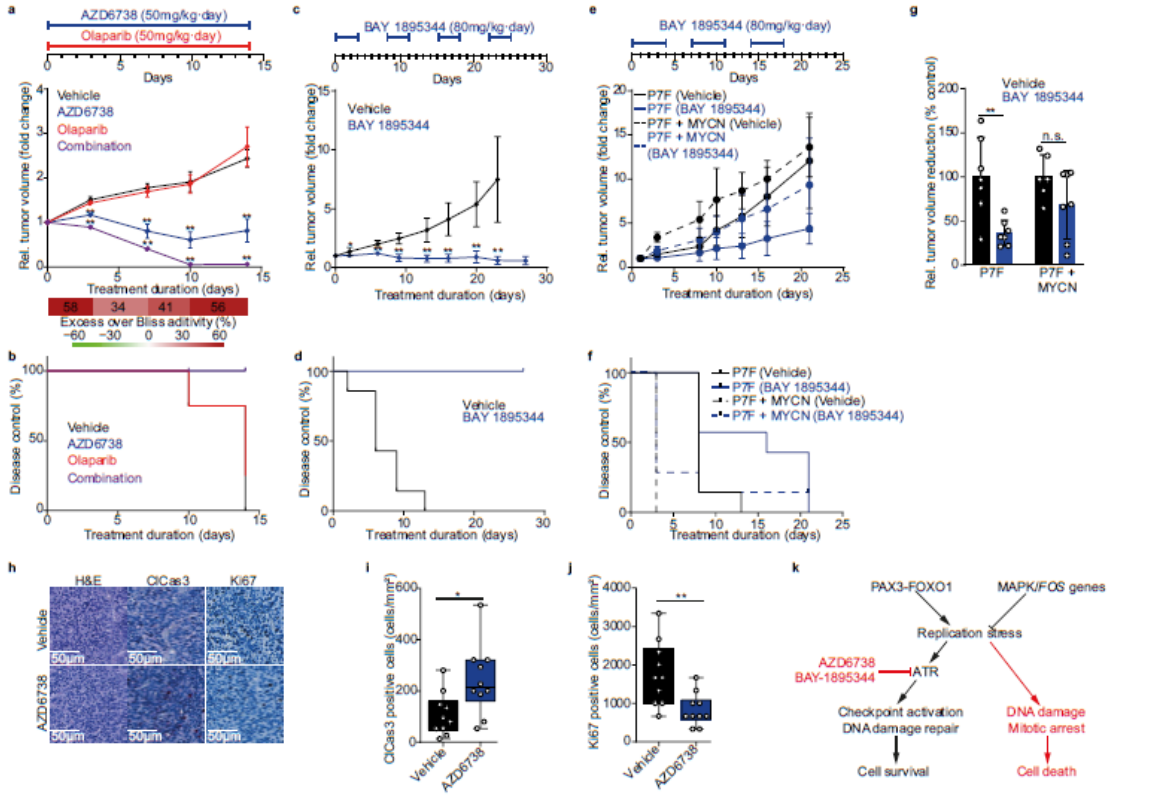

Fig. 7 | ATR inhibition sensitizes ARMS PDXs to PARP1 inhibition in vivo. **a** Tumor volume change of an ARMS PDX treated with AZD6738, olaparib or both compared to control ($n = 4$ mice per group; bottom, excess over Bliss additivity, ** $P < 0.01$). **b** Kaplan–Meier curve showing tumor doubling time after treatment. **c** Tumor volume change of the ARMS PDX treated with BAY 1895344 as compared to control ($n = 7$ mice per group; top, timeline of the drug schedule, ** $P < 0.01$). **d** Kaplan–Meier curve showing tumor doubling time after treatment. **e** Tumor volume change of an ARMS PDX harboring a PAX7-FOXO1 and a relapse with an additional MYCN amplification, treated with BAY 1895344 as compared to control ($n = 7$ mice per group; top, timeline of the drug schedule). **f** Kaplan–Meier curve showing tumor doubling time after treatment. **g** Tumor volume reduction at the endpoint of the treatment with BAY 1895344 or vehicle in a PAX7-FOXO1 ARMS PDX and a PAX7-FOXO1 MYCN amplified ARMS PDX ($n = 6$ mice for vehicle and $n = 7$ mice for BAY 1895344 treatment; $P = 0.004$; 0.117, respectively.) **h** Representative immunohistochemistry staining for cleaved Caspase3 and Ki67. Quantification of cleaved Caspase3 (i) and Ki67 (j) ($n = 10$ sections of 275µmx275µm; $P = 0.005$). **k** Schematic of our proposed model. PAX3-FOXO1 induces replication stress, which activates the ATR signaling pathway, promoting checkpoint activation and DNA repair. With ATR inhibitors, replication stress cannot be repaired, leading to DNA damage accumulation, mitotic arrest, and cell death. A proposed counteractive measure is the activation of the RAS-MAPK pathway, in particular *FOS* genes, to reduce replication stress. All statistical analyses correspond to two-sided student's t-test; data presented as mean value ± error bars representing standard deviation. Box plots (i and j) show center line as median, box limits as upper and lower quartiles, whiskers as minimum to maximum values.

Ki67 staining compared to tumors from mice treated with the vehicle control, suggesting that ATR inhibitor treatment led to increased cell death and decreased cell proliferation (Fig. 7h–j). Addition of olaparib to AZD6738, as currently explored in clinical trials in other tumor entities (NCT03682289), significantly potentiated the anti-tumor effects, leading to full regression of the PDX tumors (Fig. 7a). Loss of mouse weight after 10 days of combined AZD6738 and olaparib treatment, however, indicated increased toxicity compared to single agent treatment (Supplementary Fig. 10f). Thus, ATR inhibition has anti-tumor activity against preclinical ARMS models, which may be clinically translatable.

Discussion

We have found that preclinical models of ARMS are sensitive to pharmacological ATR inhibition. Consistent with previous reports of other oncogenic fusion genes inducing replication stress (e.g., in Ewing sarcoma[31]), expression of PAX3-FOXO1 was sufficient to increase replication stress, which required both DNA damage repair and DNA damage signaling, resulting in apoptosis if impaired by the selective inhibition of ATR (Fig. 7k). Untransformed mouse myoblast cells engineered to express PAX3-FOXO1, as well as PAX3-FOXO1-expressing rhabdomyosarcoma cell lines, accumulated unrepaired DNA damage and underwent apoptosis upon treatment with selective inhibitors of ATR signaling. These effects, observed particularly in PAX3-FOXO1-expressing rhabdomyosarcoma cells, were associated with on-target effects of ATR inhibition, such as decreased phosphorylation of BRCA1 and homologous recombination activity, and were accompanied by induction of genomic instability, increased mitotic arrest and apoptosis. In turn, single-agent treatment with two different inhibitors of ATR exhibited potent antitumor activity against high-risk patient-derived ARMS models. Moreover, decreased BRCA1 and homologous recombination activity through pharmacological ATR inhibition sensitized cells to PARP1 inhibition. When combined, ATR and PARP1 inhibitors exhibited strong antitumor activity against patient-derived ARMS models resistant to the current standard-of-care treatment.

Human cancers require active DNA damage repair for survival. As a result, selective inhibitors of ATR-mediated DNA damage repair signaling are used to target tumors with intrinsic deficiencies in DNA repair or high abundance of DNA damage[20,24,27,30,31,46,47,58]. Dissecting the molecular mechanisms of susceptibility to ATR inhibitors has been the subject of extensive investigations in the past years[59]. We and others have found inducers of ATR inhibitor susceptibility, such as PGBD5 recombinase activity in embryonal tumors[21], oncogene-induced replication stress, *ATM* loss, and TP53 deficiency[20,27,60]. Our current work revealed a specific dependency conferred by high steady-state replication stress in alveolar, PAX3-FOXO1-expressing rhabdomyosarcoma. In contrast to previous reports, we did not observe a statistically significant association between these factors and ATR inhibitor sensitivity in ARMS cell lines, suggesting that additional factors influence DDR pathway dependencies in ARMS. In line with the elimusertib phase I/II clinical trial data showing lack of response in 7 out of 11 patients with ATM aberrations, we also did not find *ATM* loss to be associated with increased ATR inhibitor sensitivity in ARMS cells. Pharmacological inhibition of DNA damage signaling kinases exhibited a specific response profile, with ATR- selective inhibitors showing enhanced replication stress-dependent anti-tumor activity. Notably, CHK1, a downstream target of ATR, is inhibited by prexasertib, which is currently being clinically investigated in combination with chemotherapy for patients with relapsed rhabdomyosarcoma (NCT04095221). Given their varied potency and selectivity, it is possible that other selective DNA damage signaling inhibitors can also effectively target replication stress-induced dependencies in rhabdomyosarcoma. Because ATR is also activated by specific DNA structures such DNA–RNA hybrid R-loops, which can be the cause of oncogene-induced DNA replication stress[31], the preferential activity of ATR inhibitors in PAX3-FOXO1-expressing cells may also be due to the formation of such structures. We provide evidence that PAX3-FOXO1 expression, at least in part, contributes to replication stress and sensitivity to ATR inhibition, which is consistent with previous reports of fusion oncogene-induced replication stress in Ewing sarcoma[30,31].

MYCN has been described as a direct target of PAX3-FOXO1 and is itself a potent inducer of replication stress[61]. High MYCN expression was also detected in PAX3-FOXO1-expressing cells and was positively associated with ATR inhibitor sensitivity, but ectopic MYCN expression did not lead to increased ATR inhibitor sensitivity. Furthermore, ATR inhibitors showed higher antitumor activity in a PDX harboring a PAX7-FOXO1 fusion compared to a PDX from the same patient with a *MYCN* amplification. Thus, MYCN does not seem to contribute to ATR inhibitor sensitivity in ARMS to the same extend as it does in other tumor entities.

ATR is essential for intra-S phase and G2/M checkpoint activation[13,16,25,32]. When checkpoints are constitutively active, cells can undergo checkpoint adaptation to continue proliferating despite the presence of DNA damage[62,63]. We anticipate that susceptibility to ATR inhibitors may also depend on tumor-specific mechanisms of checkpoint adaptation. CHK1 and CDK1 can promote checkpoint adaptation by mediating forced mitotic entry[64,65]. Inhibition of ATR could exacerbate the effect of checkpoint adaptation by suppressing checkpoint activation. Consistently, we observed accumulation of cells in mitosis and increased activation of CDK1 targets in our phosphoproteomic profiling after ATR inhibition. In line with checkpoint adaptation promoting DNA damage accumulation and genomic instability[63], we observed high degrees of genomic instability in PAX3-FOXO1-expressing cells treated with ATR inhibitors. Intriguingly, PAX3-FOXO1 can itself promote checkpoint adaptation in rhabdomyosarcoma cells through induction of PLK1 expression, which in turn activates CDK1 and forces mitotic entry[66]. It is tempting to speculate that PAX3-FOXO1-induced checkpoint adaptation may also influence ATR inhibitor sensitivity.

Even though results of clinical trials with ATR inhibitors in adults have shown promising single agent antitumor activity in various tumor entities, some patients progress or relapse after some time[67,67]. Thus, identifying molecular mechanisms of ATR inhibitor resistance is of paramount clinical importance, as it may enable the identification of clinical biomarkers that help predict ATR inhibitor susceptibility and can be used to monitor resistance development. Our genome wide CRISPRa screen and models of ATR inhibitor resistance identified the RAS-MAPK pathway and its downstream effectors, the *FOS* family of transcription factors, as modulators of ATR sensitivity. How *FOS* gene family expression leads to reduced steady-state replication stress, is still unresolved (Fig. 7h). A study in osteosarcoma showed that expression of *FOS* protects cells from replication stress by inducing CHK1 and facilitates transformation by RAS-MAPK[68]. Based on our findings and previous reports, it is tempting to speculate that pharmacological RAS-MAPK inhibition may enhance ATR inhibitor sensitivity or delay onset of resistance in ARMS.

In conclusion, we here present preclinical evidence supporting a molecularly targetable therapeutic option for ARMS, for which current treatment options have been exhausted and prognosis remains dismal. Our findings warrant the future investigation of ATR inhibitors in clinical trials, such as the currently undergoing phase I/II trial of BAY 1895344 (Elimusertib) in relapsed PAX3-FOXO1-expressing rhabdomyosarcoma (NCT05071209). We hope that our in-depth analysis of molecular factors influencing ATR inhibitor sensitivity will help guide predictive biomarker development.

Methods

Study design

The purpose of this study was to examine the effects of ATR inhibition in preclinical models of rhabdomyosarcoma and identify potential biomarkers to select patients that could benefit from small molecule ATR inhibitor treatment. We first determined the inhibitory activity of the ATR inhibitors in rhabdomyosarcoma cell models, and compared these cells based on known determinants of ATR inhibition sensitivity, as well as PAX3-FOXO1, a molecular feature of ARMS. We analyzed the effects of AZD6738 treatment on genomic instability (including double strand break formation, micronucleation, and apoptosis) and on protein phosphorylation. This study was performed following the guidelines recommended by Carola A.S. Arndt for childhood and adolescent tumors, namely five to eight cell lines per disease, for which we validated the expression of the target gene, included 72 h IC_{50} determination to each drug, and explored potential two-drug combinations[69]. Outliers were not excluded unless technical errors were present. For the CRISPRa screen, we used only one cell line and at least three independent sgRNAs per gene. All sgRNAs of interest were validated in independent experiments in two cell models. For the analysis of phosphoproteomic changes after ATR inhibition, we used three independently grown biological replicates of the same rhabdomyosarcoma cell line. For in vivo testing, sample size was decided based on previous experience with the models. Animals euthanized before the end of the experiment, due to excessive tumor growth or loss of body weight, were included in the analysis.

Reagents

All reagents were obtained from Carl Roth (Karlsruhe, Germany) unless otherwise indicated. Oligonucleotide primers were obtained from Eurofins Genomics (Luxemburg, Luxemburg, complete sequence in Supplementary Table 1). A list of antibodies and their catalog numbers can be found in Supplementary Table 2. AZD6738 (ceralasertib) was provided by Astra Zeneca (Cambridge, UK). BAY 1895344 (elimusertib) was provided by Bayer AG. All drugs were dissolved in Dimethylsulfoxid (DMSO) and stored at 10 mM concentrations at −20 °C.

Plasmid constructs

Human *PAX3-FOXO1* cDNA was PCR-amplified and isolated from a plasmid gifted by Prof. Beat Schäfer. *PAX3-FOXO1* cDNA was cloned into pENTR1A (Thermo Fisher) using the restriction enzymes SalI and NotI (New England Biolabs) and cloned into a pInducer20 (Addgene #44012) using the Gateway strategy and the manufacturer's protocol (Thermo Fisher). pLKO.1 shRNA plasmids targeting BRCA1 (TRCN0000009823, TRCN0000010305, TRCN0000039834), ATR (TRCN0000010301, TRCN0000039614, TRCN0000039615, TRCN0000039616) and control targeting GFP (shGFP) were obtained from the RNAi Consortium (Broad Institute). Plasmid containing an inducible shRNA targeting PAX3-FOXO1 (cloned in the pRSI backbone) were a kind gift from Prof. Beat Schäfer.

Cell culture

Rh41, Kym1, and Rh18 cells were a kind gift from Prof. Simone Fulda. Rh5, RMS and KFR were a kind gift from Prof. Beat Schäfer. The remaining human tumor cell lines were obtained from the American Type Culture Collection (ATCC, Manassas, Virginia). The absence of *Mycoplasma sp.* contamination was determined using a Lonza (Basel, Switzerland) MycoAlert system. Rh4, Rh5, Rh30, Rh41, RMS, KFR, RD, T174, TE381.T, C2C12, 5838, A4573, CHP, JR, SB, SK-N-MC, TC-71 and HEK293T cell lines were cultured in Dulbecco's Modified Eagle's Medium (DMEM, Thermo Fisher, Waltham, Massachusetts, USA) supplemented with 10% fetal calf serum (Thermo Fisher) and penicillin/streptomycin (Thermo Fisher). CADO-ES1, Rh18, and Kym1 cells were cultured in Roswell Park Memorial Institute (RPMI)−1640 (Thermo Fisher) supplemented with 10% fetal calf serum and penicillin/streptomycin. Twice per week, cells were washed with phosphate-buffered saline (PBS), incubated in trypsin (Thermo Fisher) for five minutes sedimented at 500 g for 5 min and a fraction was cultured in fresh media. Cells were kept in culture for a maximum of 30 passages. Resuspended cells were counted by mixing 1:1 with 0.02 % trypan blue in a BioRad (Hercules, CA, USA) TC20 cell counter.

Human primary myoblasts were established from muscle biopsies obtained from M. vastus lateralis and M. triceps brachii. Volunteers were a 41F (Myo1), 32M (Myo2), 44F (Myo3), 52F (Myo4), and 21F (Myo5) who came to the hospital with a diagnosis (myalgia, cramps, myalgia, mialgya and family history of myopathy, respectively), but had no myopathology. All donors provided informed consent, and the myoblast isolation was done at the HELIOS Hospital Berlin Buch (Berlin, Germany) with the approval by the regulatory agencies (Ethics committee of Charité Universitätsmedizin Berlin, in compliance with the Declaration of Helsinki, approval number EA2/175/17). Myoblasts were grown in Skeletal Muscle Growth Medium (Provitro, Berlin, Germany) without antibiotics. Contamination of myoblast cultures with fibroblast was assessed by anti-desmin staining and was always below 5%.

Lentiviral transduction

Lentivirus were produced as previously described[70]. In short, HEK293T cells were transfected using TransIT-LT1 (Mirus, Madison, Wisconsin, USA) in a 2:1:1 ratio of lentiviral plasmid, psPAX2, and pMD2.G plasmids following the TransIT-LT1 manufacturer's protocol. Viral supernatant was collected 48 and 72 h after transfection, pooled, filtered, and stored at −80 °C. Cells were transduced for one day in the presence of 8 μg/mL polybrene (Sigma Aldrich).

CRISPRa screening and sequencing

The genome-wide CRISPRa screen was performed as described in Konermann et al.[50]. Briefly, Rh4 cells were transduced with the lentiMPH v2 plasmid (Addgene #89308) and selected with hygromycin for 10 days (Thermo Fisher). Next, cells were transduced with the sgRNA library at a multiplicity of infection (MOI) of <0.3, ensuring at least 500 cells to be transduced with each sgRNA-encoding plasmid on average. After selection with blasticidin (Thermo Fisher) for 7 days, cells were separated in two groups, one group was incubated in the presence of AZD6738 at 750 nM concentration and the other group was incubated in the presence of DMSO. Genomic DNA was extracted and the sgRNA amplified using PCR and barcoded for Illumina sequencing. Sequencing was performed on a NextSeq500 with Mid Output, with a read length of 1 × 81 bp +8 bp Index and 20% PhiX Control v3. Samples were demultiplexed using flexbar[71] and analyzed using MAGeCK (v. 0.5.6)[72]. Pathway analysis was performed using the R package msigdbr (R version 4.0.3; RStudio v1.3.1093; msigdbr v.7.4.1), providing a ranked list of genes and log-fold change and selecting the hallmark pathways from MSigDB[73,74].

Cell viability

Cell viability was assessed using CellTiter-Glo (Promega, Madison, Wisconsin, USA). Briefly, 1000 cells were seeded in white, flat-bottom, 96-well plates (Corning, Corning, NY, USA). After 24 h, drugs were added to the medium, and cells were incubated for 72 h. CellTiter-Glo luminescent reagent was added according to the manufacturers protocol, and the luminescence signal measured on a Synergy LX (Agilent, California, USA) with BioTek Gen5 (v3.08). To evaluate if a combination of drugs is synergistic, cells were simultaneously treated with varying concentrations of drugs, and cell viability was measured with CellTiter-Glo. Synergism scores were obtained using the R package SynergyFinder (v2.2.4)[75].

Immunoblotting

Whole-cell protein lysates were prepared by lysing cells in Radioimmunoprecipitation assay buffer (RIPA) supplemented with cOmplete Protease inhibitor (Roche, Basel, Switzerland) and PhosphStop (Roche). Protein concentrations were determined by bicinchoninic acid assay (BCA, Thermo Fisher). 10 μg of protein were denatured in Laemmli buffer at 95 °C for 5 min. Lysates were loaded onto 16% or 10% Tris-Glycin (Thermo Fisher) for gel electrophoresis depending on the protein sizes of interest. Proteins were transferred onto Polyvinylidenfluorid (PVDF) membranes (Roche), blocked with 5% dry milk for 1 h, and incubated with primary antibodies overnight at 4 °C, then secondary antibodies for 1 h at room temperature. Chemiluminescent signal was detected using Enhanced chemiluminescence (ECL) Western Blotting Substrate (Thermo Fisher) and a Fusion FX7 imaging system (Vilber Lourmat, Marne-la-Vallée, France) using ImageLab (v6.0.1). Quantification was performed with ImageJ (v.1.52a).

Immunofluorescence

Cells were grown at the desired confluency on a glass coverslide for 24 h (micronuclei quantification) and treated with 1000 ng/mL doxycycline for another 48 h (for the corresponding experiment). Cells were washed with PBS three times and fixed for 10 min with 4% paraformaldehyde, washed with PBS three times and permeabilized with PBS containing 0.1% Triton-X100. For micronuclei detection, cells were mounted on a slide with DAPI-containing mounting media (Vectashield, Vec-H-1000). For immunofluorescence, cells were blocked for 40 min with 5% BSA in PBS, incubated overnight at 4 °C with the primary antibody, washed three times with PBS-T (0.05% Tween-20 in PBS), incubated for 1 h in the dark at room temperature with the secondary antibody, washed three times with PBS-T and mounted on a slide with DAPI-containing mounting media. Cells were imaged using an ECHO Revolve microscope and quantified using ImageJ (v.1.52a).

RT-qPCR

RNA from cell lines was extracted using RNeasy mini kit (QIAGEN). Synthesis of cDNA was performed using Transcription First Strand cDNA Synthesis kit (Roche). 50 ng of cDNA were combined with the corresponding primers (Supplementary Table 1), and SG qPCR Master Mix (Roboklon, Berlin, Germany), keeping the mixture and cycling conditions recommended by the manufacturer. DNA content was

measured using a CFX Connect Real-Time PCR detection system (BioRad) with the software CFX Manager (v3.1).

Fluorescence-activated cell sorting (FACS)

For cell cycle analysis, cells were incubated with 5-Ethynyl-2´-deoxyuridine (EdU) for 2 h and fluorescent labeling was performed with the Click-IT EdU Alexa Fluor 488 Flow Cytometry Assay kit (Thermo Fisher), according to the manufacturer's description. Terminal deoxynucleotidyl transferase dUTP nick end labeling (TUNEL) was performed using the APO-BrdU TUNEL Assay Kit (Thermo Fisher), according to the manufacturer's descriptions. Cell death was assessed by measuring caspase 3 cleavage using a CellEvent Caspase3/7 Green Flow Cytometry kit (Thermo Fisher), according to the manufacturer's descriptions. Stained cells were measured on a BD LSR Fortessa flow cytometer (BD Biosciences, Franklin Lakes, NJ, USA) with the BD FACS Diva (v8.0.1) and analyzed with FlowJo (v10.6.2).

Homologous recombination activity assay

All the plasmids were obtained from Addgene (pDRGFP #26475pCBA-SceI #26477; pCAG-FALSE #89689; pCAGGS-mCherry #41583). The protocol was adapted from the plasmid depositors'[76,77]. Briefly, cells were co-transfected with pCBA-SceI and pDRGFP to analyze homologous recombination. As a negative control, pCBA-SceI was substituted with the empty backbone pCAG-FALSE. Transfection efficiency was calculated using cells transfected with pCAGGS-mCherry. Two days after transfection, cells were trypsinized, washed twice with PBS and fluorescence measured with flow cytometry. When necessary, cells were treated with 750 nM AZD6738 for five days prior to flow cytometry analysis.

Phosphoproteomics sample preparation

Rh30 cells were cultured for two weeks in the presence of stable isotope labeling with amino acids (SILAC) media in DMEM, 10% dialyzed fetal calf serum, 1% Proline, 1% Glutamine, 0.025% ^{8}Lysine, and ^{10}Arginine ("Heavy") or ^{0}Lysine and ^{0}Arginine ("Light"). After labeling, cells were incubated in the presence of AZD6738 750 nM or DMSO for two hours in biological triplicates. Cells were harvested, resuspended and combined in 400 µL of 8 M urea and 0.1 M Tris-HCl, pH 8. Proteins were reduced in 10 mM dithiothreitol (DTT) at room temperature for 30 min and alkylated with 50 mM iodoacetamide (IAA) at room temperature for 30 min in the dark. Proteins were first digested by lysyl endopeptidase (LysC) (Wako Pure Chemical Industries, Ltd., Osaka, Japan) at a protein-to-LysC ratio of 100:1 (w/w) at room temperature for 3 h. Then, the sample solution was diluted to final concentration of 2 M urea with 50 mM ammonium bicarbonate (ABC). Trypsin (Promega) digestion was performed at a protein-to-trypsin ratio of 100:1 (w/w) under constant agitation at room temperature for 16 h. Tryptic digests corresponding to 200 µg protein per condition were desalted with big C18 Stage Tips packed with 10 mg of ReproSil-Pur 120 C18-AQ 5 µm resin (Dr. Maisch GmbH, Ammerbuch, Germany). Peptides were eluted with 200 µL of loading buffer (80% ACN (v/v) and 6% TFA (v/v). Phosphopeptides were enriched using a microcolumn tip packed with 0.5 mg of TiO_2 (Titansphere, GL Sciences, Tokyo, Japan)[78]. The TiO_2 tips were equilibrated with 20 µL of the loading buffer via centrifugation at 100 × *g*. 50 µL of the sample solution was loaded on a TiO_2 tip via centrifugation at 100 × *g* and this step was repeated until the sample solution was loaded. The TiO_2 column was washed with 20 µL of the loading buffer, followed by 20 µL of washing buffer (50% ACN (v/v) and 0.1% TFA (v/v)). The bound phosphopeptides were eluted using successive elution with 30 µL of elution buffer 1 (5% ammonia solution), followed by 30 µL of elution buffer 2 (5% piperidine)[79]. Each fraction was collected into a fresh tube containing 30 µL of 20% formic acid. 3 µL of 100% formic acid was added to further acidify the samples. The phosphopeptides were desalted with C18 Stage Tips prior to nanoLC-MS/MS analysis.

NanoLC-MS/MS analysis

Peptides were separated on a 2 m monolithic column (MonoCap C18 High Resolution 2000 (GL Sciences), 100 µm internal diameter × 2000 mm at a flow rate of 300 nL/min with a 5–95% acetonitrile gradient on an EASY-nLC II system (Thermo Fisher Scientific). 240 min gradient was performed for phosphoproteome analyses. A Q Exactive plus instrument (Thermo Fisher Scientific) was operated in the data dependent mode with a full scan in the Orbitrap followed by top 10 MS/MS scans using higher-energy collision dissociation (HCD). For whole proteome analyses, the full scans were performed with a resolution of 70,000, a target value of 3×10^6 ions, and a maximum injection time of 20 ms. The MS/MS scans were performed with a 17,500 resolution, a 1×10^6 target value, and a 20 ms maximum injection time. For phosphoproteome analyses, the full scans were performed with a resolution of 70,000, a target value of 3×10^6 ions, and a maximum injection time of 120 ms. The MS/MS scans were performed with a 35,000 resolution, a 5×10^5 target value, and a 160 ms maximum injection time. Isolation window was set to 2 and normalized collision energy was 26.

Raw data were analyzed and processed using MaxQuant (v1.5.1.2)[80]. Search parameters included two missed cleavage sites, fixed cysteine carbamidomethyl modification, and variable modifications including L-[$^{13}C_6$,$^{15}N_4$]-arginine, L-[$^{13}C_6$,$^{15}N_2$]-lysine, methionine oxidation, N-terminal protein acetylation, and asparagine/glutamine deamidation. In addition, phosphorylation of serine, threonine, and tyrosine were searched as variable modifications for phosphoproteome analysis. The peptide mass tolerance was 6 ppm for MS scans and 20 ppm for MS/MS scans. Database search was performed using Andromeda[81] against uniprot-human 2014-10 with common contaminants. False discovery rate (FDR) was set to 1% at both peptide spectrum match (PSM) and protein level. The 're-quantify' and 'match between runs' functions were enabled. Phosphorylation sites were ranked according to their phosphorylation localization probabilities (P) as class I ($P > 0.75$), class II ($0.75 > P > 0.5$), and class III sites ($P < 0.5$), and only class I sites were used for further analyses. Data normalization was performed using the default settings of the R package DEP[82]. In short, peptides not identified in at least two replicates in both conditions were removed. Intensity values were normalized based on the variance stabilizing transformation, and missing values were imputed using random draws from a Gaussian distribution centered around a minimal value ($q = 0.01$). For pathway enrichment analysis, we used a single sample gene set enrichment analysis (ssGSEA) as previously described[38], ranking genes according to their fold change. For gene ontology (GO) analysis, we followed the ClusterProfiler R package (v3.16.1)[83]. *P*-values were calculated using hypergeometric distribution (one-sided Fisher exact test) and corrected for multiple comparisons (Holm–Bonferroni method), selecting phosphopeptides with a fold change >1 or <−1 and a FDR < 0.01, and reporting the top 10 GO terms enriched in the subset.

Patient-derived xenograft (PDX) treatment

The establishment of PDX models was conducted as previously described[84] in collaboration with Experimental Pharmacology & Oncology GmbH (EPO, Berlin, Germany). Briefly, a tumor fragment was serially transplanted in mice at least three times prior to the experiments. All experiments were conducted according to the institutional animal protocols and the national laws and regulations and approved by the Charité University Medicine and MSKCC IACUC. Fusion status was determined by PCR at time of diagnosis. Tumor fragments from rhabdomyosarcoma patients were transplanted into NOD.Cg-*Prkdc*^{scid} *Il2rg*^{tm1Sug}/*JicTac* female mice between 6 and 8 weeks old (Taconic, Rensselaer, NY, USA) or NSG-H (NOD.Cg-*Prkdc*^{scid} *Hprt*^{em1Mvw} *Il2rg*^{tm1Wjl}/*MwwJ*; for the PAX7-FOXO1 ARMS PDXs) male and female mice mix between 6 and 8 weeks old. Animals were IVC housed under sterile and standardized conditions (22 °C +/−1 °C, 50% relative humidity, 12-hour

light-dark cycle, autoclaved food, bedding material and tap water ad libitum). Tumor growth was monitored with caliper measurements. Tumor volume was calculated with the formula length x width^2/2. PDX were serially transplanted in mice at least three times prior to the experiments. Mice were randomized into four groups with at least 3 mice to receive AZD6738 (50 mg/kg day, oral), olaparib (50 mg/kg day, oral), a combination of AZD6738 and olaparib, or vehicle. For in vivo treatment, AZD6738 was dissolved in DMSO at 62.5 mg/ml and mixed 1:10 in 40% propylene glycol and 50% sterile water, resulting in a final AZD6738 concentration of 6.25 mg/ml. Olaparib was dissolved in 4% DMSO, 30% polyethylene glycol 300 and sterile water. For the BAY 1895344 study, mice were administered 40 mg/kg body weight on a 3 days on/ 4 days off regime twice daily (orally). BAY 1895344 was dissolved in 60% polyethylene glycol 400, 10% ethanol, and 30% water to a 4 mg/ml solution. Ifosfamide was dissolved in 0.9% sodium chloride and administered intravenously at a 50 mg/mL concentration up to 80 mg/kg body weight per day twice weekly. Vincristine was dissolved in 0.9% sodium chloride and administered daily intravenously at 1 mg/mL up to 1 mg/kg body weight per day. Solutions in which the drugs were dissolved were used as vehicle controls respectively. Mice were sacrificed by cervical dislocation once the tumor volume exceeded 2000 mm^3 or body weight loss was higher than 10%. For the toxicity study, blood was drawn, and blood count was analyzed by Synlab (Berlin, Germany). Organ tissue was collected, fixed with formalin and embedded into paraffin, sliced, and stained with hematoxylin & eosin following the standard diagnostics protocol. For immunohistochemistry staining of cleaved caspase 3 and Ki67, snap frozen tumor fragments were cut and stained following the standard protocol using the antibodies listed in Supplementary Table 2.

RNA-seq of ATR inhibitor resistant cells

To generate cells resistant to ATR inhibitors, cells were cultured with an IC10 of the corresponding ATR inhibitor for at least three passages. The concentration was doubled for a total of four months. At that point, pellets were collected and prepared for RNA-seq using TruSeq Standard mRNA library prep according to the manufacturer's instructions. Samples were sequenced using a NextSeq500 mid output using pair ended reads (2x75bp). Reads were filtered by sequence quality using trimGalore!, aligned to the reference genome (hg19 [https://www.ncbi.nlm.nih.gov/assembly/GCF_000001405.13/]) using STAR[85] and counted using HTSeq[86]. For pathway analysis, we used the package gage and selected the hallmark pathways from MSigDB[73,74].

Statistics and reproducibility

All statistical tests were done using GraphPrism7 (student's two-sided t-test) or were part of the R package used for the analysis (MAGeCK-VISPR, DEP, CePa, msigdbr, gage). All computational analyses were performed using Python 3.7 (MAGeCK-VISPR v.0.5.6, TrimGalore! v.0.6.1, STAR v.2.7.9a, HTSeq v.1.99.2) or RStudio v.1.3.1093 (R v.4.0.3, biomaRt v.2.44.4, CePa v.0.7.0, clusterProfiler v.3.16.1, DEP v.1.10.0, gage v.2.38.3, msigdbr v.7.4.1, org.Hs.eg.db v.3.11.4, synergyfinder v.2.2.4, tidyverse v.1.3.1).

Western immunoblots (in Figs. 2a, b, h, i, 3d, e, 4a, h, 5g, h, l, 6g, h, Supplementary Figs. 2a, e, 4a, 5a, 6a, 8f, g, and 10a) were done in one independent experiment, but include different biologically independent cell models (Figs. 2h, i, 3d, e, 5g, h and Supplementary Figs. 6f, g, and Fig. 5a), two independent small molecule inhibitors (Figs. 2a, b, h, i, 3d, e, and 6g, h) or include at least three independent shRNA or sgRNA, respectively (Figs. 4h, 5g, h, l and Supplementary Figs. 2a, e, 4a, 8f, g). Immunofluorescence experiments (Figs. 2d, 4b) were repeated three times. For micronucleation (Fig. 2d, e), each replicate includes 50 cells. Histochemistry experiments (Fig. 7h and Supplementary Fig. 10a, p) were performed once. Quantification of immunohistochemistry (Fig. 7i, j) was performed in 10 representative 275 μm × 275 μm sections per group.

Reporting summary

Further information on research design is available in the Nature Research Reporting Summary linked to this article.

Data availability

The reference genome hg19 [https://www.ncbi.nlm.nih.gov/assembly/GCF_000001405.13/] used in this study is publicly available. The proteomics data which support the findings in this study have been deposited in the ProteomeXchange Consortium via jPOST partner repository with the dataset identifier JPST001683 and the accession code identifier PXD035131.

The CRISPR reads generated in this study are available from the NCBI Sequence Read Archive (SRA) Sequence Read Archive (SRA) under the BioProject code PRJNA856804. The RNA-seq reads generated in this study have been deposited in the SRA, accessible under the BioProject code PRJNA856799. Source data are provided with this paper.

References

1. Ognjanovic, S., Linabery, A. M., Charbonneau, B. & Ross, J. A. Trends in childhood rhabdomyosarcoma incidence and survival in the United States, 1975–2005. *Cancer* **115**, 4218–4226 (2009).
2. Douglass, E. C. et al. A specific chromosomal abnormality in rhabdomyosarcoma. *Cytogenet Cell Genet.* **45**, 148–155 (1987).
3. Douglass, E. C. et al. Variant translocations of chromosome 13 in alveolar rhabdomyosarcoma. *Genes Chromosomes Cancer* **3**, 480–482 (1991).
4. Keller, C. et al. Alveolar rhabdomyosarcomas in conditional Pax3:Fkhr mice: Cooperativity of Ink4a/ARF and Trp53 loss of function. *Genes Dev.* **18**, 2614–2626 (2004).
5. Perkins, S. M., Shinohara, E. T., DeWees, T. & Frangoul, H. Outcome for children with metastatic solid tumors over the last four decades. *PLoS One* **9**, e100396 (2014).
6. Crist, W. et al. The third intergroup rhabdomyosarcoma study. *J. Clin. Oncol.* **13**, 610–630 (1995).
7. Shern, J. F. et al. Comprehensive genomic analysis of rhabdomyosarcoma reveals a landscape of alterations affecting a common genetic axis in fusion-positive and fusion-negative tumors. *Cancer Discov.* **4**, 216–231 (2014).
8. Cheung, N. K. & Dyer, M. A. Neuroblastoma: Developmental biology, cancer genomics, and immunotherapy. *Nat. Rev. Cancer* **13**, 397–411 (2013).
9. Hartwell, L. H., Szankasi, P., Roberts, C. J., Murray, A. W. & Friend, S. H. Integrating genetic approaches into the discovery of anticancer drugs. *Science* **278**, 1064–1068 (1997).
10. Farmer, H. et al. Targeting the DNA repair defect in BRCA mutant cells as a therapeutic strategy. *Nature* **434**, 917–921 (2005).
11. Fong, P. C. et al. Inhibition of poly(ADP-ribose) polymerase in tumors from BRCA mutation carriers. *N. Engl. J. Med.* **361**, 123–134 (2009).
12. Kotsantis, P., Petermann, E. & Boulton, S. J. Mechanisms of oncogene-induced replication stress: Jigsaw falling into place. *Cancer Discov.* **8**, 537–555 (2018).
13. Saldivar, J. C., Cortez, D. & Cimprich, K. A. The essential kinase ATR: Ensuring faithful duplication of a challenging genome. *Nat. Rev. Mol. Cell Biol.* **18**, 622–636 (2017).
14. Bass, T. E. et al. ETAA1 acts at stalled replication forks to maintain genome integrity. *Nat. Cell Biol.* **18**, 1185–1195 (2016).
15. Haahr, P. et al. Activation of the ATR kinase by the RPA-binding protein ETAA1. *Nat. Cell Biol.* **18**, 1196–1207 (2016).

16. Buisson, R., Boisvert, J. L., Benes, C. H. & Zou, L. Distinct but concerted roles of ATR, DNA-PK, and Chk1 in countering replication stress during S phase. *Mol. Cell* **59**, 1011–1024 (2015).
17. Feijoo, C. et al. Activation of mammalian Chk1 during DNA replication arrest: A role for Chk1 in the intra-S phase checkpoint monitoring replication origin firing. *J. Cell Biol.* **154**, 913–923 (2001).
18. Fokas, E. et al. Targeting ATR in DNA damage response and cancer therapeutics. *Cancer Treat. Rev.* **40**, 109–117 (2014).
19. Kwok, M. et al. Synthetic lethality in chronic lymphocytic leukaemia with DNA damage response defects by targeting the ATR pathway. *Lancet* **385**, S58 (2015).
20. Kwok, M. et al. ATR inhibition induces synthetic lethality and overcomes chemoresistance in TP53- or ATM-defective chronic lymphocytic leukemia cells. *Blood* **127**, 582–595 (2016).
21. Henssen, A. G. et al. Therapeutic targeting of PGBD5-induced DNA repair dependency in pediatric solid tumors. *Sci. Transl. Med.* https://doi.org/10.1126/scitranslmed.aam9078 (2017).
22. Foote, K. M., Lau, A. & Nissink, J. W. Drugging ATR: Progress in the development of specific inhibitors for the treatment of cancer. *Future Med. Chem.* **7**, 873–891 (2015).
23. Morgado-Palacin, I. et al. Targeting the kinase activities of ATR and ATM exhibits antitumoral activity in mouse models of MLL-rearranged AML. *Sci. Signal* **9**, ra91 (2016).
24. Middleton, F. K. et al. Common cancer-associated imbalances in the DNA damage response confer sensitivity to single agent ATR inhibition. *Oncotarget* **6**, 32396–32409 (2015).
25. Karnitz, L. M. & Zou, L. Molecular pathways: Targeting ATR in Cancer Therapy. *Clin. Cancer Res.* **21**, 4780–4785 (2015).
26. Chen, T. et al. Development of pharmacodynamic biomarkers for ATR inhibitors. *Mol. Oncol.* **9**, 463–472 (2015).
27. Roeschert, I. et al. Combined inhibition of Aurora-A and ATR kinase results in regression of MYCN-amplified neuroblastoma. *Nat. Cancer* **2**, 312–326 (2021).
28. Wengner, A. M. et al. The novel ATR inhibitor BAY 1895344 is efficacious as monotherapy and combined with DNA damage-inducing or repair-compromising therapies in preclinical cancer models. *Mol. Cancer Ther.* **19**, 26–38 (2020).
29. Yap, T. A. et al. First-in-human trial of the oral ataxia telangiectasia and RAD3-related (ATR) inhibitor BAY 1895344 in patients with advanced solid tumors. *Cancer Discov.* **11**, 80–91 (2021).
30. Nieto-Soler, M. et al. Efficacy of ATR inhibitors as single agents in Ewing sarcoma. *Oncotarget* **7**, 58759–58767 (2016).
31. Gorthi, A. et al. EWS-FLI1 increases transcription to cause R-loops and block BRCA1 repair in Ewing sarcoma. *Nature* **555**, 387–391 (2018).
32. Cimprich, K. A. & Cortez, D. ATR: An essential regulator of genome integrity. *Nat. Rev. Mol. Cell Biol.* **9**, 616–627 (2008).
33. Zeman, M. K. & Cimprich, K. A. Causes and consequences of replication stress. *Nat. Cell Biol.* **16**, 2–9 (2014).
34. Zhang, C. Z. et al. Chromothripsis from DNA damage in micronuclei. *Nature* **522**, 179–184 (2015).
35. Xu, B. et al. Replication stress induces micronuclei comprising of aggregated DNA double-strand breaks. *PLoS One* **6**, e18618 (2011).
36. Gurley, L. R., Walters, R. A. & Tobey, R. A. Cell cycle-specific changes in histone phosphorylation associated with cell proliferation and chromosome condensation. *J. Cell Biol.* **60**, 356–364 (1974).
37. Lakin, N. D., Hann, B. C. & Jackson, S. P. The ataxia-telangiectasia related protein ATR mediates DNA-dependent phosphorylation of p53. *Oncogene* **18**, 3989–3995 (1999).
38. Krug, K. et al. A curated resource for phosphosite-specific signature analysis. *Mol. Cell Proteom.* **18**, 576–593 (2019).
39. Downing, K. H. Structural basis for the interaction of tubulin with proteins and drugs that affect microtubule dynamics. *Annu. Rev. Cell Dev. Biol.* **16**, 89–111 (2000).
40. Gatei, M. et al. Ataxia telangiectasia mutated (ATM) kinase and ATM and Rad3 related kinase mediate phosphorylation of Brca1 at distinct and overlapping sites. In vivo assessment using phospho-specific antibodies. *J. Biol. Chem.* **276**, 17276–17280 (2001).
41. Helt, C. E., Cliby, W. A., Keng, P. C., Bambara, R. A. & O'Reilly, M. A. Ataxia telangiectasia mutated (ATM) and ATM and Rad3-related protein exhibit selective target specificities in response to different forms of DNA damage. *J. Biol. Chem.* **280**, 1186–1192 (2005).
42. Kang, Y. et al. Protein phosphatase 5 is necessary for ATR-mediated DNA repair. *Biochem. Biophys. Res Commun.* **404**, 476–481 (2011).
43. Jeggo, P. A., Pearl, L. H. & Carr, A. M. DNA repair, genome stability and cancer: A historical perspective. *Nat. Rev. Cancer* **16**, 35–42 (2016).
44. Beckta, J. M. et al. Mutation of the BRCA1 SQ-cluster results in aberrant mitosis, reduced homologous recombination, and a compensatory increase in non-homologous end joining. *Oncotarget* **6**, 27674–27687 (2015).
45. Cortez, D., Wang, Y., Qin, J. & Elledge, S. J. Requirement of ATM-dependent phosphorylation of brca1 in the DNA damage response to double-strand breaks. *Science* **286**, 1162–1166 (1999).
46. Lloyd, R. L. et al. Combined PARP and ATR inhibition potentiates genome instability and cell death in ATM-deficient cancer cells. *Oncogene* **39**, 4869–4883 (2020).
47. Kim, H. et al. Targeting the ATR/CHK1 Axis with PARP inhibition results in tumor regression. *Clin Cancer Res.* **23**, 3097–3108 (2017).
48. Hanna, J. A. et al. PAX3-FOXO1 drives miR-486-5p and represses miR-221 contributing to pathogenesis of alveolar rhabdomyosarcoma. *Oncogene* **37**, 1991–2007 (2018).
49. Vasan, N., Baselga, J. & Hyman, D. M. A view on drug resistance in cancer. *Nature* **575**, 299–309 (2019).
50. Konermann, S. et al. Genome-scale transcriptional activation by an engineered CRISPR-Cas9 complex. *Nature* **517**, 583–588 (2015).
51. Shaulian, E. & Karin, M. AP-1 in cell proliferation and survival. *Oncogene* **20**, 2390–2400 (2001).
52. Whitmarsh, A. J. & Davis, R. J. Transcription factor AP-1 regulation by mitogen-activated protein kinase signal transduction pathways. *J. Mol. Med.* **74**, 589–607 (1996).
53. Vitorino, F. N. L. et al. FGF2 antiproliferative stimulation induces proteomic dynamic changes and high expression of FOSB and JUNB in K-Ras-driven mouse tumor cells. *Proteomics* **18**, e1800203 (2018).
54. Vallejo, A. et al. An integrative approach unveils FOSL1 as an oncogene vulnerability in KRAS-driven lung and pancreatic cancer. *Nat. Commun.* **8**, 14294 (2017).
55. Tomicic, M. T. et al. Delayed c-Fos activation in human cells triggers XPF induction and an adaptive response to UVC-induced DNA damage and cytotoxicity. *Cell Mol. Life Sci.* **68**, 1785–1798 (2011).
56. Christmann, M. & Kaina, B. Transcriptional regulation of human DNA repair genes following genotoxic stress: trigger mechanisms, inducible responses, and genotoxic adaptation. *Nucleic Acids Res.* **41**, 8403–8420 (2013).
57. Dillon, M. T. et al. PATRIOT: A phase I study to assess the tolerability, safety, and biological effects of a specific ataxia telangiectasia and Rad3-related (ATR) inhibitor (AZD6738) as a single agent and in combination with palliative radiation therapy in patients with solid tumours. *Clin. Transl. Radiat. Oncol.* **12**, 16–20 (2018).
58. Reaper, P. M. et al. Selective killing of ATM- or p53-deficient cancer cells through inhibition of ATR. *Nat. Chem. Biol.* **7**, 428–430 (2011).
59. Lecona, E. & Fernandez-Capetillo, O. Targeting ATR in cancer. *Nat. Rev. Cancer* **18**, 586–595 (2018).
60. Menezes, D. L. et al. A synthetic lethal screen reveals enhanced sensitivity to ATR inhibitor treatment in mantle cell lymphoma with ATM loss-of-function. *Mol. Cancer Res.* **13**, 120–129 (2015).

61. Mercado, G. E. et al. Identification of PAX3-FKHR-regulated genes differentially expressed between alveolar and embryonal rhabdomyosarcoma: focus on MYCN as a biologically relevant target. *Genes Chromosomes Cancer* **47**, 510–520 (2008).
62. Kato, T. A., Okayasu, R. & Bedford, J. S. Signatures of DNA double strand breaks produced in irradiated G1 and G2 cells persist into mitosis. *J. Cell Physiol.* **219**, 760–765 (2009).
63. Deckbar, D. et al. Chromosome breakage after G2 checkpoint release. *J. Cell Biol.* **176**, 749–755 (2007).
64. Gheghiani, L., Loew, D., Lombard, B., Mansfeld, J. & Gavet, O. PLK1 activation in late G2 sets up commitment to mitosis. *Cell Rep.* **19**, 2060–2073 (2017).
65. Syljuåsen, R. G., Jensen, S., Bartek, J. & Lukas, J. Adaptation to the ionizing radiation-induced G2 checkpoint occurs in human cells and depends on checkpoint kinase 1 and Polo-like kinase 1 kinases. *Cancer Res.* **66**, 10253–10257 (2006).
66. Kikuchi, K. et al. Cell-cycle dependent expression of a translocation-mediated fusion oncogene mediates checkpoint adaptation in rhabdomyosarcoma. *PLoS Genet.* **10**, e1004107 (2014).
67. Thomas, A. et al. Phase I study of ATR inhibitor M6620 in combination with topotecan in patients with advanced solid tumors. *J. Clin. Oncol.* **36**, 1594–1602 (2018).
68. Schulze, J. et al. Fos-dependent induction of Chk1 protects osteoblasts from replication stress. *Cell Cycle* **13**, 1980–1986 (2014).
69. Arndt, C. A. S. *Sarcomas of Bone and Soft Tissues in Children and Adolescents* 1 edn 180 (Springer, 2021).
70. MacArthur, I. C. et al. Prohibitin promotes de-differentiation and is a potential therapeutic target in neuroblastoma. *JCI Insight* https://doi.org/10.1172/jci.insight.127130 (2019).
71. Dodt, M., Roehr, J. T., Ahmed, R. & Dieterich, C. FLEXBAR-flexible barcode and adapter processing for next-generation sequencing platforms. *Biology* **1**, 895–905 (2012).
72. Li, W. et al. MAGeCK enables robust identification of essential genes from genome-scale CRISPR/Cas9 knockout screens. *Genome Biol.* **15**, 554 (2014).
73. Subramanian, A. et al. Gene set enrichment analysis: A knowledge-based approach for interpreting genome-wide expression profiles. *Proc. Natl Acad. Sci. USA* **102**, 15545–15550 (2005).
74. Liberzon, A. et al. The Molecular Signatures Database (MSigDB) hallmark gene set collection. *Cell Syst.* **1**, 417–425 (2015).
75. He, L. et al. Methods for high-throughput drug combination screening and synergy scoring. *Methods Mol. Biol.* **1711**, 351–398 (2018).
76. Pierce, A. J., Johnson, R. D., Thompson, L. H. & Jasin, M. XRCC3 promotes homology-directed repair of DNA damage in mammalian cells. *Genes Dev.* **13**, 2633–2638 (1999).
77. Bennardo, N., Cheng, A., Huang, N. & Stark, J. M. Alternative-NHEJ is a mechanistically distinct pathway of mammalian chromosome break repair. *PLoS Genet.* **4**, e1000110 (2008).
78. Rappsilber, J., Mann, M. & Ishihama, Y. Protocol for micro-purification, enrichment, pre-fractionation and storage of peptides for proteomics using StageTips. *Nat. Protoc.* **2**, 1896–1906 (2007).
79. Kyono, Y., Sugiyama, N., Imami, K., Tomita, M. & Ishihama, Y. Successive and selective release of phosphorylated peptides captured by hydroxy acid-modified metal oxide chromatography. *J. Proteome Res.* **7**, 4585–4593 (2008).
80. Cox, J. & Mann, M. MaxQuant enables high peptide identification rates, individualized p.p.b.-range mass accuracies, and proteome-wide protein quantification. *Nat. Biotechnol.* **26**, 1367–1372 (2008).
81. Cox, J. et al. Andromeda: A peptide search engine integrated into the MaxQuant environment. *J. Proteome Res.* **10**, 1794–1805 (2011).
82. Zhang, X. et al. Proteome-wide identification of ubiquitin interactions using UbIA-MS. *Nat. Protoc.* **13**, 530–550 (2018).
83. Yu, G., Wang, L. G., Han, Y. & He, Q. Y. clusterProfiler: An R package for comparing biological themes among gene clusters. *OMICS* **16**, 284–287 (2012).
84. Timme, N. et al. Small-molecule dual PLK1 and BRD4 inhibitors are active against preclinical models of pediatric solid tumors. *Transl. Oncol.* **13**, 221–232 (2020).
85. Dobin, A. et al. STAR: Ultrafast universal RNA-seq aligner. *Bioinformatics* **29**, 15–21 (2013).
86. Anders, S., Pyl, P. T. & Huber, W. HTSeq—A Python framework to work with high-throughput sequencing data. *Bioinformatics* **31**, 166–169 (2015).

Acknowledgements

We thank Experimental Pharmacology & Oncology GmbH for technical support. We thank Astra Zeneca for providing AZD6738 (ceralasertib) and olaparib for the compassionate use, as well as Emma Dean, Alan Lau, Andrew Pierce and Bienvenú Loembé for the fruitful discussions. We thank Bayer AG for providing BAY1895344 (elimusertib) and support for preclinical study design using that drug. The project that gave rise to these results received the support of a fellowship from "la Caixa" Foundation (ID 100010434). H.D.G. received this fellowship, whith the code is LCF/BQ/EU18/11650037. A.G.H. is supported by the *Deutsche Forschungsgemeinschaft* (DFG, German Research Foundation) – 398299703 and the *Wilhelm Sander Stiftung*. This project has received funding from the European Research Council (ERC) under the European Union's Horizon 2020 research and innovation program (grant agreement No. 949172; A.G.H and H.D.G.). This research was financially supported by the Charité 3R, Charité - Universitätsmedizin Berlin (A.G.H.). A.G.H. is supported by the German Cancer Consortium (DKTK). A.G.H. is a participant in the BIH-Charité Clinical Scientist Program funded by the Charité – *Universitätsmedizin Berlin* and the Berlin Institute of Health. M.V.O. is supported by Cannonball Kids' cancer, the ASCO Conquer Cancer Foundation, and the NIH/NCI via P30 CA008748. This work was supported by the *Deutsche Krebshilfe* (German Cancer Aid) – 70114107 (Mildred-Scheel Professorship), 70113870 and 70113871 (A.G.H.). F.D. is participant in the BIH Charité Junior Clinician Scientist Program funded by the Charité-Universitätsmedizin Berlin and the Berlin Institute of Health at Charité (BIH). We thank the patients and their parents for granting access to the tumor specimen and clinical information that were analyzed in this study.

Author contributions

H.D.G. and A.G.H. contributed to the study design, collection and interpretation of the data and wrote the manuscript. H.D.G., F.P., Y.B., J.v.S., G.I., K.G., K.I., S.M., N.T., R.C.G., I.M., C.Y.C., J.S., C.F., and B.L. performed experiments, analyzed data and reviewed this manuscript. H.D.G., K.He, and K.Ha performed the analysis of the CRISPR screening. D.G., J.R., and V.B. collected and prepared PDX samples. A.M.W., A.E., G.S., P.H., M.K., P.M., M.Se, A.L., F.D., D.H., J.H.S., S.S., D.Y., F.D.L., A.L.K., M.d.V., M.Sc, and M.O. contributed to study design. A.G.H. led the study design, to which all authors contributed.

Funding

Open Access funding enabled and organized by Projekt DEAL.

Competing interests

A.M.W. is employed by Bayer AG. A.G.H. has received research funding from Bayer AG. The remaining authors declare no competing interests.

Additional information

Supplementary information The online version contains supplementary material available at https://doi.org/10.1038/s41467-022-32023-7.

Correspondence and requests for materials should be addressed to Anton G. Henssen.

Peer review information *Nature Communications* thanks Giorgio Galli, Beat Schäfer, and the other, anonymous, reviewer(s) for their contribution to the peer review of this work.

[1]Experimental and Clinical Research Center (ECRC) of the MDC and Charité Berlin, Berlin, Germany. [2]Department of Pediatric Oncology and Hematology, Charité – Universitätsmedizin Berlin, corporate member of Freie Universität Berlin, Humboldt-Universität zu Berlin, Berlin, Germany. [3]Max Delbrück Center for Molecular Medicine, Berlin, Germany. [4]Department of Pediatrics, Memorial Sloan Kettering Cancer Center, New York City, NY, USA. [5]Experimental Pharmacology and Oncology (EPO), Berlin, Germany. [6]Charité - Universitätsmedizin Berlin, Corporate Member of Freie Universität Berlin and Humboldt-Universität zu Berlin, Experimental and Clinical Research Center, Charité Campus Buch, Lindenberger Weg 80, 13125 Berlin, Germany. [7]Bayer AG, Berlin, Germany. [8]Berlin Institute of Health, 10178 Berlin, Germany. [9]Institute of pathology, Charité – Universitätsmedizin Berlin, corporate member of Freie Universität Berlin, Humboldt-Universität zu Berlin, Berlin, Germany. [10]Berlin Institute of Health at Charité – Universitätsmedizin Berlin, BIH Biomedical Innovation Academy, BIH Charité Junior Clinician Scientist Program, Charitéplatz 1, 10117 Berlin, Germany. [11]Department of chemistry, biochemistry and pharmacy, Free University of Berlin, Berlin, Germany. [12]German Cancer Consortium (DKTK), partner site Berlin, and German Cancer Research Center (DKFZ), Heidelberg, Germany. ✉e-mail: henssenlab@gmail.com

Supplementary Information for

Therapeutic targeting of ATR in alveolar rhabdomyosarcoma

Heathcliff Dorado García, Fabian Pusch, Yi Bei, Jennifer von Stebut, Glorymar Ibáñez, Kristina Guillan, Koshi Imami, Dennis Gürgen, Jana Rolff, Konstantin Helmsauer, Stephanie Meyer-Liesener, Natalie Timme, Victor Bardinet, Rocío Chamorro González, Ian C. MacArthur, Celine Y. Chen, Joachim Schulz, Antje M. Wengner, Christian Furth, Birgit Lala, Angelika Eggert, Georg Seifert, Patrick Hundsoerfer, Marieluise Kirchner, Philipp Mertins, Matthias Selbach, Andrej Lissat, Frank Dubois, David Horst, Johannes H. Schulte, Simone Spuler, Daoqi You, Filemon Dela Cruz, Andrew L. Kung, Kerstin Haase, Michela di Virgilio, Monika Scheer, Michael V. Ortiz, Anton G. Henssen*

*Corresponding author. Email: henssenlab@gmail.com

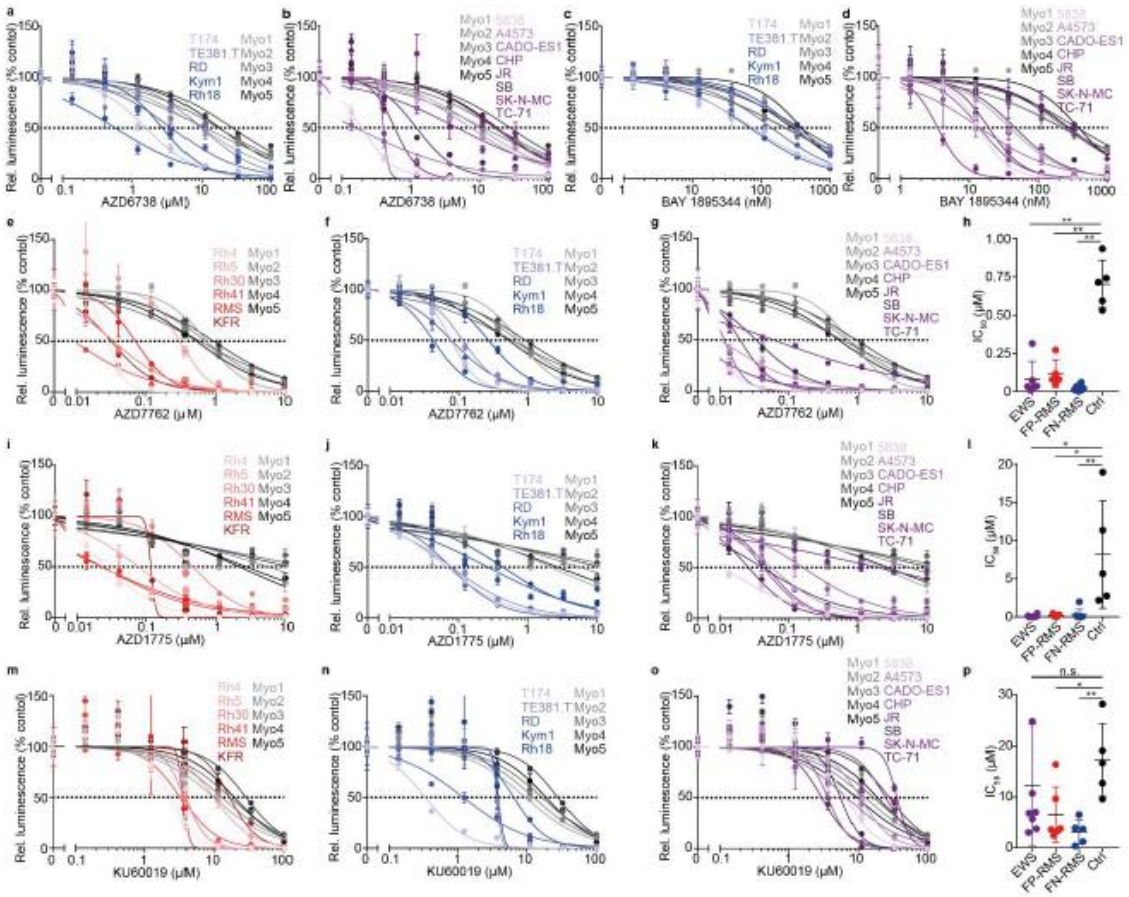

Supplementary Fig. 1. Effects of DNA Damage Response inhibitors in RMS and EWS cell lines (a-b) Dose-response curves of cell viability for FN-RMS (a) and EWS cell lines (b) treated with the ATR inhibitor AZD6738 compared to primary myoblasts (n=3). **(c-d)** Dose-response curves of cell viability for FN-RMS (c) and EWS cell lines (d) treated with the ATR inhibitor BAY 1895344 compared to primary myoblasts (n=3). **(e-g)** Dose-response curves of cell viability for FP-RMS (e) FN-RMS (f) and EWS cell lines (g) treated with the CHK1/2 inhibitor AZD7762 compared to primary myoblasts (n=3). **(h)** IC_{50} values for FP-RMS, EWS, FN-RMS and Ctrl cells treated with AZD7762 (P=6.95x10^{-8}; 3.29x10^{-5}; 8.45x10^{-5} for EWS, FP-RMS and FN-RMS vs Ctrl, respectively; from left to right, n=8, 6, 5 and 5 biologically independent cells). **(i-k)** Dose-response curves of cell viability for FP-RMS (i) FN-RMS (j) and EWS cell lines (k) treated with the WEE1 inhibitor AZD1775 compared to primary myoblasts (n=3). **(l)** IC_{50} values for FP-RMS, EWS, FN-RMS and Ctrl cells treated with AZD1775 (P=0.008; 0.020; 0.035 for EWS, FP-RMS and FN-RMS vs Ctrl, respectively; from left to right, n=8, 6, 5 and 5 biologically independent cells). **(m-o)** Dose-response curves of cell viability for FP-RMS (m) FN-RMS (n) and EWS cell lines (o) treated with the ATM inhibitor KU60019 compared to primary myoblasts (n=3). **(p)** IC_{50} values for FP-RMS, EWS, FN-RMS and Ctrl cells treated with KU60019 (P=0.421; 0.020; 0.030 for EWS, FP-RMS and FN-RMS vs Ctrl, respectively; from left to right, n=8, 6, 5 and 5 biologically independent cells). All statistical analyses correspond to two-sided student's t-test; data presented as mean value ± error bars representing standard deviation. Source data are provided as a Source Data file.

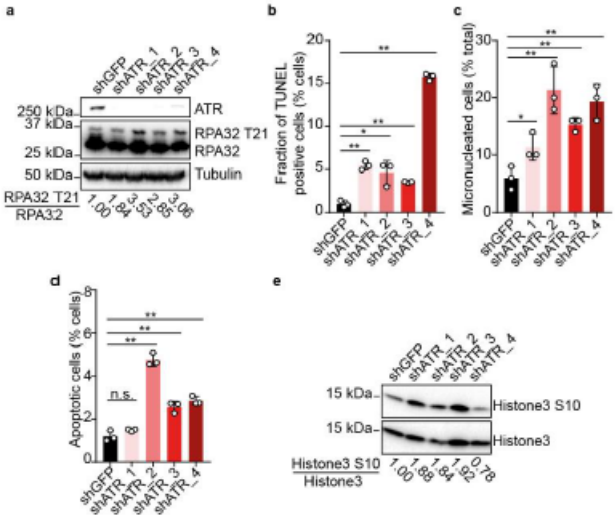

35

36 **Supplementary Fig. 2. ATR knockdown leads to increased DNA damage and**
37 **genomic instability. (a)** Western immunoblot of ATR and RPA32 phosphorylation at
38 T21 in Rh4 cells expressing shRNAs targeting ATR compared to shGFP expressing cells.
39 **(b)** Quantification of TUNEL signal in Rh4 cells expressing shRNAs targeting ATR
40 compared to shGFP expressing cells. (n = 3; from left to right, P = 2.74x10^{-4}; 0.012;
41 3.93x10^{-4}; 1.52x10^{-6}). **(c)** Fraction of micronucleated Rh4 cells expressing shRNAs
42 targeting ATR compared to shGFP expressing cells. (n = 3, with 50 nuclei counted per
43 replicate; P = 0.039; 0.005; 0.002; 0.003). **(d)** Fraction of apoptotic Rh4 cells expressing
44 shRNAs targeting ATR compared to shGFP expressing cells. (n = 3; from left to right, P
45 = 0.121; 8.61x10^{-5}; 0.003; 7.72x10^{-4}). **(e)** Western immunoblot of Histone 3
46 phosphorylation at S10 in Rh4 cells expressing shRNAs targeting ATR compared to
47 shGFP expressing cells. All statistical analyses correspond to two-sided student's t-test; data
48 presented as mean value ± error bars representing standard deviation. Source data are provided as
49 a Source Data file.

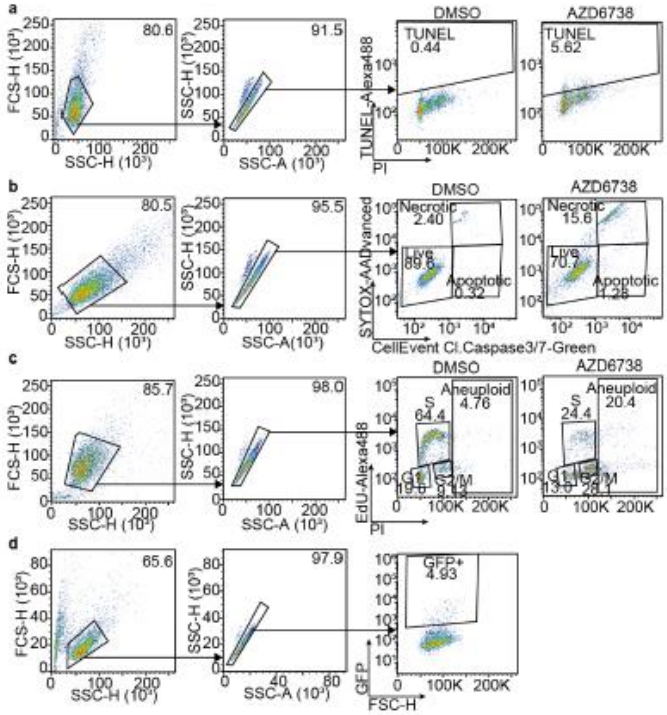

Supplementary Fig. 3. Representative FACS gating used in the study. (**a**) Representative gating of unrepaired DSBs measured by TUNEL. (**b**) Representative gating of cells stained for Caspase3/7 cleavage and SYTOX. (**c**) Representative gating of cell cycle phase distribution and aneuploidy as measured after EdU and propidium iodide co-staining. (**d**) Representative FACS gating of cells with active HR activity, measured as GFP reconstitution based on repair of an SceI-mediated DNA lesion via homologous recombination. FSC-H: Forward scatter (height), SSC-H: Side scatter (height), SSC-A: Side scatter (area).

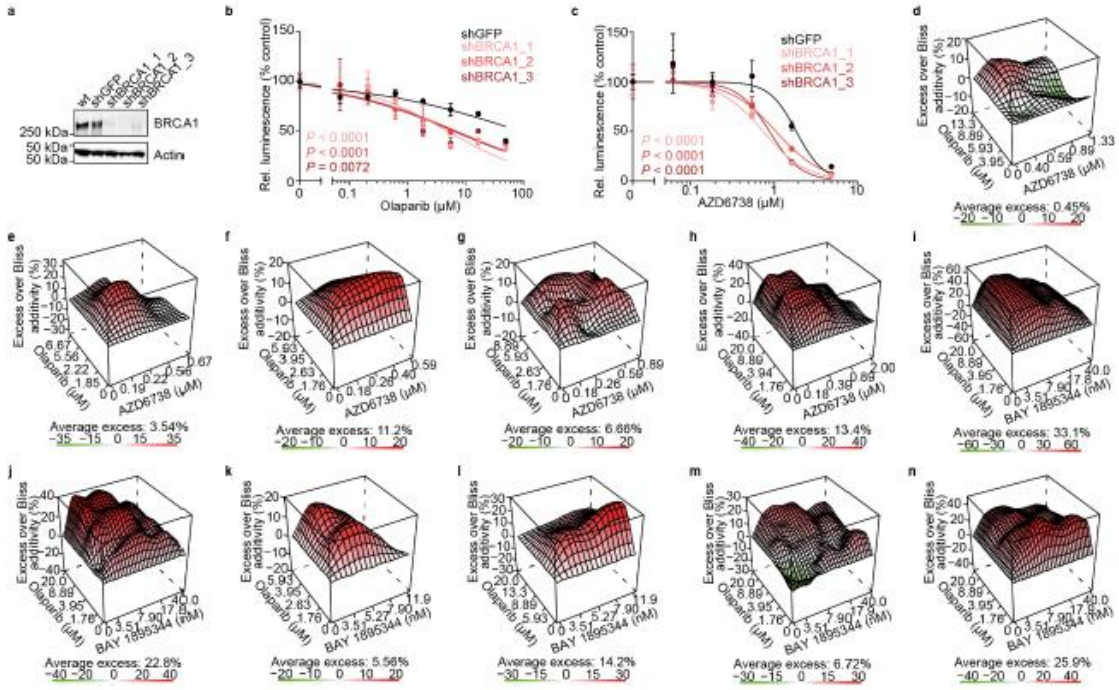

59

60 **Supplementary Fig. 4. ATR inhibition synergizes with olaparib in fusion-positive**
61 **rhabdomyosarcoma cell lines. (a)** Western immunoblot of BRCA1 in Rh4 cells of stably
62 expressing shRNAs targeting BRCA1 (shRNA targeting GFP was used as a control). **(b)**
63 Dose-response curves for Rh4 stably expressing different shRNAs targeting BRCA1 and
64 treated with PARP1 inhibitor olaparib (shRNA targeting GFP was used as a control) (n =
65 3). **(c)** Dose-response curves for Rh4 transduced with different shRNA targeting BRCA1
66 treated with ATR inhibitor AZD6738 (shRNA targeting GFP was used as a control) (n =
67 3). **(d-h)** Excess over Bliss analysis of combined treatment with olaparib and AZD6738
68 in Rh5 (d), Rh30 (e), Rh41 (f), RMS (g) and KFR (h) cells ($n = 3$). **(i-n)** Excess over Bliss
69 analysis of combined treatment with olaparib and BAY 1895344 in Rh4 (i) Rh5 (j), Rh30
70 (k), Rh41 (l), RMS (m) and KFR (n) cells ($n = 3$). All statistical analyses correspond to two-
71 sided student's t-test; data presented as mean value ± error bars representing standard deviation.
72 Source data are provided as a Source Data file.

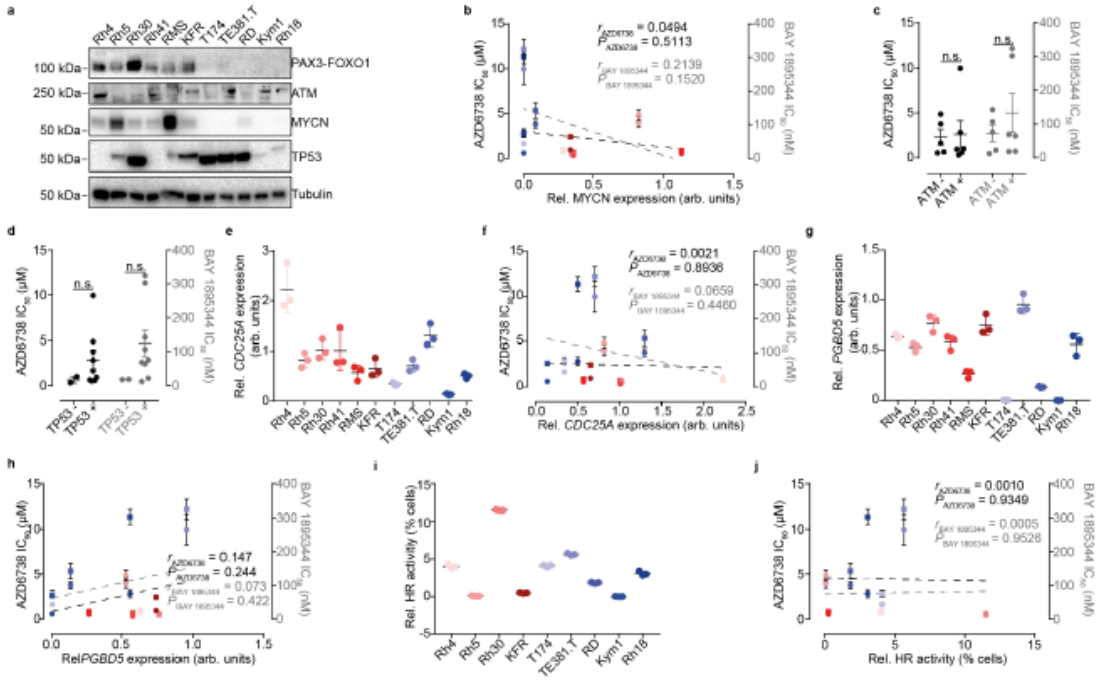

73

74 **Supplementary Fig. 5. Molecular factors associated with ATR inhibitor sensitivity**
75 **in rhabdomyosarcoma cells.** (**a**) Western Immunoblot of PAX3-FOXO1, MYCN, ATM
76 and TP53 in rhabdomyosarcoma cell lines. (**b**) Correlation of MYCN protein levels and
77 IC_{50} values for AZD6738 and BAY 1895344 (n=3 biologically independent
78 measurements of IC_{50} values). (**c-d**) Comparison of IC_{50} values for AZD6738 and BAY
79 1895344 for ATM (c; n=5 and n=6 for ATM- and ATM+, respectively; $P = 0.869$; 0.392)
80 and TP53 (d; n=2 and n=9 for TP53- and TP53+, respectively; $P = 0.356$; 0.240). (**e**)
81 mRNA expression levels of *CDC25A* in rhabdomyosarcoma cell lines ($n = 3$). (**f**)
82 Correlation of *CDC25A* expression and IC_{50} values for AZD6738 and BAY 1895344 (n=3
83 biologically independent measurements of IC_{50} values). (**g**) mRNA expression levels of
84 *PGBD5* in rhabdomyosarcoma cell lines ($n = 3$). (**h**) Correlation of *PGBD5* expression
85 and IC_{50} values for AZD6738 and BAY 1895344 (n=3 biologically independent
86 measurements of IC_{50} values). (**i**) Quantification of HR activity in RMS cells ($n = 3$). (**j**)
87 Correlation of HR activity and IC_{50} values for AZD6738 and BAY 1895344 (n=3
88 biologically independent measurements of IC_{50} values). All statistical analyses correspond
89 to two-sided student's t-test; data presented as mean value ± error bars representing standard
90 deviation. Source data are provided as a Source Data file.

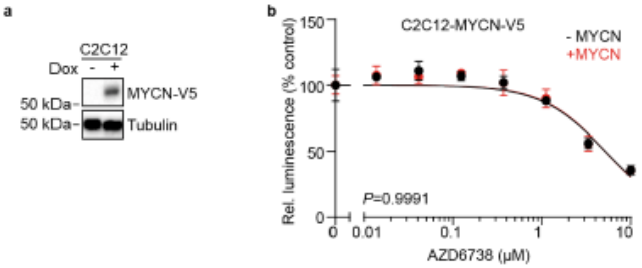

Supplementary Fig. 6. Ectopic expression of MYCN has no effect in ATR inhibitor sensitivity in C2C12 myoblasts. (a) Western immunoblotting of MYCN in C2C12 after induction with doxycycline (1000 ng/ml for 48h). **(b)** Dose-response curves in C2C12 cells treated with ATR inhibitor AZD6738 after doxycycline-induced ectopic expression of MYCN (n=3; error bars represent standard error of the mean). All statistical analyses correspond to two-sided student's t-test; data presented as mean value ± error bars representing standard deviation. Source data are provided as a Source Data file.

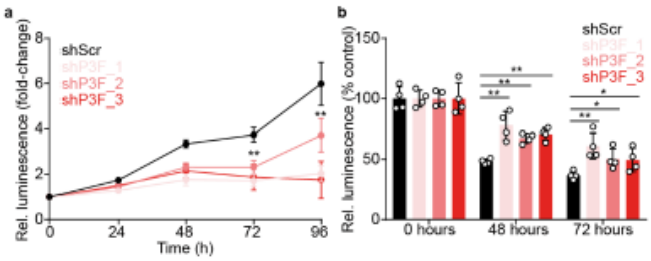

Supplementary Fig. 7. PAX3-FOXO1 knockdown reduces sensitivity to ATR inhibition (a) Proliferation of Rh4 cells over time after doxycycline-induced knockdown of PAX3-FOXO1 (n=8; P = $1.49x10^{-9}$; $2.11x10^{-7}$; $1.20x10^{-6}$; $2.76x10^{-8}$; $1.06x10^{-4}$; $1.67x10^{-7}$). **(b)** Cell viability reduction of Rh4 cells treated with AZD6738 (750 nM) after doxycycline-induced knockdown of PAX3-FOXO1 (n=4; P = 0.002; 0.001; $1.88x10^{-4}$; 0.005; 0.027; 0.048). All statistical analyses correspond to two-sided student's t-test; data presented as mean value ± error bars representing standard deviation. Source data are provided as a Source Data file.

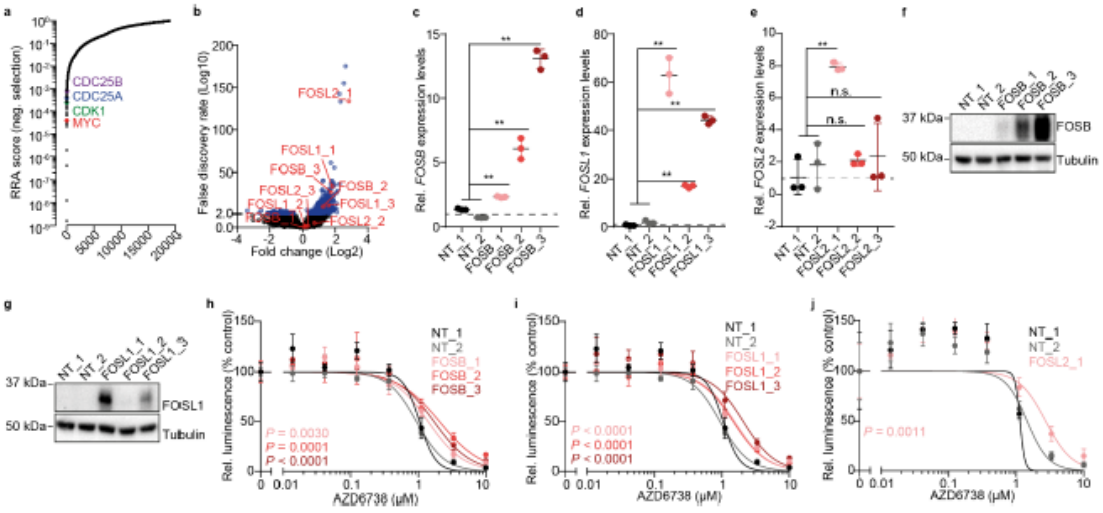

108

109 **Supplementary Fig. 8. *FOSB*, *FOSL1* and *FOSL2* expression reduces sensitivity to**
110 **ATR inhibition in rhabdomyosarcoma cells. (a)** Waterfall plot showing the negative
111 robust rank aggregation (RRA) score of sgRNAs in Rh4 cells incubated in the presence
112 of AZD6738 for 9 days compared to DMSO treated cells as analyzed using MAGeCK.
113 **(b)** Volcano plot showing the changes in sgRNA enrichment in Rh4 cells incubated in the
114 presence of AZD6738 for 9 days compared to DMSO treated cells as analyzed using
115 MAGeCK. In red, all the sgRNA corresponding to *FOSB*, *FOSL1* and *FOSL2*. **(c-e)** *FOSB*
116 (c; n=3 independent experiments; $P = 4.7\text{x}10^{-4}$, $P = 2.9\text{x}10^{-6}$ and $P = 5.1\text{x}10^{-9}$), *FOSL1*
117 (d; n=3 independent experiments; $P = 1.2\text{x}10^{-7}$, $P = 1.6\text{x}10^{-8}$ and $P = 2.2\text{x}10^{-10}$) and
118 *FOSL2* (e; n=3 independent experiments; $P = 4.2\text{x}10^{-5}$, $P = 0.400$ and $P = 0.430$) mRNA
119 expression measured using RT-qPCR in Rh4 cells expressing dCas9, lentiMPH and
120 sgRNAs targeting *FOSB*, *FOSL1* or *FOSL2* ($n = 3$). **(f-g)** Western immunoblot of FOSB
121 (f) and FOSL1 (g) in Rh4 cells stably expressing dCas9, lentiMPH and sgRNAs targeting
122 *FOSB* and *FOSL1*, respectively. **(h-j)** Relative cell viability of Rh4 cells stably expressing
123 dCas9, lentiMPH and sgRNAs targeting *FOSB* (h), *FOSL1* (i) and *FOSL2* (j) in the
124 presence and absence of AZD6738 ($n = 3$). All statistical analyses correspond to two-sided
125 student's t-test; data presented as mean value ± error bars representing standard deviation. Source
126 data are provided as a Source Data file.

127

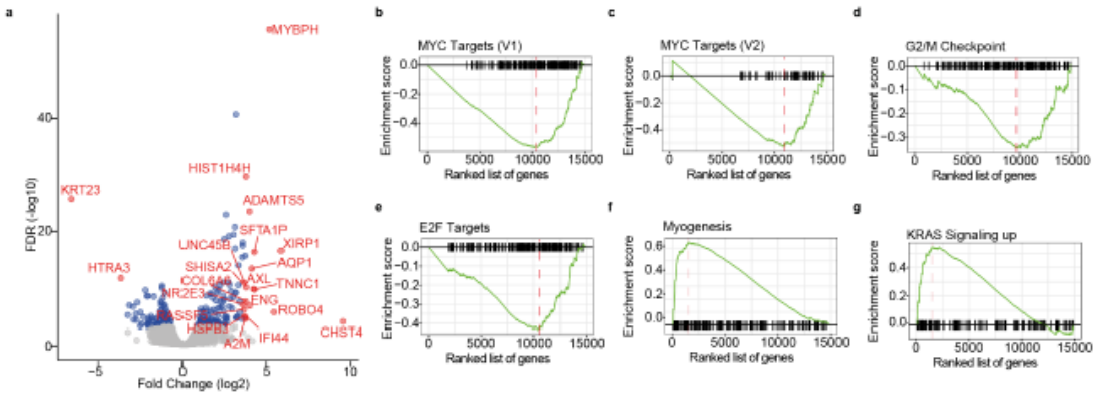

Supplementary Fig. 9. RAS-MAPK pathway is activated in Rh4 cells resistant to ATR inhibitors. **(a)** Volcano plot showing differentially expressed genes in cells incubated for 4 months with the ATR inhibitor AZD6738 vs a control population (red, top 20 differentially expressed genes). **(b-f)** GSEA plots showing enrichment of genes belonging to the MYC targets V1 (b), MYC targets V2 (c), G2/M checkpoint (d), E2F targets (e), myogenesis (f) and KRAS signaling up (g) pathways according to the GSEA hallmark pathways. Source data are provided as a Source Data file.

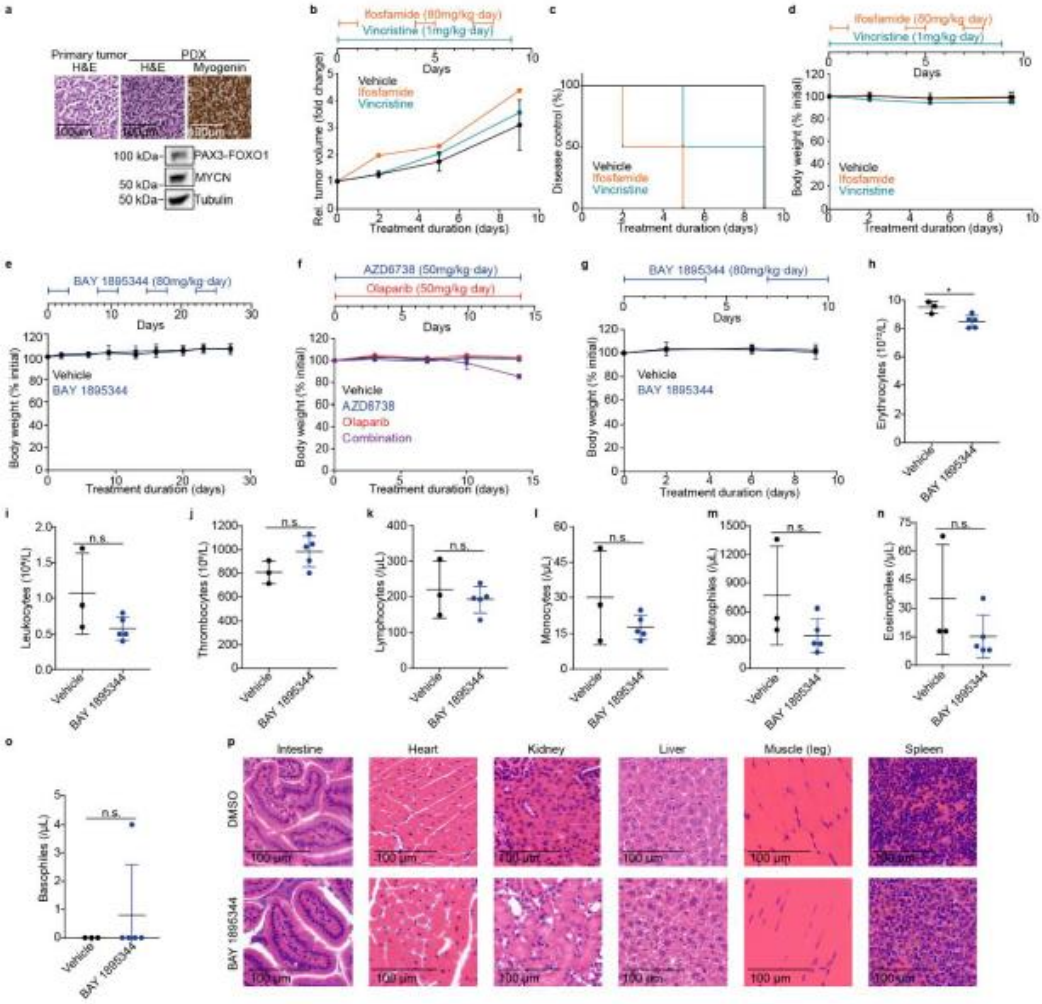

136

137 **Supplementary Fig. 10.** ***In vivo*** **treatment with ATR inhibitors has no remarkable**
138 **toxicity in mice harboring ARMS PDX models. (a)** Representative histological images
139 and western immunoblot for PAX3-FOXO1 and MYCN for the ARMS PDX model used.
140 **(b)** Tumor volume change of the ARMS PDX and treated with ifosfamide or vincristine
141 as compared to control (n=3 mice for vehicle, n=2 for treatments; top, timeline of the drug
142 schedule). **(c)** Kaplan Meier curve showing tumor doubling time after treatment. **(d)** Body
143 weight over time of mice harboring the ARMS PDX model and treated with ifosfamide,
144 vincristine or control (n=3 mice for vehicle, n=2 for treatments). **(e)** Body weight over
145 time of mice harboring the rhabdomyosarcoma PDX model and treated with BAY
146 1895344 or a vehicle control. (n=7). **(f)** Body weight over time of mice harboring the
147 rhabdomyosarcoma PDX and treated with AZD6738, olaparib, both or a vehicle control
148 (n=4). **(g)** Body weight over time of NOG mice treated with BAY 1895344 or a vehicle
149 control. (n=3 for vehicle, n=5 for BAY 1895344 treated mice). **(h-o)** Blood counts for
150 NOG mice treated with BAY 1895344 or vehicle, including erythrocytes (h; P=0.019),
151 leukocytes (i; P=0.109), thrombocytes (j; P=0.093), lymphocytes (k; P=0.512),
152 monocytes (l; P=0.217), neutrophiles (m; P=0.136), eosinophiles (n; P=0.212) and
153 basophiles (o; P=0.482) (n=3 for vehicle, n=5 for BAY 1895344 treated mice for all
154 figures from h to o). (p) Representative hematoxylin and eosin (H&E) histological images
155 of mice organs after treatment with BAY 1895344 or vehicle. All statistical analyses
156 correspond to two-sided student's t-test; data presented as mean value ± error bars representing
157 standard deviation. Source data are provided as a Source Data file.

Primer	Sequence (5'-3')
CDC25A_Fwd	ACC GTC ACT ATG GAC CAG C
CDC25A_Rv	TTC AGA GCT GGA CTA CAT CC
FOSB_Fwd	GTG AGA GAT TTG CCG GGC TC
FOSB_Rv	AGA GAG AAG CCG TCA GGT TG
FOSL1_Fwd	GCC CAC TGT TTC TCT TGA GC
FOSL1_Rv	GAT GGA GAG TGT GGC AGT GA
FOSL2_Fwd	GCC CAG TGT GCA AGA TTA GC
FOSL2_Rv	GGG CTC CTG TTT CAC CAC TA
HPRT1_Fwd	TGA CAC TGG CAA AAC AAT GCA
HPRT1_Rv	GGT CCT TTT CAC CAG CAA GCT
PGBD5_Fwd	CAG CCT CTG GGT CAG ACA AT
PGBD5_Rv	GCT TAT TCT TCA GCG CAT CC

158

159 **Supplementary Table 1.** Oligonucleotide sequences used in the manuscript.

Antibody	Company	Catalog number	Dilution
Actin	Cell Signaling Technology	3700	1:1000 in 5% milk in TBS
ATM	Cell Signaling Technology	92356	1:1000 in 5% milk in TBS
ATR	Cell Signaling Technology	13934	1:1000 in 5% milk in TBS
BRCA1	Merck Millipore	OP92-100UG	1:5000 in 5% milk in TBS
BRCA1 S1524	Bethyl Laboratories	A300-001A	1:1000 in 5% BSA in TBS
ClCas3	Cell Signaling Technology	9664	1:2000 in 3% BSA in PBS
c-Raf	Cell Signaling Technology	9422	1:1000 in 5% milk in TBS
c-Raf S338	Cell Signaling Technology	9427	1:1000 in 5% BSA in TBS
ERK1/2	Cell Signaling Technology	4695	1:1000 in 5% milk in TBS
ERK1/2 T202/T204	Cell Signaling Technology	4370	1:1000 in 5% BSA in TBS
FOSB	Cell Signaling Technology	2251	1:1000 in 5% milk in TBS
FOSL1	Cell Signaling Technology	5281	1:1000 in 5% milk in TBS
FOXO1 (And PAX3-FOXO1)	Santa Cruz Biotechnology	sc-374427	1:500 in 5% milk in TBS
Histone 2A.X S139	Merck Millipore	05-636	1:500 in 5% FBS in TBS-T
Histone 3	Cell Signaling Technology	4499	1:1000 in 5% milk in TBS
Histone 3 S10	Cell Signaling Technology	3377	1:1000 in 5% BSA in TBS
Ki67	Thermo Fisher Scientific	MA5-14520	1:20 in 3% BSA in PBS
MYCN	Santa Cruz Biotechnology	sc-53993	1:500 in 5% milk in TBS
RPA32 T21	Abcam	ab61065	1:10000 in 5% BSA in TBS
TP53	Santa Cruz Biotechnology	sc-98	1:500 in 5% milk in TBS
Tubulin	Cell Signaling Technology	3873	1:1000 in 5% milk in TBS
Anti-mouse-HRP	Thermo Fisher Scientific	62-6520	1:1000 in 5% milk or BSA in TBS
Anti-rabbit-HRP	Thermo Fisher Scientific	G-21234	1:1000 in 5% milk or BSA in TBS
Anti-mouse-Alexa488	Dianova	715-096-150	1:1000 in 5% FBS in TBS-T

Supplementary Table 2. Antibodies used in the manuscript, including dilution.

9.2. Roeschert *et al*. Combined inhibition of Aurora-A and ATR kinase results in regression of *MYCN*-amplified neuroblastoma.

https://doi.org/10.1038/s43018-020-00171-8

10. Curriculum Vitae

My curriculum vitae does not appear in the electronic version of my paper for reasons of data protection.

11. Publication list

Anton G Henssen, Casie Reed, Eileen Jiang, **Heathcliff Dorado Garcia**, Jennifer von Stebut, Ian C MacArthur, Patrick Hundsdoerfer, Jun Hyun Kim, Elisa de Stanchina, Yasumichi Kuwahara, Hajime Hosoi, Neil J Ganem, Filemon Dela Cruz, Andrew L Kung, Johannes H Schulte, John H Petrini, Alex Kentsis. Therapeutic targeting of PGBD5-induced DNA repair dependency in pediatric solid tumors. Sci Transl Med. (2017). IF: 16.71

Youjia Han, Sven Lindner, Yi Bei, **Heathcliff Dorado Garcia**, Natalie Timme, Kristina Althoff, Andrea Odersky, Alexander Schramm, Andrej Lissat, Annette Künkele, Hedwig E.Deubzer, Angelika Eggert, Johannes H. Schulte, Anton G. Henssen. Synergistic activity of BET inhibitor MK-8628 and PLK inhibitor Volasertib in preclinical models of medulloblastoma. Cancer Letters (2019). IF: 7.36

Ian C. MacArthur, Yi Bei, Heathcliff Dorado Garcia, Michael V. Ortiz,3Joern Toedling, Filippos Klironomos, Jana Rolff, Angelika Eggert, Johannes H. Schulte, Alex Kentsis, and Anton G. Henssen. Prohibitin promotes dedifferentiation and is a potential therapeutic target in neuroblastoma. JCI insight (2019). IF: 6.21

Richard P. Koche*, Elias Rodriguez-Fos*, Konstantin Helmsauer*, Martin Burkert, Ian C. MacArthur, Jesper Maag, Rocio Chamorro, Natalia Munoz-Perez, Montserrat Puiggròs, **Heathcliff Dorado Garcia**, Yi Bei, Claudia Röefzaad, Victor Bardinet, Annabell Szymansky, Annika Winkler, Theresa Thole, Natalie Timme, Katharina Kasack, Steffen Fuchs, Filippos Klironomos, Nina Thiessen, Eric Blanc, Karin Schmelz, Annette Künkele, Patrick Hundsdörfer, Carolina Rosswog, Jessica Theissen, Dieter Beule, Hedwig Deubzer, Sascha Sauer, Joern Toedling, Matthias Fischer, Falk Hertwig, Roland F. Schwarz, Angelika Eggert, David Torrents*, Johannes H. Schulte* & Anton G. Henssen*. Extrachromosomal circular DNA drives oncogenic genome remodeling in neuroblastoma. Nature Genetics, 2019. 52(1): p. 29-34. IF: 27.61

Celine Chen, **Heathcliff Dorado García**, Monika Scheer, Anton G. Henssen. Current and future treatment strategies for rhabdomyosarcoma. Front. Oncol. (2019). IF: 4.85

Natalie Timme, Youjia Han, Shuai Liu, Hailemichael O. Yosief, **Heathcliff Dorado García**, Yi Bei, Filippos Klironomos, Ian C. MacArthur, Annabell Szymansky, Jennifer von Stebut, Victor Bardinet, Constantin Dohna, Annette Künkele, Jana Rolff, Patrick Hundsdörfer, Andrej Lissat, Georg Seifert, Angelika Eggert, Johannes H. Schulte, Wei

Zhang, Anton G. Henssen, Small-Molecule Dual PLK1 and BRD4 Inhibitors are Active Against Preclinical Models of Pediatric Solid Tumors. Translational Oncology (2020). IF: 4.24

Thomas Gp Grünewald, Marta Alonso, Sofia Avnet, Ana Banito, Stefan Burdach, Florencia Cidre-Aranaz, Gemma Di Pompo, Martin Distel, **Heathcliff Dorado-Garcia**, Javier Garcia-Castro, Laura González-González, Agamemnon E Grigoriadis, Merve Kasan, Christian Koelsche, Manuela Krumbholz, Fernando Lecanda, Silvia Lemma, Dario L Longo, Claudia Madrigal-Esquivel, Álvaro Morales-Molina, Julian Musa, Shunya Ohmura, Benjamin Ory, Miguel Pereira-Silva, Francesca Perut, Rene Rodriguez, Carolin Seeling, Nada Al Shaaili, Shabnam Shaabani, Kristina Shiavone, Snehadri Sinha, Eleni M Tomazou, Marcel Trautmann, Maria Vela, Yvonne Mh Versleijen-Jonkers, Julia Visgauss, Marta Zalacain, Sebastian J Schober, Andrej Lissat, William R English, Nicola Baldini, Dominique Heymann. Sarcoma treatment in the era of molecular medicine. EMBO Mol Med. (2020) IF: 12.14

Konstantin Helmsauer, Maria E. Valieva, Salaheddine Ali, Rocío Chamorro González, Robert Schöpflin, Claudia Röefzaad, Yi Bei, **Heathcliff Dorado Garcia**, Elias RodriguezFos, Montserrat Puiggròs, Katharina Kasack, Kerstin Haase, Csilla Keskeny, Celine Y. Chen, Luis P. Kuschel, Philipp Euskirchen, Verena Heinrich, Michael I. Robson, Carolina Rosswog, Joern Toedling, Annabell Szymansky, Falk Hertwig, Matthias Fischer, David Torrents, Angelika Eggert, Johannes H. Schulte, Stefan Mundlos, Anton G. Henssen & Richard P. Koche. Enhancer hijacking determines extrachromosomal circular MYCN amplicon architecture in neuroblastoma. Nat Commun, (2020). IF: 14.92

Isabelle Roeschert, Evon Poon, Anton G. Henssen, **Heathcliff Dorado Garcia**, Marco Gatti, Celeste Giansanti, Yann Jamin, Carsten P. Ade, Peter Gallant, Christina Schülein-Völk, Petra Beli , Mark Richards, Mathias Rosenfeldt, Matthias Altmeyer, John Anderson, Angelika Eggert, Matthias Dobbelstein, Richard Bayliss , Louis Chesler, Gabriele Büchel and Martin Eilers. Combined inhibition of Aurora-A and ATR kinases results in regression of MYCN-amplified neuroblastoma. Nat Cancer (2021). IF: 23.18

Oxana Schmidt†, Nadja Nehls†, Carolin Prexler, Kristina von Heyking, Tanja Groll, Katharina Pardon, **Heathcliff Dorado Garcia**, Tim Hensel, Dennis Gürgen , Anton G. Henssen, Angelika Eggert, Katja Steiger, Stefan Burdach and Günther H. S. Richter.

Class I histone deacetylases (HDAC) critically contribute to Ewing sarcoma pathogenesis. J Exp Clin Cancer Res (2021). IF: 12.66

Mareike Berlak#, Elizabeth Tucker#, Mathurin Dorel, Annika Winkler, Aleixandria McGearey, Elias Rodriguez-Fos, Barbara Martins da Costa, Karen Barker, Elicia Fyle, Elizabeth Calton, Selma Eising, Kim Ober, Deborah Hughes, Eleni Koutroumanidou, Paul Carter, Reda Stankunaite, Paula Proszek, Neha Jain, Carolina Rosswog, **Heathcliff Dorado Garcia**, Jan Jasper Molenaar, Mike Hubank, Giuseppe Barone, John Anderson, Peter Lang, Hedwig Elisabeth Deubzer, Annette Künkele, Matthias Fischer, Angelika Eggert, Charlotte Kloft, Anton George Henssen, Michael Boettcher, Falk Hertwig, Nils Blüthgen, Louis Chesler#, Johannes Hubertus Schulte#. Mutations in ALK signaling pathways conferring resistance to ALK inhibitor treatment lead to collateral vulnerabilities in neuroblastoma cells. Mol Cancer (2022). IF: 41.44

Heathcliff Dorado García, Fabian Pusch, Yi Bei, Jennifer von Stebut, Glorymar Ibáñez, Kristina Guillan, Koshi Imami, Dennis Gürgen, Jana Rolff, Konstantin Helmsauer, Stephanie Meyer-Liesener, Natalie Timme, Victor Bardinet, Rocío Chamorro González, Ian C MacArthur, Celine Y Chen, Joachim Schulz, Antje M Wengner, Christian Furth, Birgit Lala, Angelika Eggert, Georg Seifert, Patrick Hundsoerfer, Marieluise Kirchner, Philipp Mertins, Matthias Selbach, Andrej Lissat, Frank Dubois, David Horst, Johannes H Schulte, Simone Spuler, Daoqi You, Filemon Dela Cruz, Andrew L Kung, Kerstin Haase, Michela DiVirgilio, Monika Scheer, Michael V Ortiz, Anton G Henssen. Therapeutic targeting of ATR in alveolar rhabdomyosarcoma. Nat Commun. (2022). IF: 17.69

12. Acknowledgments

First and foremost, I would like to thank my family for their continuous support and validation through my PhD and the rest of my life. They not only provided the resources needed to achieve my career goals, but I feel them by my side even when we are thousands of kilometers away.

I am also very fortunate to have met incredible friends along this journey, which also became part of the family we choose. Not only have they inspired me, and continue to do so, but they also have helped me find myself and become the person I am proud to be. I cherish every moment we spent together. I can only wish that we will share many more stories together and that we will continue to enrich our lives for as many years as possible.

I would like to mention specially my friends from the lab, which have been there for me in the toughest parts of the PhD and have celebrated with me every academic achievement. This experience could not have happened without you, and I hope I can be there to celebrate your graduations and future milestones. Thank you for having built this incredible environment and keep being the support for future lab members.

I would also like to extend my gratitude to Anton for his supervision, and for providing me with this opportunity. This could not have been possible if it were not for your perseverance and guidance. Special thanks also to Michela and Johannes for their insightful comments and discussions, which were essential for shaping and improving this project.

Finally, I would like to thank all the patients who willingly and selflessly donated material for research. Their unvaluable contribution will help future children to have a second chance, and a better life experience. I hope my contribution, together with many others currently working on this field, can be translated into a durable and safe therapy that provides a good quality of life to as many patients as possible. I would like to specially thank M.B. and their family for their brave contribution, and for never losing the hope and remind us all why we are doing this.